Investigation of inoculation Routes on Chronic Wasting Disease Progression in Cervidized Mouse Model: A Foundation for Microbiota-Pathogenesis Research

Nisanth Thavarajah

Thesis submitted to the University of Ottawa in partial Fulfillment of the requirements for the Master of Science in Cellular and Molecular Medicine

Department of Cellular and Molecular Medicine

Faculty of Medicine

University of Ottawa

Abstract

Chronic wasting disease (CWD) is an infectious and fatal prion disorder of cervids that is rapidly expanding across North America. Although extensively studied in natural hosts, the early tissue and route-specific events that govern prion seeding and amplification remain poorly defined. This thesis employed transgenic mice that express transgenic elk prion protein (TgElk) to investigate the effects of inoculation routes on CWD prion seeding and distribution in selected tissues.

TgElkPrP mice were inoculated with CWD positive brain homogenate via the intragastric (IG) or intracerebral (IC) routes. Prion seeding activity and amplification were determined using real-time quaking-induced conversion (RT-QuIC), and the CWD positivity in animals was confirmed by immunohistochemistry.

Prion seeding activity was detected in brain and spleen tissues as early as 8 weeks post-IC inoculation. In contrast, prion seeding activity was minimally expressed in mice by 56 weeks post-IG inoculation, suggesting a longer incubation time is required for disease manifestation. These findings indicate differential disease progression rates and incubation processes caused by different inoculation routes.

This work also provides a foundation for future investigations into the interaction between CWD progression and the dynamics of gut microbiome composition, with the potential to identify gut microbial species as a biomarker for early detection of CWD and to understand how gut microbial communities influence animal susceptibility to CWD.

Acknowledgements

I would like to first extend my sincerest gratitude to my thesis supervisor, Dr. Wandong Zhang from the National Research Council of Canada, for working on this project. His wealth of knowledge, as well as his guidance throughout this project, was both strongly encouraging and essential to its completion.

I would also like to thank my thesis co-supervisor, Dr. Jiewen Guan, for allowing me to complete this work in her laboratory at the Canadian Food Inspection Agency. Her input and help throughout were valuable and supportive.

My thesis advisory committee, Dr. Marceline Côté and Dr. Gerard Jansen, also deserve recognition and thanks for their input, collaboration, and support.

Lastly, I would like to thank my wife, Sharmi, and my mother, Jeya, for their love, support, encouragement, and motivation, as this work would have been inconceivable without them.

Table of Contents

Abbreviations

BSE – Bovine Spongiform Encephalopathy

CJD – Creutzfeldt-Jakob Disease

CNS – Central Nervous System

Ct – Cycle Threshold

CWD – Chronic Wasting Disease

DNA – Deoxyribonucleic Acid

EDTA – Ethylenediaminetetraacetic Acid

ELISA – Enzyme-Linked Immunosorbent Assay

FFI – Fatal Familial Insomnia

GPI – Glycosylphosphatidylinositol

GSS – Gerstmann-Sträussler-Scheinker Syndrome

IC – Intracerebral

IG – Intragastric

IHC – Immunohistochemistry

IP – Intraperitoneal

IV – Intravenous

MWCO – Molecular Weight Cut-Off

NaCl – Sodium Chloride

NGS – Next-Generation Sequencing

PBS – Phosphate Buffered Saline

PCR – Polymerase Chain Reaction

PMCA – Protein Misfolding Cyclic Amplification

PrP – Prion Protein

PrP^{C}– Cellular Prion Protein

PrP^{Sc}– Scrapie/Pathogenic Prion Protein

PrP^{CWD}– Chronic Wasting Disease–associated Prion Protein

PRNP – Prion Protein Gene

qPCR – Quantitative Polymerase Chain Reaction

recPrP – Recombinant Prion Protein

RFU – Relative Fluorescence Units

RNA – Ribonucleic Acid

ROC – Receiver Operating Characteristic

RT-QuIC – Real-Time Quaking-Induced Conversion

rRNA – Ribosomal RNA

SCFA – Short-Chain Fatty Acid

SDS – Sodium Dodecyl Sulphate

SD – Standard Deviation

TgElk – Transgenic Elk Prion Protein Mouse Model

ThT – Thioflavin T

TSE – Transmissible Spongiform Encephalopathy

vCJD – Variant Creutzfeldt-Jakob Disease

WB – Western Blo

Introduction

With the beginning of the 18th century, observers witnessed abnormal behaviour being displayed by Merino sheep, which consisted of altered gait, excessive licking, and an intense itch, compelling these sheep to scrape their backs against fences aggressively (Zabel & Reid, 2015). To classify this unusual behaviour, pathologists Creutzfeldt and Jakob in the early 20th century described a neurodegenerative disease that, along with scrapie, would be included in a group of diseases known as transmissible spongiform encephalopathies (TSEs) (Zabel & Reid, 2015). By the end of that century, the growing evidence forced some scientists to break with the dominant biological dogma that governed pathogen replication. In 1950's, Watson and Crick had convincingly shown how to crack the genetic code. TSEs seemed to ignore this new dogma. J.S. Griffith formulated the possible mechanisms by which a pathogenic protein could record its own blueprint for replication independent of a genetic code. Stanley Prusiner referred to this proteinaceous infectious agent as a prion. The narrative surrounding investigations of proteins that elicit anomalous chemical and biological paradigms, such as prion proteins, provides a compelling and controversial narrative informing our understanding of biological dogma, and ultimately protein biochemistry and mediated storage and transfer of biological information.

Prion diseases represent a distinct group of infectious neurodegenerative diseases characterized by the accumulation of misfolded prion proteins (Zhu & Aguzzi, 2021). Prions lack nucleic acids, unlike traditional infectious pathogens (Das & Zou, 2016). They nevertheless exhibit a propensity to propagate through the misfolding and aggregation of host proteins, resulting in a progressive and fatal neurodegenerative disease characterized by encephalopathy. The protein misfolds and acts as a template, which leads to the misfolding and accumulation of endogenous PrP^{C} proteins in the host brain (Kupfer et al., 2009). The resultant accumulation of PrP^{Sc} at lesion sites leads to neuronal cell death, spongiform change in the surrounding tissue, and ultimately, progressive neurodegeneration. Prion disease affects cognitive and motor function, leading to dementia, ataxia, and finally, death (Soto & Satani, 2010). These diseases are

always fatal, and no effective treatment is available (Gilch et al., 2011). These infectious proteinopathies include Creutzfeldt-Jakob disease (CJD), variant CJD, Gerstmann-Sträussler-Scheinker syndrome (GSS), and Fatal Familial Insomnia (FFI) in humans, as well as prion diseases of mutton in animals such as Chronic Wasting Disease (CWD) in cervids, scrapie in sheep and goats, and Bovine Spongiform Encephalopathy (BSE) in cattle. Although rare, prion diseases carry tremendous public health relevance due to their long incubation periods, hardiness against PrP^{Sc} decontamination, and potential for iatrogenic transmission. The ability of prions to cross species lines is particularly concerning in relation to zoonotic transmission, as is the case with chronic wasting disease in cervids.

Chronic wasting disease (CWD) is now acknowledged as the most rapidly spreading prion epizootic disease from a captive mule deer pen in Colorado, now covering over 36 U.S. states and 5 Canadian provinces (British Columbia, Alberta, Saskatchewan, Manitoba, and Quebec) (USGS, 2025) (Fig. 1). This disease has spread, in part, due to biological characteristics that differ from other prion diseases. First, misfolded prion proteins (PrP^{Sc}) adhere to clay minerals and quartz, remaining infectious in soil for years and thereby producing persistent environmental reservoirs (Johnson et al., 2006). Second, infected cervids shed prion protein in saliva, urine, and feces for months and, at times, years, before showing clinical signs of CWD (weight loss and ataxia), which makes subclinical infected cervids mobile infection waves (Haley et al., 2011). This disease is always fatal, and animals typically die within months to years of showing clinical signs (Henderson et al. 2020). Within adult deer, death usually occurs between 16 months and 4 years (Miller, Wilds & Williams, 1998; Williams, 2005). The disease affects many species of cervids, including deer (white-tailed, mule, black-tailed, red, and sika deer), elk (wapiti), moose, and reindeer (caribou). Therefore, there is a need to understand the earliest cellular and molecular circumstances regarding PrP^{Sc} entry into the host, peripheral amplification, and eventual neuroinvasion to strategize measures to control the spread of CWD.

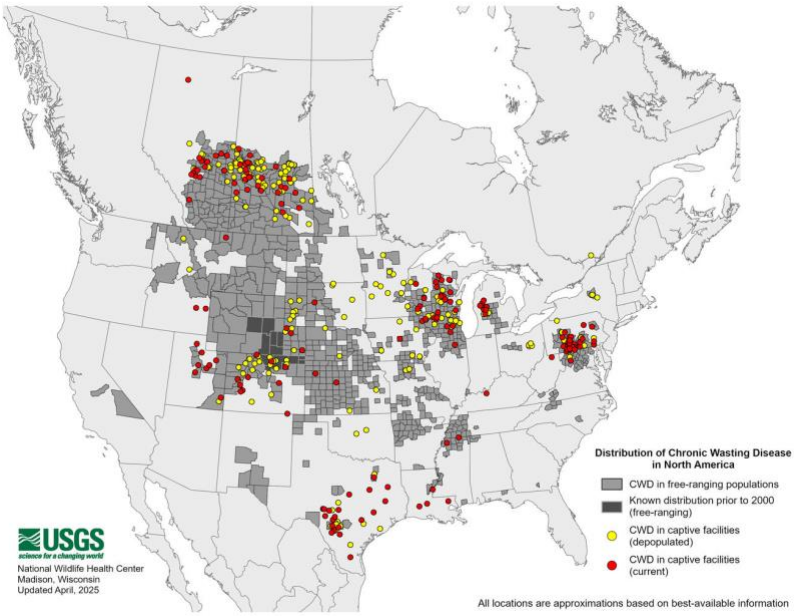

Figure 1. Distribution of Chronic Wasting Disease in North America, updated April 11, 2025.
Chronic wasting disease has been detected in free-ranging deer cervids in 36 U.S. states and four Canadian provinces and in captive cervid facilities in 22 states and three provinces.

Over the past decade, advances in imaging, transgenic models, and ultrasensitive seeding assays have dismantled the narrative of oral ingestion to the brain and replaced it with a multistage, tissue-resolved pathway of propagation. High-resolution microscopy can track PrP^{Sc} uptake by the intestinal microfold cells and enterocytes (Kujala et al., 2011). Gene knockout studies have confirmed Peyer's patches as indispensable replication niches, and longitudinal biopsy studies in deer have timed the leap from lymphoid tissues to the vagus nerve with month-scale precision (Takakura et al., 2011). Current research suggests that although only one polymorphism can extend incubation for multiple years (Moazami-Goudarzi et al., 2021), antibiotic-induced dysbiosis can expedite neuroinvasion (Trichka & Zou, 2021). These items add to the complexity of genetics, microbiota, and the environment. In fact, one moose that was diagnosed with CWD post-mortem exhibited no clinical signs even though there was evidence of spongiform encephalopathy in the brainstem and cervical spinal cord (Baeten et al., 2007).

Overview of Chronic Wasting Disease

The normal cellular prion protein (PrP^{C}) is a glycosyl-phosphatidylinositol (GPI)–anchored glycoprotein that is predominantly α-helical, soluble, and readily digested by proteases. In contrast, the misfolded, disease-associated/abnormal isoform (PrP^{Sc}) adopts a β-sheet–rich structure that aggregates into amyloid fibrils and exhibits marked resistance to protease K. The spontaneous conversion of PrP^{C} into PrP^{Sc} occurs when native PrP^{C} undergoes this α-to-β conformational transition, and the resulting PrP^{Sc} acts as a template to recruit and refold additional PrP^{C}. This templated misfolding drives fibril elongation and fragmentation, creating new growth ends and a self-propagating cycle of prion replication (Prusiner, 1998).

The mechanism for this is described by nucleation-dependent polymerization (Figure 2). The core mechanism for forming infectious prions begins with a misfolded PrP^{C} converting to its pathogenic, beta-sheet-rich conformation; this is a relatively slow process due to the energy barrier that forms the initial nucleus (Silva et al., 2022). Subsequently, once a critical nucleus is generated, rapid elongation occurs as more PrP^{C} molecules become misfolded and recruited. Ultimately, this leads to rapid, incremental generation of amyloid fibrils to exponentially grow the amyloid material (Soto, 2012), and ultimately a self-replicating process that underlies the transmissible and progressive accumulation of prions in exposed hosts contributing to the pathogenesis associated with prion diseases such as CWD, Creutzfeldt-Jakob Disease (CJD), and Scrapie. Currently there have been no selective methods to inactivate prions, including ionizing radiation, UV radiation, boiling / heat inactivation, nucleases, proteases, formalin, or autoclaving (121 °C, 20 min, standard practice in microbiology). Ingestion is the dominant route for entry of prion acquisition, as demonstrated by the consumption or contamination of crops or coprophagy (Bravo-Risi et al., 2021). Of particular note, infectious prions have been evidenced in bodily fluids, at low

concentrations, such as the urine and saliva of CWD-infected deer (Haley et al., 2009; Mathiason et al., 2009). These findings support the possibility that abnormal prions can be detected via bodily fluids excreted from the animal, which could offer potential ante-mortem detection for diagnostic purposes. Present evidence suggests that abnormal prions can be detected ante-mortem through blood and fecal samples. Vertical transmission has also been documented within CWD prions within the fetal tissues of CWD-affected, naturally infected white-tailed deer (Bravo-Risi et al., 2021).

In addition, propagation of CWD prions is influenced by variations in the prion protein gene (PRNP), where specific polymorphisms can modify host susceptibility and alter the rate of disease progression across cervid species (Moazami-Goudarzi et al., 2021). Environmental factors can drive CWD prion persistence and propagation by reducing degradation and mobility of infectious particles. Soil organic matter, such as humic acids, can bind and stabilize prions, thereby lowering effective dose and facilitating long-term environmental infectivity (Kuznetsova et al., 2018). The route of transmission also shapes prion strain characteristics: peripheral transmission maintains natural strain properties of elk and deer prions, whereas intracerebral transmission can generate divergent strains (Defranco et al., 2024). Chronic wasting disease is invariably fatal. Infected cervids typically die within months to years after the onset of clinical signs, with adult deer succumbing within approximately 16 months to 4 years (Williams, 2005; Miller, Wilds & Williams, 1998; Henderson et al., 2020). The disease affects a broad range of cervid species, including mule deer, white-tailed deer, Rocky Mountain elk, and moose. Susceptibility varies among species and populations, as genetic differences in the prion protein gene influence both infection risk and disease progression (Benestad & Telling, 2018). CWD prions (PrP^{CWD}) exhibit a wide tissue tropism. They accumulate at highest concentrations in the central nervous system, lymphoid tissues, and excretory organs, but can be detected in many peripheral tissues throughout the body (Hoover et al., 2017). Infection can occur through direct or indirect exposure, most often via the gastrointestinal tract, where specialized M cells facilitate prion uptake and subsequent neuroinvasion (Minich et al., 2021).

PrP^{CWD} is detected in alimentary associated lymphoid tissues (AALTs) shortly after infection and reflects the earliest locations of prion accumulation after oral exposure. As disease progression continues, prions spread into other tissues including the brain, salivary glands, urinary bladder, and distal intestinal tract (Haley et al. 2011). The peripheral nervous system (PNS) is also affected as prions replicate in neuronal tissues including the myenteric plexus and vagosympathetic trunk indicating that neuronal pathways are involved in prion trafficking and invasion of organs (Sigurdson et al., 2001). In addition, prions can be found in other endocrine tissues, such as in the pituitary gland, adrenal medulla, and pancreatic islets indicating the widespread tissue tropism of PrP^{CWD} (Sigurdson et al. ,2001). Research conducted through serial protein misfolding cyclic amplification (sPMCA) indicated the highest PrP^{CWD}-generating activity existed in the salivary glands, urinary bladder, and distal intestinal tract of cervids that had been exposed to CWD (Haley et al., 2011); however, these tissues did not demonstrate any detectable prion protein (PrP^{CWD}) by standard western blotting, indicating either a lower prion burden or the presence of protease-sensitive forms.

PrP^{CWD} has distinct regions of engagement of peripheral tissues depending on the route of inoculation; in oral inoculation studies, PrP^{CWD} deposition occurs quickly and extensively in lymphoid tissues before spreading to the central and peripheral nervous system tissue and eventually, other organs late in the disease (Fox et al., 2006). This progression seems to reflect prion movement from the initial site of peripheral entry to the spread of infectivity to the central nervous system along the neural route. CWD has been transmitted to deer by aerosol route, with a prion dose over 20 times less than that used for oral inoculation, implying inhalation may be a feasible pathway for CWD transmission (Denkers et al., 2012), which challenges the premise oral exposure is the predominant route of natural transmission.

Prion Protein Gene (PRNP) Characteristics

PRNP encodes the prion protein (PrP), which plays a crucial role in the pathology of chronic wasting disease (CWD) among cervids. The PRNP gene is highly conserved within the Cervidae family, exhibiting only 16 amino acid polymorphisms within the 256-amino-acid open reading frame of its third exon (Orge et al., 2021). Specific polymorphisms in PRNP significantly influence susceptibility to CWD, with certain variants associated with reduced infection rates and slower disease progression (Moazami-Goudarzi et al., 2021).

Polymorphisms within *prnp* shape how efficiently PrP^{CWD} replicates, which in turn affects whether cervids become infected and how quickly they succumb. Mouse models expressing cervid PrP variants have been instrumental in teasing apart these genetic influences. One of the earliest polymorphisms studied was at codon 96 of the white-tailed deer PRNP gene, where glycine can be replaced by serine. Transgenic mice carrying the glycine allele (96G) developed CWD in approximately 160 days and accumulated abundant PrP^{Sc} in their brains, indicating high susceptibility. In contrast, mice expressing the serine allele (96S) remained free of clinical disease and protease-resistant PrP for more than 600 days. Heterozygous 96G/96S mice exhibited a delayed onset of disease relative to homozygous 96G animals, indicating a partial protective effect. Another polymorphism in white-tailed deer, codon 95 (H95), is rare but essential; transgenic mice with histidine at this position showed no disease when inoculated with common CWD strains. However, a novel prion strain dubbed $H95^{+}$ can emerge and overcome this barrier, causing disease in H95 mice after much longer incubation periods.

The Rocky Mountain elk exhibits a polymorphism at codon 132 (equivalent to human codon 129) at which methionine can be substituted by leucine. Methionine (M132) expressing mice readily propagate CWD prions, whereas leucine (L132) expressing mice remain free of the disease. In mule deer, there is

polymorphism at codon 225, where homozygous 225F deer are considerably less likely to become infected with CWD than individuals with the most common serine allele; in transgenic mice with the phenylalanine substitution, the incubation time is prolonged, yet attack rates are low, and only a small percentage go on to develop disease. For codon 226, elk has glutamate (E) and white-tailed deer has glutamine (Q), and in a disease-targeted mouse strain E226 elk exhibited a 20-38% shorter disease onset than Q226 white-tailed deer, suggesting glutamate may facilitate more efficient prion replication.

There are other polymorphisms, some of which have been explored more recently. A rare A-to-G change at codon 116 in white-tailed deer does not prevent infection but alters strain characteristics. Mice inoculated with CWD prions from 116G animals have a survival time of about two months longer than mice infected with wild-type prions, and the strain can infect otherwise resistant 96S transgenic mouse. Polymorphism S138N, is even rarer and has only been found in reindeer, fallow deer, and in a very small number of white-tailed deer. Interbreeding with these polymorphisms in gene-targeted mice heterozygous for N138 and S138 remain asymptomatic over 600 days in isolation, but retain low-level prion seeding activity, suggest that asparagine at codon 138 operates under a dominant-negative principle for prion conversion. Finally, there are only reports of polymorphisms such as Q95H, A117V, etc. in European cervids, and it remains unknown if these possibly influence CWD susceptibility.

Overall, these polymorphisms indicate that a simple change in an amino acid of PrP can have a big impact on disease manifestation.

Polymorphisms such as 96S, H95, L132, F225, and N138 confer very strong resistance by either preventing prion conversion or significantly extending the incubation interval. On the other hand, polymorphisms such as 96G, M132, and E226 promote fast prion replication and clinical disease. Some polymorphisms such as G116 and L138 can generate new strains capable of breaking through established resistant boundaries to infection. Knowledge gained through mouse models has helped frame the observations

made for PRNP alleles in populations of wild cervids. Further, data from these models would support strategies (e.g., breeding or surveillance) that exploit genotype for CWD susceptibility.

Animal Models for CWD Research

Various animal models have been utilized to investigate CWD, each providing unique insights into different aspects of the disease. Cervids, including deer, elk, and moose, are the most relevant models because of their status as natural hosts for CWD (Mathiason, C, K. 2022). These animals enable researchers to study disease progression, transmission dynamics, and species-specific susceptibility in wild populations, as well as to investigate the impact of environmental factors on the spread of CWD.

Mice are the most widely used laboratory animals for studying diseases due to their manageability, short generation time, and ease of genome manipulation. Mouse models possess the ability to recapitulate aspects of the neuropathological and biochemical characteristics of several human and animal diseases in a shorter period.

Transgenic mice can be generated to express a *prnp* gene matched to the species and prion strain under investigation. Most often, the transgenes are represented on a *prnp* null background ($prnp^{0/0}$), to avoid partial or complete suppression of disease caused by the co-expression of wild-type *prnp*. The expression levels of *prnp* in the models may affect prion disease susceptibility and incubation periods (Pruisner et al., 1990). While transgenic models are extremely valuable for understanding aspects of the disease, the downsides to classic transgenic mouse models include the potential for variable copy numbers of the transgene at undefined genomic locations due to random integration of transgene insertion sites. This aspect inhibits the standardization of experiments and may affect the repeatability of animal disease. Gene targeting, which directly replaces the mouse PrP gene with the species-specific PrP gene, offers advantages over traditional transgenic mice and appears to provide a more accurate representation of

disease by demonstrating peripheral pathogenesis and mechanisms of horizontal transmission. These models have revealed differences between CWD prions from Norway and North America, as well as distinctive strain properties in Finland's moose CWD (Sun et al., 2023).

Bank voles and ferrets provide valuable information on interspecies transmission and strain adaptation of CWD prions. Bank voles are highly susceptible to various prion strains and exhibit short incubation periods, whereas ferrets offer insights into the potential risks to carnivores and other non-cervid species. In a study investigating the potential for CWD transmission to different wildlife species, four species of epidemic-sympatric rodents [meadow vole (*Microtus pennsylvanicus*), red-backed vole (*Myodes gapperi*), white-footed mouse (*Peromyscus leucopus*), deer mouse (*Peromyscus maniculatus*)] were intracerebrally inoculated with CWD prions. The efficient intracerebral transmission observed in all species, particularly blank voles, highlights their high experimental susceptibility to CWD prions and underscores their value as models for studying interspecies transmission and prion strain adaptation (Heisey et al., 2009).

Furthermore, fetuses of white-tailed deer from dams infected with CWD have been studied to explore the potential for mother-to-offspring transmission (Nalls et al., 2021). Non-human primates are essential models for assessing potential zoonotic risks and evaluating possibility of CWD transmission in humans. Two non-human primate species, cynomolgus macaques and squirrel monkeys, have been used as NHP models to assess CWD susceptibility (Race et al., 2014). Interestingly, squirrel monkeys showed a higher susceptibility to CWD than cynomolgus macaques, suggesting potential resistance in species that are evolutionarily closer to humans (Race et al., 2009).

Effects of Routes of Prion Exposure and Inoculation on CWD Pathogenesis

Various inoculation modalities are available to study CWD in mice, each providing different insights into pathogenesis, transmission, and host susceptibility. Each route used to inoculate an animal will initiate a different rate of transmission, the specificity of tissue tropism, and the ultimate progression of disease; thus, it has an impact on experimental designs and the applicability to future translational work.

One of the most commonly used experimental methods for CWD transmission is intracerebral (IC) inoculation, which directly introduces prions into the brain tissue. This highly invasive technique requires microsurgical precision and stereotaxic equipment. By bypassing peripheral immune barriers and avoiding the need for prion amplification in lymphoid tissues, IC inoculation places infectious material directly into the central nervous system (CNS), resulting in the shortest incubation periods of any known method, usually around 150–200 days in transgenic mouse models expressing cervid PrP.

Including examples of intracerebral CWD transmission in cattle and sheep provides context for the mouse data by illustrating that direct brain exposure can overcome natural species barriers. These cross-specific findings underscore that the intracerebral route is a powerful tool for revealing the fundamental capacity of CWD prions to infect diverse mammalian hosts, complementing the detailed observations made in the TgElkPrP mouse model. For example, cattle intracerebrally inoculated with CWD-infected brain homogenates from mule deer exhibited a gradual amplification of proteinase-resistant PrP (PrP^{res}) in various brain tissues in some subjects, with little or no evidence of neuropathological lesions associated with transmissible spongiform encephalopathies (Hamir et al., 2005). Similarly, intracerebral inoculation of sheep with CWD prions derived from mule deer resulted in clinical disease in a subset of sheep (Hamir et al., 2006). In the same model, inoculation of transgenic mice with CWD-derived homogenates intracerebrally resulted in clinical signs of disease in all mice that received the homogenate within a defined shortest incubation period of 180 days (Seelig et al., 2010).

Oral transmission has been established experimentally (Nichols et al., 2013). Contrasting with IC, oral inoculation mimics the way in which animals would naturally be exposed and results in longer and less consistent incubation periods in comparison to IC inoculation. This route entails directly administering CWD-infected brain homogenates to the mouth or esophagus, usually preceded by fast to maximize uptake. Oral transmission necessitates prion traversal across the gastrointestinal epithelium, amplification within gut-associated lymphoid tissues (GALT), and access to peripheral nerves to finally reach the CNS. Incubation times for oral inoculations to mice range from around 200 days to upwards of 400 days, depending on prion strain, dose, and genetics of host.

In oral inoculation studies, questions about the alimentary tract-associated lymphoid tissues suggest their importance as early sites of prion replication. PrP^{Sc}, when inoculated orally into mule deer fawns, was detected in alimentary tract-associated lymphoid tissues as early as 42 days post-inoculation (Sigurdson et al., 1999). This study indicates that lymphoid tissues draining the gastrointestinal tract may be important for entry and amplification of prions (Sigurdson et al., 1999). Thus, the efficient horizontal transmission, scored in relation to oral inoculation studies is aligned with free ranging cervids oral transmission patterns of prion disease, which has ecological relevance to this mode of transmission (Sigurdson et al., 1999).

Intravenous (IV) inoculation injects the infectious agent directly into circulation and is typically a lateral tail vein route; incubation times to clinical signs observed are intermediate relative to the IC or oral routes. Research indicates approximate incubation periods of 200 ± 7 days following an intravenous (IV) exposure (Seelig et al., 2010). This route bypasses mucosal barriers and delivers prions directly to secondary lymphoid tissues enabling research into hematogenous spread and contributions of peripheral tissues.

Intraperitoneal (IP) inoculation has been beneficial in studying tissue tropism and peripheral replication of CWD prions. In this route the inoculum is directly delivered to the peritoneal cavity, allowing an infected tissue systemic access to visceral lymphoid structures. Seelig et al. (2010) noted disseminated PrP^{Sc} accumulation was detected in the spleen and mesenteric lymph nodes of mice inoculated intraperitoneally with cervid-born CWD prions. Neuronal pathological changes appear later, as a secondary observation, following detection of prion deposition in the spinal cord and brainstem. Reported survival periods post-inoculation ranged from 220 - 330 days, and early prion propagation was predominantly detected in lymphoreticular tissue consistent with neuroinvasion taking place after peripheral inoculation.

Aerosolized exposures models closely mimic environmental routes of transmission and are critical in advancing understanding of prion infectivity by inhalation in the respiratory tract. In aerosolized models, mice are exposed to aerosolized CWD prions in a controlled chamber, and it is possible to ecologically control important parameters such as intranasal particle size, inoculation dose, and exposure period. Incubation times following aerosol inoculation of CWD prions are usually > 250 - 400 days. Denkers et al. (2012) demonstrated successful transmission of CWD to transgenic mice expressing cervid PrP, and it occurred via aerosol exposures, even at doses less than necessary for oral infection. Transmission efficiency was greater in animals with small mucosal injuries, even minor abrasions on the oral epithelium—showing that compromised mucosal barriers may present naked prion proteins (or infectious agents) with an increased opportunity to establish infection (Denkers et al., 2010). This is significant for environmental transmission risk and biosafety in that the inhalation of prion-laden particles, as might be encountered at mineral licks or in dust-laden environments, may be a feasible route of infection (Plummer et al., 2018). In addition, due to their relevance to scenarios of environmental transmission, routes of intranasal have also been researched. Most importantly, Denkers et al and Telling et al. (2010)

demonstrated a potential of aerosol exposure to induce disease in transgenic mice expressing cervid PrP. This adds to the potential for pathogenicity to be connected to inhalation of prions. Related, the clay-based intranasal delivery may mimic inhalation of contaminated dust and support the hypothesis that these environmental particulates could play a role in the spread of disease (Nichols et al., 2013).

Taken together, there is a continuing need to study the comparative efficiency, tissue targeting and environmental relevance of various inoculation routes. Each model provides a different way of consideration how prion enters the host organism, replicates, and spreads, and understanding this process is critical for surveillance, intervention and establishing biosafety practices under both experimental labs and wild conditions.

To further support an infectious respiratory exposure route, experimental intranasal inoculation has been conducted using brain homogenates mixed with clay particles. According to Nichols et al. (2013), intranasal exposure of white-tailed deer with these inoculations resulted in CWD, with PrP^{Sc} detected in several tissues via immunohistochemistry. This represents an inoculation method that simulates the natural inhalation of environmental particulates, including contaminated soil or dust and promotes the relevance of inhaled exposure conditions in field settings.

To summarize, experimental studies have advanced our understanding of CWD pathogenesis through regard to comparisons of inoculation routes. Oral exposure is the most ecologically relevant method of transmission, with intracerebral and intraperitoneal models allowing researchers to establish manipulative control for mechanistic studies.

Roles of Gut Microbiota in the Pathogenesis of Chronic Wasting Disease

The gut microbiota refers to the complex community of bacteria, archaea, viruses, and fungi that inhabit the gastrointestinal tract and play essential roles in host metabolism, immune function, and neuroimmune signalling (Thaiss et al., 2016; Sommer & Bäckhed, 2013). In this study of prion-infected mice, measurable changes occur in gut microbiota diversity and community composition. Prion-inoculated mice exhibit lower overall alpha diversity (within-sample diversity) during late-stage disease; however, beta diversity (between-sample community differences) diverges significantly even in the early stages of the disease (Losa et al., 2024). Scientists from the paper mentioned above utilized a murine scrapie prion disease model. Infected mice exhibited distinct differences in fecal microbiome composition for up to 12 weeks, preceding the onset of observable overt clinical symptoms, indicating a pre-symptomatic change in the microbial community. The variation in fecal microbiome composition continued to diverge in mid- to late-term disease, marked by prion-infected mice clustering apart from control mice during principal coordinate analyses of microbiomes. These results collectively suggested that prion disease generated a dysbiosis (an ecological disturbance in microorganisms), which was slow and progressed over time, consistent with the progressive course of the disease.

Relative abundance of one or more bacterial taxa has been observed in PrP^{Sc} infected mice. Specifically, some bacteria classified as opportunistic or inflammation-associated increase in abundance, while others decrease in abundance in groups associated with healthy gut conditions (Trichka & Zou, 2021). For example, prion-infected mice exhibited increased relative abundance of Proteobacteria, a phylum of many Gram-negative bacteria (such as *Escherichia* or *Helicobacter*) that may act as opportunistic pathogens or become more dominant during gut inflammation. An increase in Proteobacteria is the typical signature of gut dysbiosis across different diseases (Shin et al., 2015). In murine prion disease models, the relative abundance of the Helicobacteraceae family (which is categorized under

Proteobacteria) was characterized with increased relative abundance in infected mice compared to controls . An overall increase in the presence of *Helicobacter spp*. may reflect a prion-associated change in gut immunity or motility that allowed for the proliferation of this bacterium (Konturek, 2005). Firmicute families, specifically Lachnospiraceae and Ruminococcaceae, were found to be more abundant during the prion infection in mice. These families include members that produce short-chain fatty acids (SCFAs) (e.g., butyrate). Losa et al. (2024) found relative increases in Lachnospiraceae and Ruminococcaceae during symptomatic stages of disease in mice intracereberally inoculated with the Rocky Mountain Laboratory 6 (RML6) prion strain, suggesting a shift in microbes that ferment dietary fibres into SCFAs. They hypothesized that this could be associated with elevated SCFA levels in the gut during prion disease and could be impactful for the host's immune state. Further, the relative increase in abundance of Lachnospiraceae has been found in other neurodegenerative disorders including Parkinson's disease, suggesting similar microbial responses to pathophysiological neurodegeneration (Koutsokostas et al., 2024).

In association with these increases, mice infected with prions have shown decreases in those bacterial groups implicated in fibre degradation and gut health. For example, the family Prevotellaceae, which belong to the Bacteroidetes phylum, are often implicated in carbohydrate fermentation/anti-inflammatory activity, and were less abundant in the prion-infected mice compared to healthy controls (Yang et al., 2019). Additionally, studies have documented increased levels of Lactobacillaceae (family containing *Lactobacillus spp*.) in prion diseased mice. Lactobacilli are commonly regarded as probiotics that assist or maintain gut barrier function and their increase could be either a compensatory response or an effect of altered diets/intake in clinically ill animals (Dempsey & Corr, 2022). However, a rise in Lactobacillaceae might also alter the gut's producing more lactic acid; but the effects on prion pathogenesis are unknown.

The above downregulated taxonomic trends in mice are similar, at least to a certain degree, to findings seen in CWD-positive cervids. In a study involving wild and farmed CWD+ and CWD- white-tailed deer, the gut microbiota profiles in CWD+ deer were significantly different than in CWD- deer (Minich et al., 2021). In particular, CWD infection in deer is associated with an increase in the abundance of Akkermansia (a mucin degradation genus), an unclassified Lachnospiraceae UCG-010 genus, and RF39 group of bacteria (Li et al., 2022). Higher level of Akkermansia is associated with a mucosal layer thinning (it eats mucus) and has been observed in weight loss and metabolic stress, which might be related to wasting symptoms seen in CWD (Tingler & Engevik, 2025). The enrichment of Lachnospiraceae in deer and mice studies similarly suggests SCFA producing bacteria respond to prion infection. Collectively, the observed microbial changes that occur in prion disease either in the natural host or in mice models suggest dysbiosis characterized by an increase in certain Firmicutes and Proteobacteria in parallel with a decrease in some Bacteroidetes and other commensal bacteria. Importantly, these changes were not haphazard but likely driven by physiological changes that occur during prion disease (i.e., neurodegeneration influence gut function; differences in diet or motility in sick animals; or inflammation) and likely continue to influence disease processes.

In PrP^{Sc} infected mice, the altered microbiota is also accompanied by changes in microbial metabolic output. A detailed metabolomic analysis of fecal samples from mice infected with scrapie, a model of prion disease relevant to CWD, showed broad alterations in the metabolome (Yang et al., 2019). Of the total 145 fecal metabolites that differed between prion-infected mice and healthy mice, it was observed that 114 were lipid metabolites. In addition to prion infection, there were also decreases in metabolites believed to be protective, such as species of phosphatidylcholine in gut tissue of prion-infected mice, and increases in metabolites believed to be harmful, such as increases in secondary bile acids, with increases in four hydrophobic bile acids being statistically significant. It was also noteworthy that short-chain fatty acids (SCFAs) were decreased - all eight SCFAs (acetic acid, propionic acid, isobutyric acid, butyric acid,

isovaleric acid, valeric acid, isohexanoic acid, caproic acid) were decreased in prion-infected mice. SCFAs, such as acetate, propionate, and butyrate, are metabolites produced from the fermentation of fibre by gut bacteria and are essential for maintaining gut integrity and immune homeostasis. Decreases and changes in SCFAs could suggest less beneficial fermenters, or more likely an alternative fermentative state, during prion disease. The same study reported alterations in amino acids. Cysteine and tyrosine were increased while histidine, tryptophan and arginine, were decreased in prion-infected mice. The alterations in metabolism further show prion disease driven dysbiosis is much more than taxonomic anomaly, there physiological implications of the biochemical pathology occurring in the gut. Alterations in SCFA's, bile acids and amino acids, can have independent effector roles and are non-fibrous substrates of commensal gut bacteria that may influence inflammation and neurophysiology in health and disease (O'Riordan et al., 2025). For example, low butyrate could signify a compromised intestinal barrier and diminished anti-inflammatory signaling, while an increase in hydrophobic bile acids might facilitate gut permeability and local inflammation. This means that changes to the gut microbiome of CWD-inoculated mice could involve changes in community composition, richness and diversity and metabolic functionality that could all affect the host's disease pathology (Yang et al., 2020; (Recharla et al., 2023).

With these correlations in mind, a lingering question is how the gut microbiota may impact CWD prion infection and disease progression. M cells in the intestinal epithelium act as gatekeepers that transcytose luminal antigens (including prions) to the underlying lymphoid tissues. The intestinal microbiota are known to modulate the density and maturation of M-cells, which also potentially impact how easily prions transcytose through the gut (Donaldson et al., 2016). The association between increased M-cell density and increased prion transfer is clear: an experiment designed to enhance M-cell density in mice, through the administration of Receptor Activator of Nuclear factor Kappa-B Ligand (RANKL), produced substantially higher prion absorption from the gut and reduced survival time after exposure to an oral inoculation of prion (Kujala et al., 2011). Conversely, depletion of M-cells has the opposite effect. In an

experiment where RANKL-neutralizing antibody was administered to mice to eradicate M-cells, prions delivered by oral inoculation was inhibited (Donaldson et al., 2012). RANKL-generalized mice showed no early pre-productive accumulation of prions in their Peyer's patches and no neuro-invasion after prion exposure by mouth, defining the importance of M-cells for prion entry from the gut lumen to lymphoid tissue. These results suggest that any factor influencing M-cells may also influence prion susceptibility to CWD. The gut microbiota is a factor, as certain commensal microorganisms or their products are known to influence M-cell quantity. For example, gut inflammation (often from microbial dysregulation or infection) will generally facilitate M-cell density, which may be mediated by upregulated RANKL expression in the gut tissue. Furthermore, aging, or chronic exposure to microbial stimuli, results in elevated M-cell quantity. Thus, dysbiosis may be associated with low-grade intestinal inflammation and increased RANKL signalling, which would increase M-cell quantity, leading to increased efficacy to oral prion infections (eg, ingestions of CWD) (Takakura et al., 2011). Conversely, a healthy microbiome may support homeostatic immune signalling which may keep M-cells in floor thereby potentially reducing prion entry.

The gut microbiome is a pivotal factor in educating and regulating the mucosal immune system. Commensal bacteria induce gut-associated lymphoid tissues leading to IgA responses and modulate pro- and anti-inflammatory responses in the intestinal mucosa. The immune system could contribute to the spread of prion disease once an infection has developed in peripheral lymphoid tissues. For example, CWD prions are deposited in Peyer's patches after oral infection and then found in other lymphoid tissues, such as the spleen and lymph node, prior to neuroinvasion. The success of this process may depend, in part, on the immediate immune milieu. For example, microbiota that is skewed toward an anti-inflammatory response (e.g. Clostridia that induce regulatory T cells) may reduce the accumulation of prion in tissues through increased immune responses that contain the infection in gut-associated lymphoid tissues.

Alternatively, a dysbiotic community (e.g., enriched in pathogenic Proteobacteria) can result in chronic mucosal inflammation that could contribute to tight junction disruption, compromising the barrier function of the gut. Increased intestinal permeability (or "leaky gut") could allow prion disease to develop systemically, or at a minimum, increase exposure to prions in submucosal tissue. Additionally, we show that microbes can modulate the differentiation of follicular dendritic cells (FDC) in Peyer's patches, which are the cells that trap and support replication of prions. If the microbial community influences the maturation of FDC or the expression of PrPC, this could influence amplification of the prion in gut-associated lymphoid follicles. While direct evidence remains to be demonstrated *in vivo* models of CWD, it is reasonable to hypothesize that the gut barrier health and homeostasis of the mucosal immune "system" (partially microbiota-mediated) would make it less likely or systemic spread of infectious prions from the gut. On the other hand, microbiota-mediated immune dysregulation may induce more favorable or accelerate prion pathogenesis in the periphery. An example of this includes an expansion of Helicobacteraceae in prion-infected mice that could promote a well-cataloged inflammation pattern (Th1) in the gut, which would theoretically increase prion spread through the carrying of an immune cell with a prion or by cytokine or barrier rupture.

The gut microbiota produces a broad spectrum of metabolites that generally have robust effects on host physiology (beyond the gut), many of which are candidates in CWD. Potentially the most impactful are the short-chain fatty acids (SCFAs), as they are key energy substrates for colonocytes and are signaling molecules that modulate inflammation and possibly neurofunction. SCFAs may influence, or be influenced by, the progression and pathology of prion diseases. For example, butyrate is an SCFA that modulates inflammation, and promotes gut barrier function by energizing colonocytes; and thus, in a likewise, loss of butyrate production (and therefore a compromised gut barrier function) would be concomitant with a reduced level of butyrate if prion-infected mice elicit a higher level of systemic inflammation which might induce pathology while exacerbating potential neurodegenerative aspects of the disease .

Additionally, SCFAs can translocate into the bloodstream and cross the blood-brain barrier, potentially impacting microglia, the resident innate immune cells of the brain. Germ-free mice (and germ-free rats) showed microglia with disrupted structural and functional characteristics, likely due to the absence of SCFAs and other bacterial signals. While not definitively linked to prion disease, microglial activation and dysregulation may contribute to the neuroinflammatory and neurodegenerative aspects of the condition. Generally, if SCFA levels are adequate, they may help microglia maintain a homeostatic, anti-inflammatory state. Conversely, a deficiency or excess of SCFAs could trigger a dysregulated inflammatory response related to prion replication in the brain or spleen or potentially alter the host's inflammatory response (Erny et al., 2021). Lachnospiraceae, a bacterium highly involved in SCFA production, was found to be increased in later stages of prion disease in a different model (Yang et al. 2020). An overall rise in certain bacterial genera, such as Lachnospiraceae, was abnormally elevated at levels that might activate an SCFA surge, leading to context-dependent changes that could either promote or hinder host protein responses. Additionally, other metabolites tested in earlier models, like bile acids, were produced directly or indirectly through microbiome changes. These metabolites can activate receptors (such as TGR5 or FXR), which have the potential to influence gut motility and barrier function, thereby impacting systemic inflammatory responses (Wahlström et al., 2016). The increased production of secondary bile acids in prion-infected mice could also augment a significantly altered inflammatory response in the gut and possibly affect liver function, ultimately influencing prion clearance or toxicity.

The gut microbiota can interface with the central nervous system through either the gut-brain-axis, special neural pathways (the vagus nerve), immune signalling and microbial mediators, etc. In relation to prion pathology, it is plausible that direct neuroinflammation occurs in brains of individuals infected due to activated microglial and astrocyte communication by way of cytokines - and furthermore other inflammatory mediators. Therefore, a pro-inflammatory gut microbiome could potentially induce neuroinflammation by varying degrees depending on the extensive capacity to essentially "prime" the

CNS to respond (protectively or not) to anything it may encounter. For example, lipopolysaccharide (LPS) that comes from Gram-negative bacteria (such as Enterobacteriaceae family and α-proteobacteria) is a significant endotoxin (or bacterial substance) that when translocated to circulation (e.g., via a leaky gut or dysbiosis), and excessive amounts causes systemic inflammation and microglial activation, resulting in neuro-inflammation in the brain. A feed-forward loop is a possibility in neurodegenerative diseases. For example, pathology from prion infection in the brain may impact gut physiology physiologically or through hormonal pathways, ultimately resulting in dysbiosis. The dysbiosis provides the signals amplifying the neuro-inflammation that has already been elicited. In prion-infected mice of a prior study, there was no disease augmentation in the absence of microbes, indicating that there is still dynamic composition, and a significant microbiome dynamic and metabolic composition was noted. This possibly suggests a bidirectional component: that the prion pathology from the brain affects the gut microbiome and/or vice-versa which contributes to modulation of the neuro-inflammation. Mechanistically, the vagus nerve provides a pathway of communication. Prion diseases theoretically have pathology in consecutive areas of the brainstem where the vagal nuclei are. Innate gut signals can travel vagally to the brain from the inflamed gut or there could be impaction in the vagal signaling, due to prion pathology, to impact gut function (i.e. motility and secretion) creating disturbance in microbial habitats. There are also bacterial products [for example, associated with gamma-aminobutyric acid (GABA] that will travel, potential cross-seed or provide something to amplify the likely misfolded host protein (i.e. bacterial amyloids like curli proteins with E. coli). Although there are no direct experiments proving the concept for PrP, it has been documented for other neurodegenerative disorders, such as several models of Parkinson's disease, where bacterial amyloid has been shown to drive α-synuclein aggregation in both the gut and brain (Chen et al., 2016). By analogy, one might theorize that more chronic exposure to microbial amyloids or even endotoxins would impact either the rate (or pattern) of prion aggregation or microglial activation phenotypes in CWD.

Investigators have begun testing the ideas mentioned above, in regard to hypotheses via experimental interventions in mouse models. While the results are questionable, they indicate that the role of microbiota is significant, but likely not just an on/off effect, but one of its influences being context-dependent/modulatory effect. An approach to test causality is to fully deplete the microbiota and see whether prion disease outcomes change. To this end, Bradford et al. (2017) conducted such experiments by infecting germ-free mice (that for prions involved the use of mouse-passaged scrapie prions) with prions and comparing the disease course to conventionally raised mice. Notably, there were no differences in clinical disease onset or survival times between germ-free and conventionally raised mice. Germ-free mice affected by both intraperitoneal and intracerebral prion inoculations developed the disease in a similar time frame as standard mice, and the associated neuropathological features (PrPSc deposition, spongiform change) were comparable between groups. Collectively, results from these studies suggest that a commensal microbiota is not required for prion replication or the development of PrP pathology in the tested models. Prion disease can develop similarly in mice devoid of gut microbes. However, this does not mean that microbiota do not have any effects on the disease, but that the effects may be context-dependent, or potentially subtle (affecting the oral route of infection as well as brain invasion situations). Interestingly, earlier studies had shown some different outcomes with regard to microbiota studies in mice and prions. For instance, a study in the 1980s reported that germ-free mice survived longer than conventional mice infected intracerebrally with prions, which was suggested to be due to impairment of microglial activation in germ free mice. In another report, germ-free mice survived significantly longer only in situations where prions were infected peripherally, not intracerebrally. Given that the same pathogen was used, these differences in Montana model studies could be explained by differences in prion strains, mouse genetic background or microbiota status (germ-free, antibiotic free, specific pathogen-free). Overall, based on the germ-free studies above, it appears that while microbiota are not a make-or-break aspect of prion disease initiation/development, they can modulate aspects of

the disease process under certain conditions (especially during/after peripheral infection and during neuroinvasion).

Several researchers have monitored microbiome changes naturally as prion disease progresses (not modelling them) in parallel to germ-free studies. For example, Losa et al. (2024) published a longitudinal fecal sequencing project with mice inoculated with RML prions. The authors note the microbiome of prion-infected mice differed significantly from controls, in the weeks leading up to symptom onset, with perturbations observed prior to the appearance of clinical signs, and significant beta diversity changes prior to clinical signs. Furthermore, the authors suggest these findings indicate that changes observed in the microbiome may occur in response to the disease and may be used as an indicator of prion disease onset. The authors report that, as it relates to microbial taxa (increase SCFA-producers, etc.), the changes were small in absolute abundance, but consistent, as related to perturbations in the microbiome. The authors suggest that the observed changes in the microbiome were "limited to a number of taxa as opposed to major compositional shifts". While some taxa were depleted or increased over time, the changes were easier to observe when viewing dissimilarity to the community rather than raw counts. These findings suggest prion diseases likely displace keystone species (or functional groups) of the microbiome instead of remapping the gut community. Furthermore, a "temporal microbiome signature" in prion disease suggests that the microbiota is responding in real time as prion disease is ongoing and could be utilized as a biomarker for stages of (or timing) of prion disease in animal models.

If the gut microbiome is indeed contributing to the pathogenesis of prion disease, the gut microbiome could potentially be targeted to modify the course outcome of the disease. Along with germ-free studies, consideration of use of antibiotics or probiotics could potentially be other options to modify gut flora. There is some evidence to suggest that some antibiotics may slow the course of prion disease. Notably, as an antibiotic, doxycycline affects the gut microbiome (and favors inhibition of bacterial protein

synthesis). While doxycycline may be acting independently of a microbiome-mediated benefit, that possibility cannot be ruled out. Trichka and Zou (2021) note that the successful testing of doxycycline in preclinical prion models and even clinical studies emphasizes the "relevance and involvement of the microbiome in prion pathology." In other words, gut microbiota might be one downstream target/direction through which doxycycline exerts its benefit (for example, by inhibiting pro-inflammatory gut microbes or by ameliorating bacteria-induced neuroinflammation). As of now (to our knowledge), no studies published have used probiotics or fecal transplants (Bokoliya et al., 2021) to alter the course of prion disease, although the potential is on the horizon. While other neurodegenerative disease models (like Alzheimer's and Parkinson's) have been shown to modify the disease course by altering the microbiome (e.g., fecal microbiota transplants form healthy mice donors modify the Alzheimer's pathology in mouse models), it is certainly plausible to predict such approaches with prion disease as well (Wang et al., 2022). In fact, a recent review suggested more consideration of microbiota-based therapeutic modalities for alleviating neuroinflammation in prion and prion-like diseases.

Emerging evidence supports a close link between CWD and gut microbial dynamics. Indirect biomarkers of prion infection may be detectable in fecal microbiota, allowing non-invasive diagnostic approaches. For example, Minich et al. (2021) found CWD-positive deer had increased abundance of taxa such as *Akkermansia*, suggesting that reproducible microbial signatures could indicate infection status and may contribute to disease pathogenesis rather than being incidental. Extending this concept to experimental models, Didier et al. (2024) reported coordinated changes in both microbial and metabolic communities in CWD-infected mice prior to the onset of clinical signs, proposing a panel of microbial features as an early infection signature. In a related longitudinal study, Losa et al. (2024) used 16S rRNA sequencing of fecal samples from mice intracerebrally inoculated with mouse-adapted CWD/scrapie prions and observed pronounced shifts in microbiota at mid- to late stages. These included enrichment of Lachnospiraceae, Ruminococcaceae, and the fibre-degrading Muribaculaceae family, along with

significant beta-diversity differences between infected and control mice, even as alpha-diversity measures remained relatively stable. Together, these studies highlight the promise of defining a reproducible "microbiomic signature" of CWD that reflects both compositional and functional alterations of the gut microbiome and could ultimately support early detection and deepen understanding of prion–microbiota interactions.

The context of studies with CWD-affected deer should help frame future study findings, including a recently published field study that assessed the fecal microbiomes of cervids naturally infected with CWD, confirming the approximate measures referred to in earlier studies with mice. In summary, Minich et al. (2021) observed greater relative abundances of Akkermansia, Lachnospiraceae UCG-010, and FIR39 (Mollicutes) in CWD-positive white-tailed deer compared to healthy controls (Delgado et al., 2017). They observed community-wide differences in gut microbiota that were associated with CWD status, sex, and geographic location within the sampled individuals. Greater bacterial diversity was exhibited, along with differences in community structure in CWD-affected deer (Minich et al., 2021). Moreover, Didier et al. (2024) found differences in microbiomes between CWD-negative and CWD-positive deer from somewhat disconnected locations; over 90 taxa were different, while CWD status was consistent between the groups. The same differences in CWD infection were observed between Firmicutes and Actinobacteria, consistently showing sufficient discriminatory accuracy (70%) in classifying prion infection status via machine learning. Differences in microbiomes observed between CWD-affected and non-CWD-infected deer suggest microbiota could be non-invasive biomarkers of CWD. In addition, the observations of dysbiotic gut microbiomes in association with prion infections were not just the conclusions of studies using mouse subjects. Similarities in dysbiosis between prion-infected mice and deer suggest that prion infection can produce similar outcomes of gut dysbiosis, regardless of the taxon; however, it is challenging to attribute causation associations in wild populations.

In summary, there is strong experimental evidence affirming that the gut microbiota is affected by prion diseases and can, in turn, influence disease outcomes to some degree. Germ-free experiments demonstrate that prion disease can occur in the absence of microbes, and evidence suggests that microbes can influence the time to disease onset and severity, depending on various factors. Mouse models allow simultaneous monitoring of prion disease progression and associated changes in the gut microbiome. Manipulating the microbiome – for example through targeted antimicrobial or probiotic treatments- has been proposed as a way to delay or modulate prion replication and disease course. Although published findings are not completely consistent likely reflecting differences in prion strain, host genotype, or baseline microbial communities across facilities, most studies converge on the conclusion that gut bacteria exert a role on prion pathogenesis.

The Use of Real-Time Quaking-Induced Conversion for Investigating Chronic Wasting Disease

Real-time quaking-induced conversion (RT-QuIC) is an ultrasensitive assay that detects pathological aggregates of misfolded prion proteins in biospecimens (Figure 2). It was developed as a diagnostic assay for multiple neurodegenerative diseases, particularly prion diseases, including Creutzfeldt-Jakob disease (CJD). In the RT-QuIC system, the mixture of a recombinant prion protein (recPrP) and thioflavin T (THT) dye initiates a rapid conformational change to amyloid which can be excited and measured in real time (Peden et al., 2012).

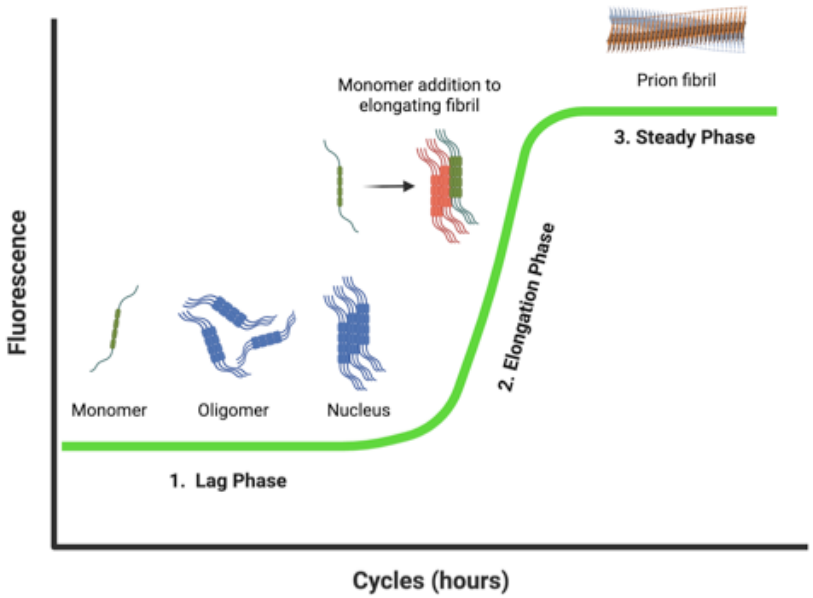

Figure 2. A schematic diagram showing the nucleation-dependent polymerization model of amyloid fibril formation. During the lag phase (nucleation), monomeric forms of the amyloid-forming peptides self-aggregate into soluble oligomers (including disordered oligomers, B-barrels, and bilayer b-sheets) and nuclei. During the elongation phase, the nucleus is extended rapidly and grows into fibrils. Then, fibrilation reaches a stage called the steady phase. Aggregation processes produce a sigmoidal kinetic curve (green) that is depicted in the figure.

RT-QuIC has impressive sensitivity and specificity for diagnosis of prion diseases. In fact, RT-QuIC demonstrated 85% sensitivity and 99% specificity in diagnosing prion diseases from cerebral spina fluid (CSF) samples (Cramm et al., 2015). RT-QuIC is being adapted to identify other misfolded proteins in neurodegenerative diseases such as, alpha-synuclein in Parkinson's disease, dementia with Lewy bodies, or tau in Alzheimer’s disease and other tauopathies (Fairfoul et al., 2016; Tennant et al., 2020).

RT-QuIC provides an opportunity for early and precise diagnosis. The assay has shown promise in detecting prion-seeding activity in various tissues including CSF and skin samples (Baranová et al., 2024; Mammana et al., 2020). Developing technologies such as Nanoparticle-enhanced Quaking-induced Conversion (nano-QuIC) have further augmented sensitivity and allowed application to more matrix accessible sample types such as blood plasma (Christenson et al., 2024). This innovation has the potential

to facilitate non-invasive, blood-based testing for early identification and management of neurodegenerative diseases, including prion disease.

RT-QuIC is routinely thought to be faster, more sensitive, and more specific than protein misfolding cyclic amplification (PMCA) in the detection of prions (Peden et al., 2012). RT-QuIC utilizes recombinant prion protein as a substrate and employs shaking cycles during the misfolding process, whereas Protein Misfolding Cyclic Amplification (PMCA) utilizes sonication (Schmitz et al., 2016). RT-QuIC enables real-time monitoring of amyloid formation and thioflavin T fluorescence, allowing for high-throughput analysis (Orrú et al., 2012; Schmitz et al., 2016). In terms of sensitivity, RT-QuIC has been shown to be at least 10,000 times more sensitive than conventional methods, including enzyme-linked immunosorbent assay (ELISA) and Western blotting for the detection of scrapie in goat brain samples (Dassanayake et al., 2015).

Interestingly, despite their similarities, RT-QuIC and PMCA may differ in important aspects of performance when identifying specific prion strains. For example, RT-QuIC was reported to be less efficient in detecting abnormal PrP associated with variant CJD compared to PMCA under the same conditions (Peden et al., 2012). Both RT-QuIC and PMCA have been modified to detect α-synuclein aggregates in synucleinopathies, such as in Parkinson's disease, with high sensitivity and specificity, even in pre-clinical stages (Grossauer et al., 2023; Paciotti et al., 2018). Overall, while both RT-QuIC and PMCA techniques are valuable, RT-QuIC seems to offer many advantages of speed, sensitivity, and ease of use for many applications within prion and protein misfolding research.

RT-QuIC is still undergoing validation and comparison to established diagnostic tests. While it has demonstrated high sensitivity and specificity in the detection of CWD prions, it is currently being evaluated against the existing gold standard testing methods, including ELISA and immunohistochemistry (IHC) (Holz

et al., 2022). The USDA has not fully approved RT-QuIC testing for routine CWD diagnostic testing because of challenges for federal approval regarding practical validation aspects (Darish et al., 2024).

There are several contradictions and interesting facts regarding some aspects of RT-QuIC's performance. Though it has presented high sensitivity in some test studies, there have been reports of modest sensitivity and negative predictive values (Bryant et al., 2025). The performance of the assay also varies depending on the sample type and location. For example, ear pinna punches and third eyelids may be conveniently collected samples for RT-QuIC testing, but the diagnostic ability of each location may vary (Cooper et al., 2019; Ferreira et al., 2021) which may be due to the fact that different tissues may have different levels of prions.

In summary, although RT-QuIC represents a robust method for detection of CWD, including the ability to detect prions in various tissues and bodily fluids (Cooper et al., 2019; Ferreira et al., 2021; Henderson et al., 2013), it is not fully utilized within the established routine diagnostic protocols and processes. Additional research studies and multi-laboratory validations are addressing the remaining uncertainty regarding variability, analytical sensitivity and specificity (Holz et al., 2022). As these efforts continue and progress is reported, acceptance and implementation for RT-QuIC may become a viable diagnostic test for CWD.

Hypothesis and Objectives

Prion diseases are infectious, lethal neurodegenerative disorders that arise from the misfolding of the cellular prion protein (PrP^{C}) to its pathogenic form, PrP^{Sc}. Chronic Wasting Disease (CWD), which is a prion disease that primarily affects cervid species, has been documented to spread more frequently through

North America, and to parts of Asia and Europe, and is a considerable ecological, economic and public health concern (USGS, 2025; Osterholm et al., 2019). CWD has been primarily studied as a transmissible neurological disease. The disease agent, PrP^{Sc}, mainly enters through the digestive system, seed and replicates in intestinal lymphoid tissues, and spreads to the central nervous system (CNS). Recent studies are beginning to uncover the role that gut microbiota may play a role in disease susceptibility and progression (Minich et al., 2021). Some microbial groups may actually influence the misfolding of prion proteins and may alter their seeding and accumulation in the host tissues, including brain, spinal cord, lymphoid tissues, salivary glands, muscle and excretory organs (Hoover et al. 2017). Although CWD prions interact with the immune cells and exploit lymphoid tissues, they generally do not elicit a classical inflammatory or adaptive immune response; immune involvement is largely permissive rather than protective (Mabbott et al., 2020). While these recent studies are only in their infancy, they open new frontiers for understanding CWD. They also may lead to more effective prevention, diagnostic, and treatment applications related to CWD. However, the influence of inoculation routes on prion seeding activity, amplification and tissue distribution in animals is still largely unexploited. In addition, the mechanisms that lead to the effect of microbiota change on prion disease etiology are currently not well understood. This thesis hypothesizes that intracerebral (IC) inoculation would result in earlier and more uniform prion seeding and disease progression compared to intragastric (IG) inoculation, due to the direct introduction of prions into the central nervous system. In contrast, IG inoculation was expected to produce delayed and more heterogeneous prion seeding, reflecting biological barriers associated with gastrointestinal uptake and peripheral neuroinvasion. The primary objective of this thesis is to determine how the routes of prion inoculation influence chronic wasting disease (CWD) prion seeding dynamics and tissue distribution in TgElkPrP transgenic mice. This will be accomplished by systematically quantifying prion seeding activity in brain, spleen, and small-intestine tissues using Real-Time Quaking-Induced Conversion (RT-QuIC) and confirming deposition with immunohistochemistry. A second objective is to

characterize changes in the gut microbiome and evaluate their association with prion seeding activity and disease progression in this model.

Together, these objectives are designed to generate mechanistic insights into the interplay between inoculation routes, tissue-specific prion amplification, and microbiome composition, thereby informing future approaches to CWD surveillance and management.

Materials and Methods

Study Design

A total of 96 TgElkPrP mice were included in this study. Mice were divided into intragastric (IG) and intracerebral (IC) inoculation groups. The IG cohort consisted of n = [36] mice, sampled at 40 [n = 12 (6 Male + 6 Female)], 48 [n = 12 (6M+6F)], and 56 [n = 12 (6M+6F)] weeks post-inoculation (WPI). The IC cohort consisted of n = [60] mice, sampled at 8 [n = 12 (6M+6F)], 12 [n = 12 (6M+6F)], 16 [n = 12 (6M+6F)], 20 [n = 12 (6M+6F)], and 24 [n = 12 (6M+6F)] WPI. Both male and female mice were included in each group. Experiments started by studying transgenic ELK-PrP mice inoculated with 50 µL of 10% (w/v) white-tailed deer (WTD) brain homogenate positive for CWD using two methods: intragastric (IG) and intracerebral (IC) (Figure 3). All TgElkPrP mice were inoculated at 6–8 weeks of age. Age-matched male and female mice were used across all experimental and control groups to minimize age-related variability in prion susceptibility. Each group included 6–8 mice (both male and female mice) and an equal number of age-matched controls, which received 50 µL of 10% WTD brain homogenate prepared from CWD-negative deer. For IG inoculations, the 50 µL dose was administered by oral gavage directly into the stomach. For IC inoculations, 50 µL of the same 10% homogenate was injected into the right parietal cortex at the caudate-putamen area using a Hamilton syringe and stereotaxic guidance. The remaining 20-µL was deposited along the needle track to ensure even exposure. The study was designed as a time-

course investigation to evaluate prion seeding activity and disease progression after exposure via these routes. The intragastric (IG) group included three time-course cohorts (IG 40, IG 48, and IG 56), representing animals examined at 40, 48, and 56 weeks post-inoculation (WPI). The intracerebral (IC) group comprised five cohorts (IC 8, IC 12, IC 16, IC 20, and IC 24), representing animals examined at 8, 12, 16, 20, and 24 WPI, respectively. Each cohort corresponds to a specific interval between inoculation and necropsy, allowing comparison of prion replication and tissue involvement across different incubation stages and between inoculation routes. Animals were monitored longitudinally and euthanized either at predefined experimental time points (IC: 8, 12, 16, 20, 24 WPI; IG: 40, 48, 56 WPI) or earlier if humane endpoints were reached due to progressive neurological disease. No spontaneous mortality occurred prior to euthanasia; thus, time of euthanasia reflects time post-inoculation at terminal disease stages. Phenotypic scoring was based on the presence and progression of established prion-associated clinical signs, including ataxia, tremors, kyphosis, slowed movement, tail rigidity, and hyper-responsiveness. Animals exhibiting two or more neurological signs within a short interval were considered symptomatic and closely monitored until euthanasia. Mouse fecal pellets were collected every 4 weeks in the IC group and every 8 weeks in the IG group, then stored at −80 °C for later microbiome DNA extraction and sequencing.

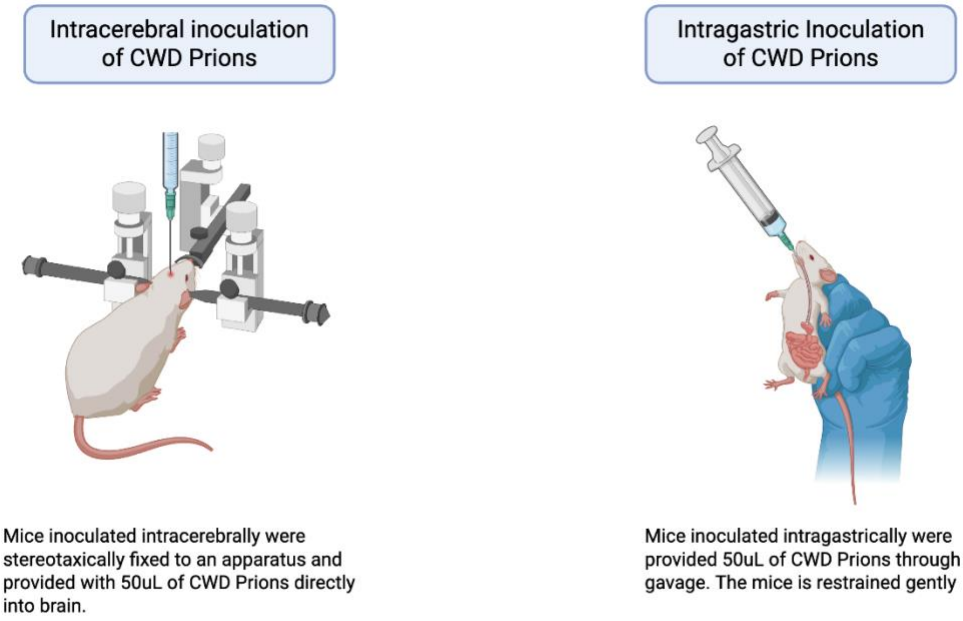

Figure 3. Intracerebral and intragastric inoculation of CWD prions.
Schematic representation of two inoculation routes used in this study. Intracereberal (IC) inoculation was performed by stereotaxic injection of 50uL of CWD Prions directly into the brain. Intragastric (IG) inoculation was performed by oral gavage, where 50uL of 10% +CWD brain homogenate was delivered directly into the stomach while the mouse is gently restrained.

The clinical symptoms used to assess the mouse CWD model include ataxia, tremors, head bobbing, kyphosis, paralysis, hyper-responsiveness, tail rigidity, and slowed movements. Medical manifestations, such as weight loss, rough/dull haircoat, abdominal distension, rectal/genital prolapse, and ocular abnormalities, were noted once a week by technicians working in the Small Animal Colony of CFIA. Mice presenting two or three neurological symptoms within 3-20 days suggest the development of prion disease. In cases where animals reached humane endpoints or died before scheduled necropsy, the time post-inoculation at death was recorded and used descriptively. Once the mice reached their designated end point or ready for euthanization due to disease advancements, they were anesthetized using isoflurane, and CO_2 asphyxiated to ensure euthanization, and the tissues were harvested and divided into portions for placement in both 1.7mL centrifuge tube for preservation in a -80°C freezer for RT-QuIC

analysis and in formalin jars for later detection of PrPSc positivity through immunohistochemical (IHC) analysis (found below). The harvested tissues included the brain, spleen, mesenteric lymph nodes, colon, small intestine, fecal pellets, skin, ear, cecum, and cecum content.

RT-QuIC: Buffers and reagents were prepared freshly or verified for expiration prior to each run. All solutions were filter-sterilized through 0.22 μm membranes. A 0.05% (w/v) Sodium dodecyl sulfate (SDS) working solution was prepared by diluting 1% SDS stock into distilled water. Sodium phosphate buffer (Na_3PO_4) was formulated by combining monobasic (NaH_2PO_4) and dibasic (Na_2HPO_4) stocks to achieve a final concentration of 50 mM (pH 7.3-7.4), and 300 mM sodium chloride (NaCl) was added to this buffer. A 1 mM Ethylenediaminetetraacetic acid (EDTA) solution was prepared by diluting a 100 mM Ethylenediaminetetraacetic acid (EDTA) stock solution. Thioflavin T (ThT) stock solution (10 mM) was prepared by dissolving ThT powder in distilled water, followed by filtration and protection from light. A 500 μM ThT working solution was generated by diluting the stock solution immediately before use. The RT-QuIC reaction solution was prepared using commercially available truncated Syrian hamster recombinant prion protein (recPrP) AA-90–231 (0.1 mg/mL, MNPROtein, Priogen Corp., St. Paul, MN), which was stored at –80 °C and cleared of aggregates by centrifugal filtration (0.2 μm MWCO; Millipore Sigma) at 8,600 rpm for 4 minutes at 4 °C.

For each RT-QuIC reaction, a master mix was prepared to contain final concentrations of 50 mM sodium phosphate, 300 mM NaCl, 1 mM EDTA, 10 μM ThT, and 0.1 mg/mL MNPROtein. Brain and spleen homogenates 19% (w/v) were thawed (as described below) and serially diluted 10-fold in 0.05% SDS to a dilution of 10^{-4} w/v. Using reverse-pipetting, 95 μL of master mix was dispensed into each well in a black-walled, clear-bottom 96-well plate, followed by 5 μL of the diluted tissue homogenate. Negative control wells received either 5 μL of 0.05% SDS or 5 μL of negative tissue homogenate. Positive controls received

previously validated prion-positive material diluted to an equivalent concentration. Plates were sealed with optically clear seals to minimize evaporation and were immediately transferred to a fluorescence plate reader (BMG FLUOstar Omega), which was incubated at 42 °C (Figure 4).

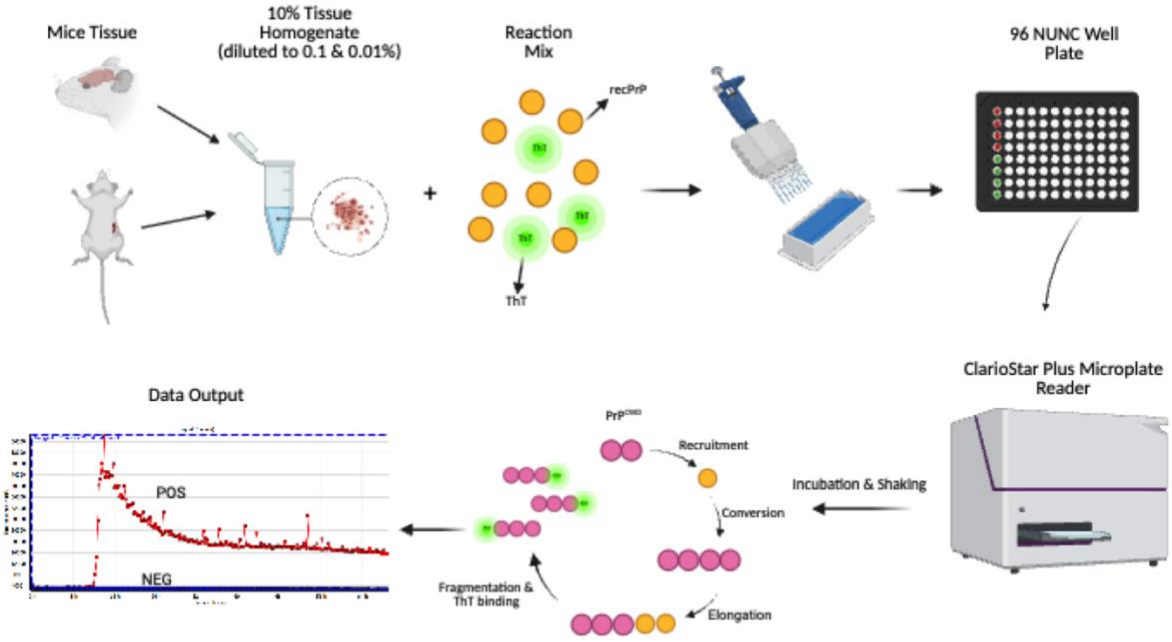

Figure 4. RT-QuIC assay workflow for prion detection
Diagram depicting the RT-QuIC amplification assay. Mouse tissues were homogenized and diluted (0.1 & 0.01%) before being added to a reaction mix containing recombinant prion protein (recPrP) and Thioflavin T(ThT). Samples were incubated in a 96-well plate and subjected to cycles of shaking and incubation in a ClarioStar Plus Plate Reader. Positive samples were identified by an increase in ThT fluorescence that passed the threshold specific to the tissue being tested.

RT-QuIC kinetics were monitored using bottom-read optics (excitation 450 nm, emission 480 nm, gain = 1,000). Each cycle consisted of 60 seconds of double-orbital shaking at 700 rpm, followed by 60 seconds of rest, and then a fluorescence read (20 flashes, 20 µs integration time). Fluorescence measurements were taken every 15 minutes for up to 60 hours or until positive control wells reached a stable plateau (Figure 4). Cycle threshold was defined as the time when the thioflavin T (ThT) signal of a reaction exceeded T_{stdev}, which was calculated as the average baseline (all readings from the fourth cycle) of all reactions in relative fluorescence units (RFU) plus 10 standard deviations. Using an R script, the time at which each replicate's ThT signal surpassed this threshold was recorded in hours. If a well did not cross the tissue-specific threshold (brain Ct=33 hr, spleen Ct=30 hr, small intestine Ct=28 hr), it was marked as

‘Negative’ or as Ct=60. The script in RStudio also calculated and reported the baseline, standard deviation, and threshold values for each RT-QuIC run in RFU. A tissue sample is considered CWD ‘+’ if all four technical replicates (4/4) crossed the tissue-specific thresholds listed above. If none of the four replicates crossed the threshold within 60 hours, the sample was classified as CWD ‘-‘. If one to three replicates tested positive, the sample was re-run in quadruplicates to obtain an eight-replicate format; in that case, at least half of the replicates (i.e., ≥4/8) needed to exceed the threshold for the tissue to be classified as CWD-positive. All negative control wells remained below the threshold throughout the test.

Data exported from MARS (both "Microplate View" and "Signal Curve" reports) were analyzed using Microsoft Excel. The fluorescence curves were plotted against time to visualize seeding kinetics and confirm reproducibility across replicates. Throughout the protocol, the reagent pH was verified daily (target range: 7.2–7.4), and any recPrP preparations that exhibited visible aggregates post-filtration were discarded. Negative-control wells and positive controls were interleaved across each plate to detect potential cross-contamination or instrument artifacts. By following this standardized RT-QuIC protocol, sensitive and reproducible detection of prion seeding activity in mouse brain and spleen tissues was achieved, consistent with institutional guidelines for prion research.

RT-QuIC Assay Preparation for Brain, Spleen and Small Intestine Tissues:

Each of brain and spleen was bisected sagittally; one hemisphere (or half of the spleen) was formalin-fixed, reserved for histopathology for downstream analysis, while the remaining half was allocated for RT-QuIC. Tissue designated for seeding was weighed and homogenized to a 10% (w/v) suspension in Phosphate Buffered Saline (PBS; pH 7.3-7.4) using the BioRad TeSeE Purification Kit Tubes placed in the Percellys 24 Tissue Homogenizer (Paris, France). Homogenates were centrifuged at 2,000 × g for 2 minutes at 4 °C to remove large debris; supernatants were collected and stored at –20 °C until use.

For small Intestine, upon homogenate preparation, the tissue designated for seeding was weighed and placed into a 1.7-mL centrifuge tube containing 1-mL BioRad homogenization buffer. Tissues underwent three brief vortex pulses to remove surface contaminants and particulates. Each sample was then weighed and noted to determine the amount of each reagent required to complete a 10% homogenate. Subsequently, tissues were transferred into BioRad TeSeE Purification Kit Tubes, and homogenization buffer supplemented with 2% $CaCl_2$, 1X PBS (pH 7.4), and Collagenase A [10103578001, Sigma-Aldrich, 100mg, 1mg/mL (0.1%, w/v)] was added to prepare a 10% (w/v) homogenate. Homogenization was performed using the Percellys 24 Tissue Homogenizer at maximum speed (5600 rpm) for six 30-second pulses, totalling 3 minutes. Homogenates were then incubated overnight at 37 °C with agitation at 650 rpm in a Fisher Scientific Thermomixer. Post-incubation, samples underwent an additional 1-minute homogenization pulse. Homogenates were centrifuged at 2,000 × g for 2 minutes at 4 °C to remove large debris, and supernatants were collected carefully to avoid disturbing the dense tissue layer at the tube's surface. If accidental disruption occurred, a re-centrifugation step was performed. Supernatants were aliquoted and stored at –20 °C until use.

DNA Extraction

Microbial DNA was extracted from mouse fecal pellets using a NucleoSpin Soil kit (Macherey-Nagel) according to the manufacturer's protocol, with minor modifications made to optimize yield and purity. One fecal pellet per sample was placed into a NucleoSpin Bead Tube Type A containing ceramic beads, followed by the addition of 700 µL of Lysis Buffer and 150 µL of SL2. 150 µL of Enhancer SX buffer was added to facilitate efficient cell disruption. Tubes were attached vertically to a homogenizer (Percellys 24 tissue homogenizer) and agitated at maximum speed for 5 min at room temperature to achieve mechanical lysis, ensuring thorough homogenization without generating excessive heat. After lysis, the

samples were centrifuged at 11,000 × g for 2 min to remove foam, and 150 µL of Lysis Buffer SL3 was added to precipitate proteins and other contaminants. The mixture was vortexed briefly, incubated in a fridge (4 °C) for 5 min, and then centrifuged again at 11,000 × g for 1 min. The clear supernatant was transferred to a fresh 2-mL collection tube and loaded onto a NucleoSpin Inhibitor Removal Column (red ring) to eliminate humic substances and other PCR inhibitors. The columns were centrifuged at 11,000 × g for 1 min, and the flow-through was retained. To adjust binding conditions, 250 µL of Binding Buffer SB was added to the inhibitor-free lysate, mixed by brief vertexing, and the entire mixture was applied to a NucleoSpin Soil Column (green ring) in a two-step loading process (550 µL per spin), each followed by centrifugation at 11,000 × g for 1 min. The silica membrane was then washed sequentially with 500 µL of SB, 550 µL of Wash Buffer SW1, and two rounds of 700 µL Wash Buffer SW2 (each wash consisting of a 2-s vortex and 11,000 × g spin for 30 s) to remove residual contaminants. A final centrifugation at 11,000 × g for 2 min ensured complete drying of the membrane. DNA was eluted by placing the column into a new microcentrifuge tube, adding 50 µL of prewarmed Elution Buffer SE (5 mM Tris-HCl, pH 8.5) directly onto the membrane, incubating for 1 minute at room temperature, and then centrifuging at 11,000 × g for 30 seconds. Eluate quality and concentration were evaluated by Nanodrop ND-1000 spectrophotometry (A_{260}/A_{280} and A_{260}/A_{230} ratios).

RT-QuIc Testing of DNA cleanness from CWD prion for 16S rRNA sequencing

After testing brains and spleens of intragastrically and intracerebrally inoculated mice, fecal samples from the mice were collected and examined to determine their suitability for 16S ribosomal RNA sequencing. Given that the samples were tested in a level 2 containment facility, it must be assessed whether removing prion-contaminated tissues from the containment is sufficiently safe to perform 16S rRNA sequencing. To determine this, DNA was extracted from fecal samples of mice from the IG groups (control and infected), including the four mice inoculated intragastrically, and tested by RT-QuIC to verify whether any prion

remained in the samples. By evaluating the safety of removing prion-contaminated tissues from the containment, I can expand the range of analytical techniques available for studying CWD while maintaining strict biosafety protocols.

To prepare the sample before running RT-QuIC, DNA was extracted from the fecal pellets using the Nucleospin Soil Kit (Macherey-Nagel GmbH & Co. KG, Düren, Germany; Cat. No. 740780.50). 100 µL of the elution buffer was used to elute 100 µL of DNA. The DNA was then prepared in a 1:19 ratio of 1.5 µL of DNA (18.5 µL of 0.1% SDS. This ratio provided the best result, avoiding any inhibition from other reagents that could interfere with signal DNA preparation and ensuring maximum signal detection while minimizing potential interference from other reagents. This carefully calibrated mixture yielded precise and reliable results for subsequent analysis. This step enables high-throughput profiling of bacterial communities in mouse feces samples to analyze the composition and diversity of microbial presence. Sequence analysis based on 16S ribosomal RNA (rRNA) gene target enables a broad taxonomical classification of bacterial presence (Figure 5).

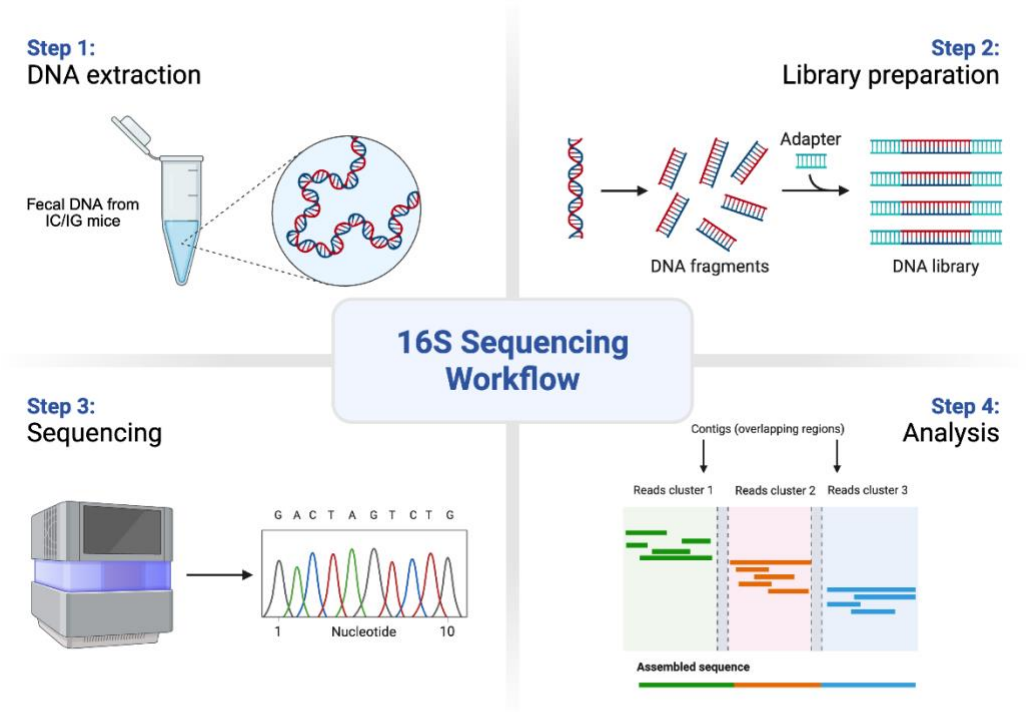

Figure 5. Workflow for next-generation sequencing of gut microbiota
Overview of the sequencing pipeline used to assess microbiota composition in inoculated mice. DNA was extracted from fecal pellets collected from IC and IG groups, followed by library preparation and sequencing. Reads were assembled into contigs and analyzed bioinformatically to identify microbial taxa and community composition.

This step enables high-throughput profiling of bacterial communities in mouse feces samples to analyze the composition and diversity of microbial presence. Sequence analysis based on 16S ribosomal RNA (rRNA) gene target enables a broad taxonomical classification of bacterial presence (Figure 5).

Immunohistochemistry Analysis

Tissues were fixed in formalin, transitioned through graded alcohols, xylene substitutes, heated at 56°C with paraffin wax, and embedded as per Canadian Food Inspection Agency SOP TS-PR006.07. Briefly, pre-warmed cassettes were introduced to the embedding centre, oriented in half-filled stainless-steel moulds, and then chilled quickly on a -15 ± 5°C cold plate to lock in the morphology. The wax was allowed to solidify, and excess wax was trimmed off, and the blocks were logged for traceability. A rotary microtome was set to a thickness of 5 µm for sectioning. The blocks were faced, chilled again, and subsequently, 5 µm

ribbons were cut using disposable blades where the trimming or cutting speed were adjusted according to the type of tissue. Sections were floated on a bath of distilled water at 34–40 °C—the temperature was balanced to the section would sit flat in the warmed water without fragmentation—picked up on pre-validated charged glass slides, drained, and air-dried. Daily readings of the equipment throughout the sectioning, maintenance logs of our microtome and other processing equipment, and entity numbers for each reagent lot were documented daily adhering to CFIA quality-assurance worksheets. Biosafety included blade guards, sharps disposed into sealed containers, and TSE decontamination of water-bath effluent; flammable solvents were kept at a safe distance away from all hot surfaces. The design of this streamlined process created uniform processing to reproducibly produce serial 5 µm sections of paraffin at a thickness suitable for either downstream hematoxylin-eosin staining, or for prion immunohistochemistry, and can be inserted directly into the Methods section of the thesis to portray tissue preparation. Sections that were formalin-fixed and paraffin-embedded 5 µm sections were stained using a Ventana DISCOVERY ULTRA autostainer (Roche) following the Canadian Food Inspection Agency (CFIA) RedMapRBAS Block program (protocol #922, v3). Slides underwent an initial re-hydration at 37 °C with continuous mixing followed by subsequent flushes with Ventana Reaction Buffer (for a total of 2). Antigen retrieval was performed by incubating the sections for 12 min with Enzyme 1 protease following a 4-min temperature equilibration. Once completed, the sections underwent EZ-Prep rinses providing minimal wash and drying. For the remainder of the procedure, endogenous reactive sites were quenched with S-Block for 4 min followed by removal of the S-Block and sequential exposure to the primary monoclonal antibody SAF-84 (Cayman Chemicals, Ann Arbor, MI, USA; Cat.189775) (2.5 µL mL^{-1}) for 32 min at 37 °C (Fig. 6). After repeated washing with the buffer, a prediluted OmniMap universal secondary antibody (Roche; proprietary concentration) was applied for 16 min. The signal amplification was performed using the Ventana RedMap alkaline-phosphatase system: Blocker R1 (4 min) → Streptavidin-alkaline phosphatase conjugate (16 min) → Activator R / Naphthol R (4 min) → Fast-Red

(8 min) x2/triple chromogen. Slides underwent a final counter stain with Ventana haematoxylin (8 min), were blued for 4 min, rinsed, dehydrated, and cover-slipped. This results in a bright red precipitate indicating PrP^{Sc} deposits, with a pale blue nuclear counter stain providing the capacity for quantitative image analysis.

Figure 6. Distribution of PrP^{CWD} deposition in brain section of a mouse orally inoculated with CWD from white-tailed deer. Tissue sections were stained with mAB SAF-84 and showed PrP^{CWD} in the (a) obex of the brainstem

Statistical Analysis

No inferential statistical analyses were performed in this study due to limited sample sizes within each experimental subgroup. Accordingly, all comparisons presented are descriptive in nature and intended to illustrate temporal and route-dependent trends rather than statistically significant differences.

ROC Analysis

To identify the validity and reliability of each replicate in each sample to be considered a true positive vs. a false positive, a Receiver Operating Characteristic (ROC) curve is used. ROC analyses have been widely applied for the evaluation of tests with dichotomous outcomes (positive/negative test results), using sensitivity and specificity as measures of accuracy in comparison with the gold standard (Hajian-Tilaki, 2013; Mandrekar, 2010). A ROC curve is a plot of sensitivity versus the false-positive rate at varying thresholds, and the area under the curve (AUC) is an effective measure of classifying power (Hajian-Tilaki,

2013). It is a graphical tool used to evaluate the diagnostic accuracy of assays by illustrating the trade-off between sensitivity (actual positive rate) and specificity (1 - false positive rate) across various threshold settings. Each point on the ROC curve represents a pair of sensitivity/specificity values corresponding to a particular decision threshold. By plotting sensitivity against 1-specificity, the ROC curve provides a comprehensive method for assessing an assay's ability to classify samples as positive or negative correctly. The significance of the ROC curve lies primarily in determining the optimal threshold that maximizes both sensitivity and specificity, thereby minimizing false positives and false negatives. The area under the ROC curve (AUC) quantifies the overall performance of the assay, with values closer to 1 indicating high discriminative ability. In contrast, values near 0.5 reflect poor performance equivalent to random chance.

To perform ROC analysis for testing small intestine tissue, distributions of RT-QuIC cycle thresholds were generated using one IHC-confirmed CWD '+' mouse small intestine, serially diluted 10-fold with IHC-confirmed CWD '-' mouse small intestine. A pool of negative small intestine samples was also included to complete the distribution needed to run the analyses. The cycle threshold was defined as the time when the ThT signal exceeded Tstdev, which was calculated as the average of the 4th cycle readings from all reactions in relative fluorescent units (RFU) plus 10 standard deviations. A cycle threshold of 60 hours was assigned to reactions where the ThT signal did not cross the threshold within the 60-hour assay (Gray et al., 2016). The cycle threshold served as a binary classifier for CWD positivity, and ROC curve analyses were conducted to compare the cycle threshold with the known CWD status of the tissue homogenates. The optimal assay duration was determined as the threshold with the highest Youden index (sensitivity + specificity – 1) (Unal, I. 2017). ROC curve calculations were performed using the RStudio ROCR package (version 1.0-11) (Sing et al., 2005).

Descriptive Statistics

Tissues from a total of 125 intracerebrally (IC) inoculated mice and 54 intragastrically (IG) inoculated mice were examined for prion seeding activity across the brain, spleen, and small intestine. Within the IC group, 125 brains**,** 125 spleens**,** and 125 small intestines were analyzed, yielding mean RT-QuIC amplification strengths (1/Ct) roughly around 0.0342, 0.0456, and 0.0287 respectively. In the IG group, 44 brains**,** 54 spleens**,** and 54 small intestines were analyzed, with corresponding median 1/Ct values of roughly 0.0132**,** 0.0205, and 0.0258 (Figure 7). These descriptive summaries, which correspond to the data visualized (Fig. 7), show consistently higher amplification strengths in IC tissues than in IG tissues. No parametric or non-parametric hypothesis testing was performed; the results are purely descriptive and intended to present the distribution of sample sizes and amplification strengths across inoculation routes and tissues.

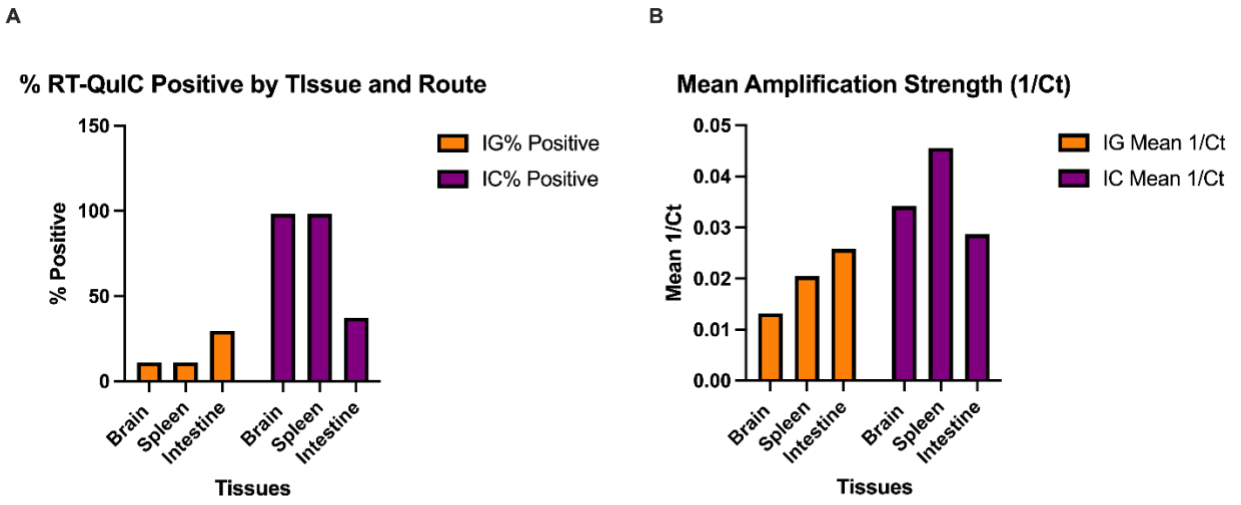

Figure 7. Comparative summary of tissue- and route-specific RT-QuIC Outcomes.
Composite summary figure illustrating (A) positivity rates (% RT-QuIC positive animals) and (B) mean amplification rates (1/Ct) for brain, spleen and small intestine tissues in IG- and IC-Inoculated mice. Results highlight route-dependent differences in prion seeding dynamics, with IC producing consistently higher positivity across tissues and IG showing greater variability and lower overal positivity.

Route	Tissue (Sheet)	Group	Total Mice	Reasons	Mean 1/Ct (positives)	IHC Results
IC	Brain	IC 12	25	END: 22, CS: 2, PID: 1	0.073448509	24
IC	Brain	IC 16	26	END: 15, CS: 9, PID: 2	0.08181784	24
IC	Brain	IC 20	26	CS 12, END: 10, PID: 4	0.071128443	22
IC	Brain	IC 24	24	CS: 11, END: 11, PID: 1, IF:1	0.067060847	23
IC	Brain	IC 8	24	END: 20, PID: 4	0.053666668	20
IC	Spleen	IC 12	25	END: 22, CS: 2, PID: 1	0.041770261	-
IC	Spleen	IC 16	26	END: 15, CS: 9, PID: 2	0.06229612	-
IC	Spleen	IC 20	26	CS: 12, END: 10, PID:4	0.069090631	-
IC	Spleen	IC 24	24	CS: 11, END: 11, PID: 1, IF: 1	0.052227367	-
IC	Spleen	IC 8	24	END: 20, PID 4	0.042184607	-
IC	Small Intestine	IC 12	25	END: 22, CS: 2, PID: 1	0.05934533	-
IC	Small Intestine	IC 16	26	END: 15, CS: 9, PID: 2	0.027834764	-
IC	Small Intestine	IC 20	26	CS: 12, END: 10, PID: 4	0.039715597	-
IC	Small Intestine	IC 24	24	CS: 11,END: 11, PID: 1,IF: 1	0.051582093	-
IC	Small Intestine	IC 8	24	END: 20, PID: 4	0.045085305	-
IG	Brain	IG40	15	END: 14, E: 1	0.022608934	1
IG	Brain	IG48	12	END: 10, MS: 1, CS: 1	0.021019698	1
IG	Brain	IG56	17	END: 7, CS: 6, IF: 1, MM 1, MPU: 1	0.021174484	2
IG	Spleen	IG40	16	END: 14, E: 1	0.025651536	-
IG	Spleen	IG48	18	END: 10, MS: 1, CS: 1, IF: 1,T: 1	0.025742853	-
IG	Spleen	IG56	20	CS: 7,END: 7, IF: 1, MM: 1, MPU: 1	0.029133507	-
IG	Intestine	IG40	16	END: 14, E: 1	0.043091846	-
IG	Intestine	IG48	18	END: 10, MS: 1, CS: 1, IF: 1,T: 1	0.037543153	-
IG	Intestine	IG56	20	END: 7, CS: 6, IF: 1, MM 1, MPU: 1	0.046319558	-

Acronyms: CS - Clinical signs, END - Endpoint, MPU - Medical Prolapse uterus, MM - Medical Malocclusion, IF- In Fighting, E - Eye Infection, PID - Post-Inoculation Death, T - Head Trauma

Table 1. Summary of RT-QuIC and IHC outcomes in IG and IC mice by tissue and cohort. Detection results for brain, spleen, and small-intestine tissues from intragastrically (IG) and intracerebrally (IC) inoculated TgElkPrP mice across time-course cohorts. For each inoculation route and tissue, the table lists the cohort (in weeks post-inoculation), the total number of mice examined, and the reasons for termination (END = natural end-stage disease, CS = clinical signs, PID = prion-induced disease, IF = intercurrent factors). RT-QuIC amplification efficiency is expressed as the mean 1/Ct of positive replicates, and immunohistochemistry (IHC) results show the number of mice with PrP^{Sc} deposits. This overview highlights tissue-specific prion propagation and compares detection by RT-QuIC with histopathological confirmation.

Descriptive analysis and time course significance was performed on this dataset. Amplification strength (1/Ct) did not differ significantly between IG and IC positives for any tissue, though brains of intracerebrally inoculated mice showed a trend toward higher values than brains of intragastrically inoculated mice. Variability was consistently greater in IG tissues, with broad distributions of 1/Ct values and a notable inverse correlation with DPI in IG intestines. Complete raw data underlying these summaries are provided in the supplementary materials (S1 & S2). The supplementary data include the full RT-QuIC fluorescence readings and complete immunohistochemistry (IHC) scoring results for all intragastrically inoculated TgElkPrP mouse tissues (brain, spleen, and small intestine), as well as for all intracerebrally inoculated TgElkPrP mouse tissues (brain, spleen, and small intestine). These tables present the complete dataset from which the summary statistics and figures in the main text were derived, allowing independent verification and future meta-analyses.

Results

Prion seeding activity was characterized in the brains, spleens, and small intestines of TgElkPrP mice that were inoculated either intragastrically (IG; *n* = 54) or intracerebrally (IC; *n* = 125) with chronic wasting disease (CWD) prions and followed for up to 400 days post-inoculation (DPI). All tissues were analyzed post-mortem using real-time quaking-induced conversion (RT-QuIC) and immunohistochemistry (IHC). Only descriptive statistics were performed; no parametric or non-parametric hypothesis testing was applied.

Across the full study period, IC inoculation produced earlier, stronger, and more consistent prion seeding than IG inoculation (Fig.11). Mean RT-QuIC amplification strengths (1/Ct) were higher in the brains (0.0342 versus 0.0132), spleens (0.0456 versus 0.0205), and small intestines (0.0287 versus 0.258) of IC-inoculated mice compared with their IG counterparts. IC mice showed uniformly high RT-QuIC positivity in brain and frequent detection in spleen and intestine, whereas IG mice showed delayed or sporadic detection, consistent with slower disease progression and longer survival times.

To establish a diagnostic threshold for classifying RT-QuIC results as positive or negative, ROC curve analysis was performed using small intestine tissue data. The ROC curve yielded an AUC of 0.918, indicating excellent discriminatory power (Fig. 8C). At the optimal cutoff of Ct = 28 h, the assay achieved both high sensitivity and specificity. This cutoff (dotted orange line, Fig. 8A) was subsequently applied across all RT-QuIC analyses presented in this study.

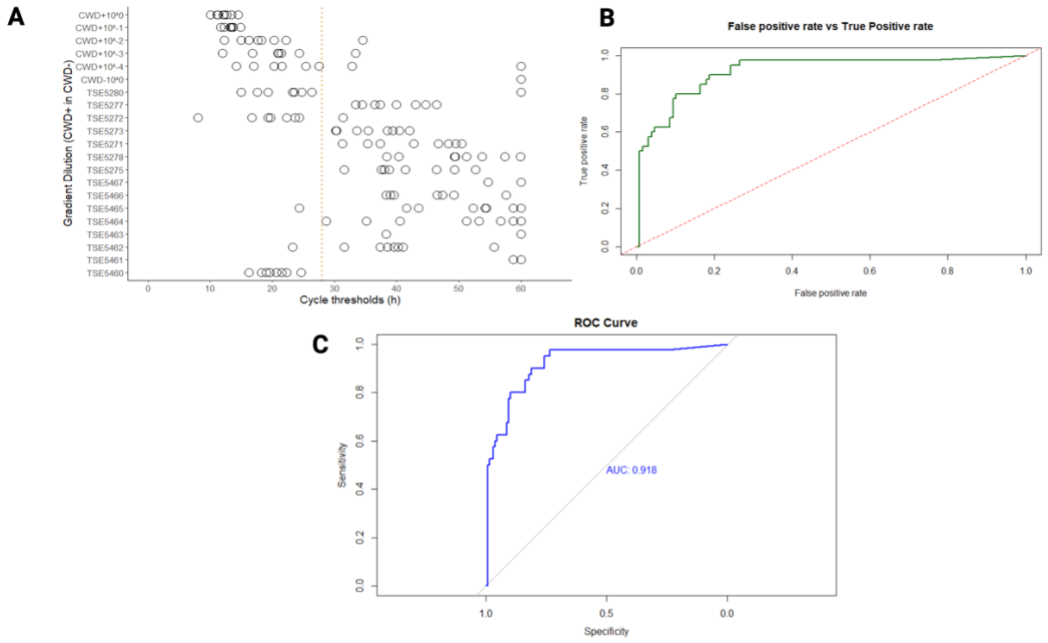

Figure 8. ROC analysis of RT-QuIC performance in small intestine tissues.
(A) Scatterplot of cycle threshold (Ct) values from serial dilutions of CWD-positive brain homogenate and small intestine experimental samples. Each open circle represents an individual replicate. The optimal diagnostic threshold (Ct = 28 h) is indicated by a dashed orange line. (B) ROC curve showing the relationship between false-positive and true-positive rates across thresholds. (C) ROC curve annotated with area under the curve (AUC = 0.918), confirming high diagnostic performance of RT-QuIC in distinguishing positive from negative small intestine tissues.

To assess the sensitivity range of the RT-QuIC assay, serial 10-fold dilutions of CWD-positive brain homogenates were prepared and analyzed in replicate (Fig. 9). Amplification was consistently observed down to a dilution of 10^{-3}, after which amplification became inconsistent and approached background levels. Based on these results, a working dilution of 0.01% (10^{-3} from 10% stock) was selected for all experimental analyses, balancing sensitivity with reproducibility and minimizing the potential for false positives in controls.

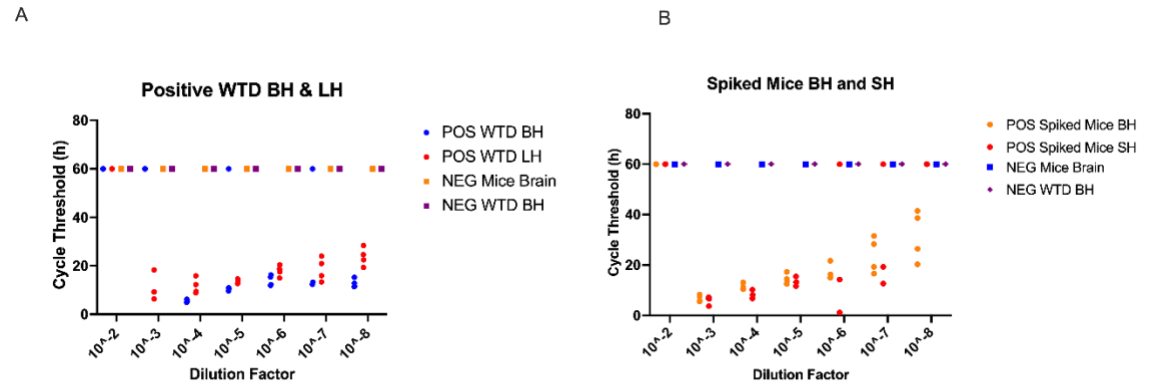

Figure 9. Measure of cycle threshold values across various dilution series (10^-2 - 10^-8). (a) dilution series for positive white-tailed deer brain and lmyphoid tissue homogenates. Replicates of 4 were used for each dilution factor. (b) dilution series for positive spiked mice brain and spleen homogenates (1:9). Replicates of 4 were used for each dilution factor. Negative controls consisted of negatiive white-tailed deer and mice tissues, each with 4 replicates respectively.

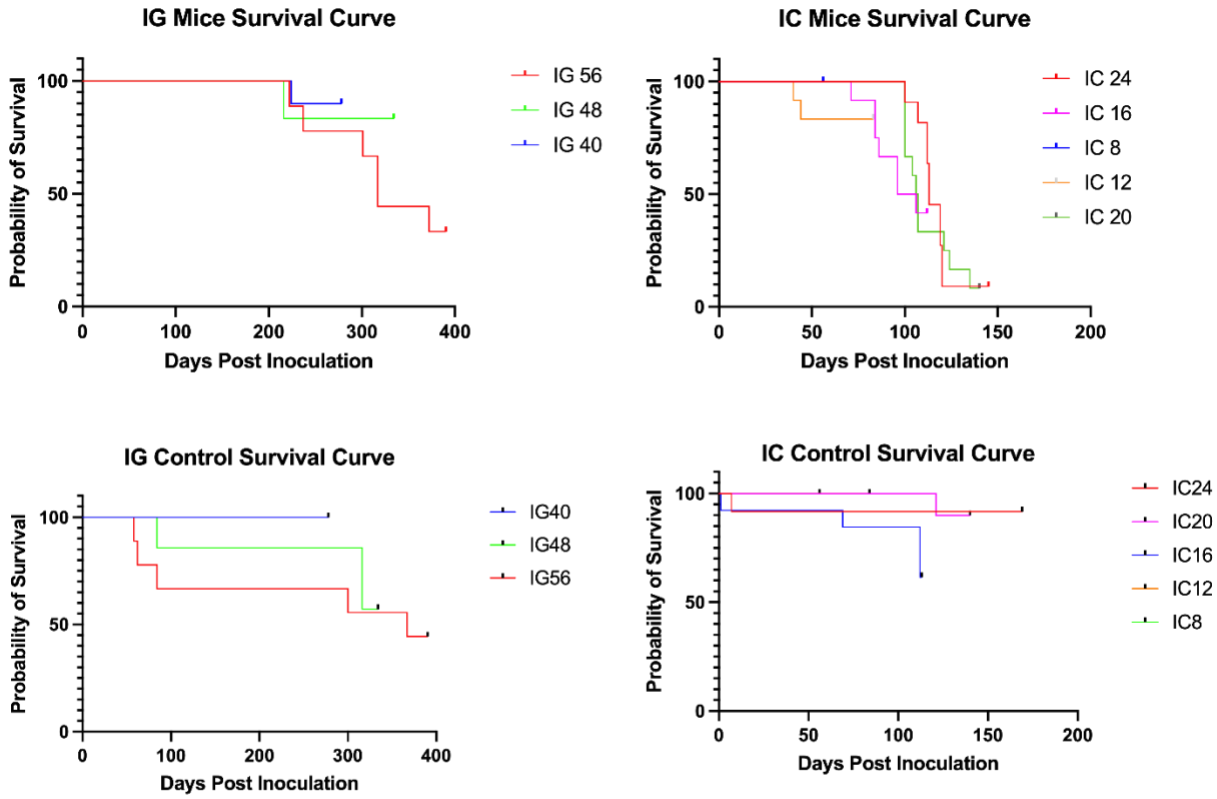

Figure 10. Kaplan-Meier curve expressing survival rate of mice from both intragastric and intracerebral inoculation. Kaplan-Meier cruve depciting probability fo the endpoints all cause mortality. A) Mice provided with white-tailed deer (WTD) CWD Inoculum through intragastric inoculation. B) Mice provided with WTD CWD Inoculum through intracerebral inoculation. C) No Treatment Control Group mice from intragastric group. D) Mice provided with negative WTD brain homogenate. Number corresponding IG or IC respective of weeks post inoculation. Both survival curves include male and female infected mice.

Kaplan–Meier survival analysis revealed significant differences in disease progression between inoculation routes (Fig. 10). The analysis revealed no significant differences among cohorts within the

intragastric group (IG40, 48, 56; log-rank test, $p > 0.05$) or within the intracerebral group (IC8,12,16,20,24; log-rank test, $p > 0.05$). However, when comparing the two inoculation routes directly, intracerebral inoculation was associated with significantly shorter survival relative to intragastric inoculation (log-rank test, $p < 0.0001$). This indicates that while survival outcomes did not differ across time-course subgroups within each inoculation route, the overall route of infection strongly influenced disease progression.

The temporal amplification patterns presented in Figures 11.1–11.3 further emphasize these route-dependent differences. In the brain (Figure 11.1), IC-inoculated mice displayed robust seeding as early as eight weeks post-inoculation, with fluorescence rising steeply and remaining high throughout the observation period, whereas IG-inoculated mice exhibited a later onset and lower overall signals, with most positives emerging only after forty weeks. In the spleen (Figure 11.2), IC mice again showed rapid and sustained prion amplification, whereas IG spleens exhibited weaker and more variable signals, reflecting slower peripheral replication. In the small intestine (Figure 11.3), IC mice demonstrated prompt and persistent amplification, while IG mice showed later, less uniform increases in seeding activity. Receiver-operating characteristic analysis of small-intestine RT-QuIC data yielded an area under the curve (AUC) of 0.918, confirming the excellent diagnostic performance of RT-QuIC for intestinal detection. Serial dilution experiments further verified the reproducibility and lower detection limit of the assay across tissues and routes.

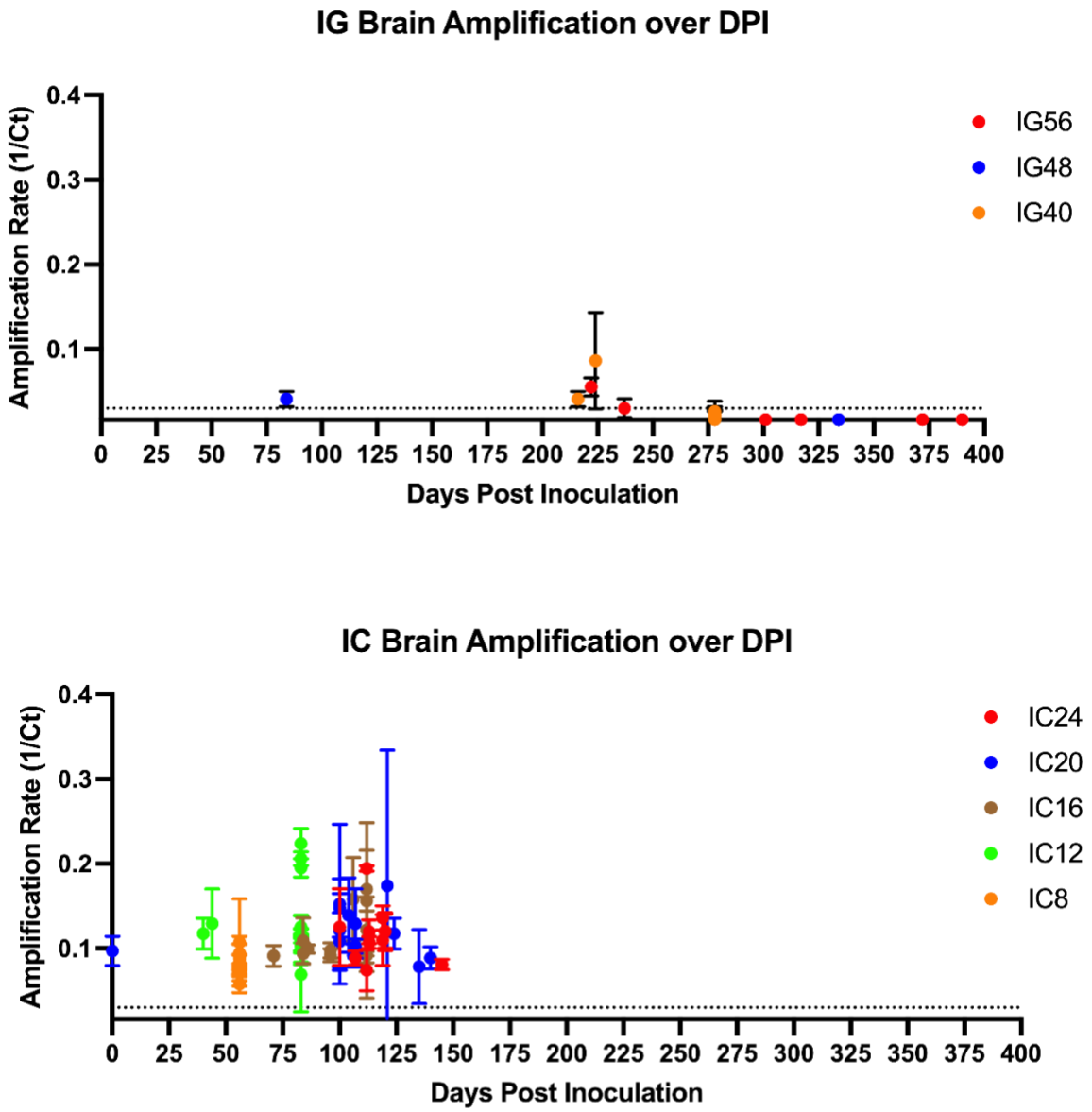

Figure 11.1. Brain RT-QuIC amplification vs DPI (IG vs IC).
IC brains show early, frequeny and consistent amplification across the DPI window, with many mice brain tissues exceeding the Ct threshold well before 200 DPI. IG brains show sparse, late positives, with only a few animals crossing threshold and substantial dispersion around the cutoff. This pattern reflects direct CNS seeding after IC, vs. inefficient/variable CNS access after IG. All negative controls were negative on RT-QuIC and IHC.

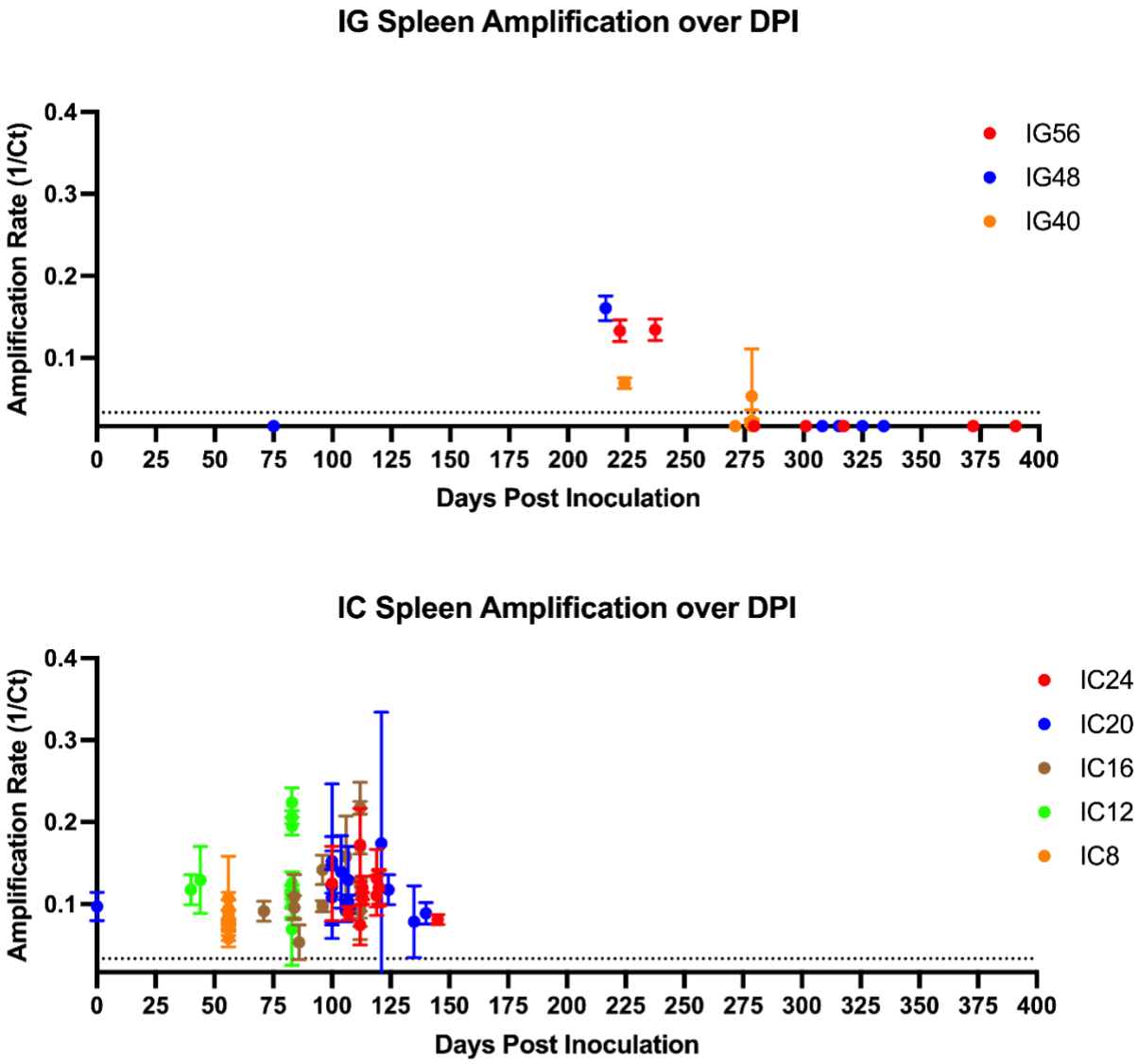

FIgure 11.2. Spleen RT-QuIC amplification vs. DPI (IG vs. IC)
IC spleens exhibit regular, early amplification across DPI, roughly parelling IC brain. IG spleens show fewer, scattered positives without a clear temporal clustering, consistent with variable immune dissemination from intestinal entry sites. All negative controls were negative on RT-QuIC and IHC.

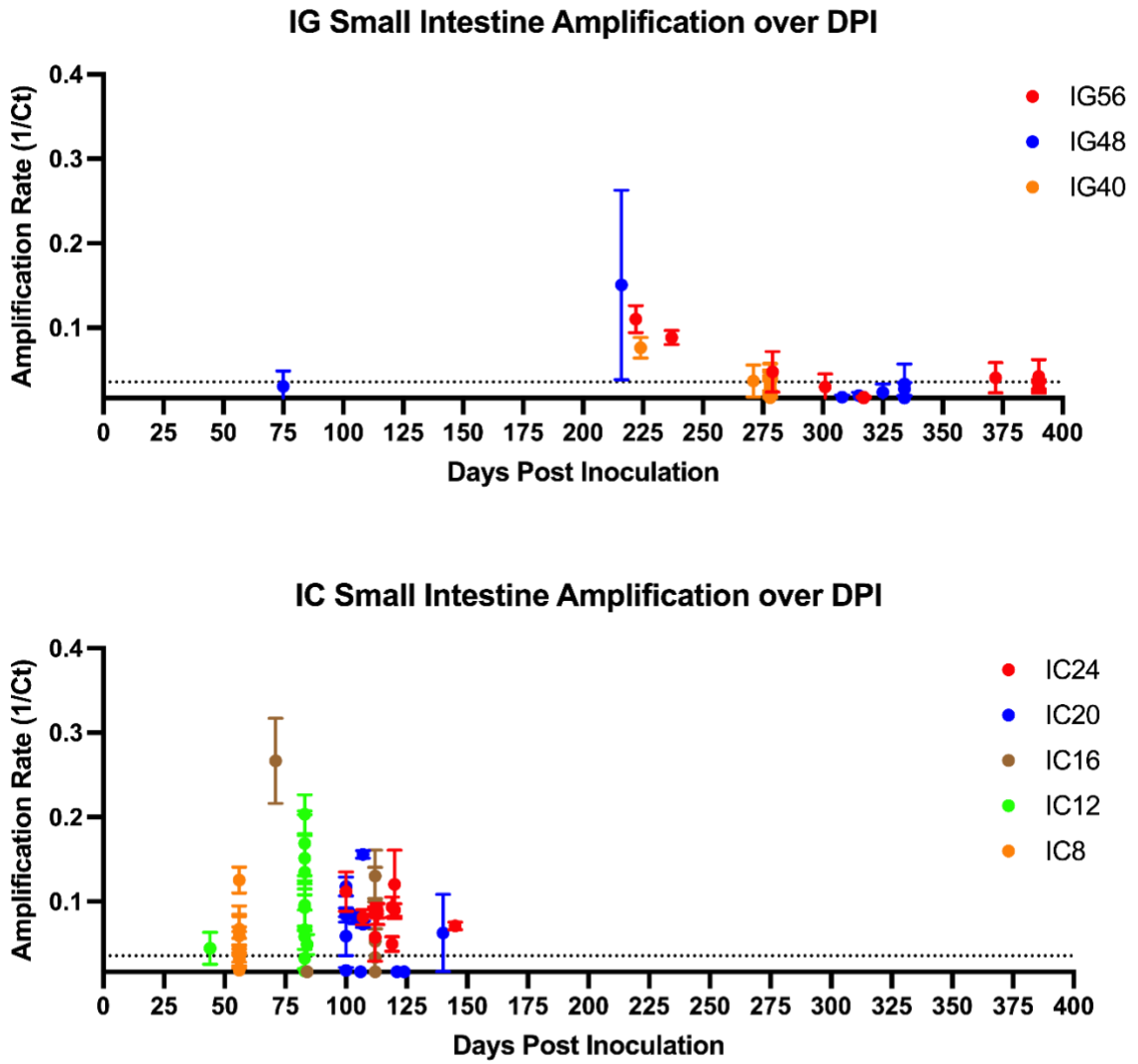

Figure 11.3 - Small Intestine RT-QuIC amplification vs. DPI (IG vs. IC)
IC small intestine shows numerous positives (secondary spread) including early DPI events. IG small intestine shows clearest relative signal among IG tissues (more intestine positives than IG brain/spleen), but with heterogeneous timing and several borderline amplifications near the threshold. This supports intestine as the primary entry site for IG despite lower absolute positivity than IC. All negative controls were negative on RT-QuIC and IHC.

Immunohistochemistry (IHC) Analysis

Formalin-fixed, paraffin-embedded brain, spleen, and small-intestine tissues from all experimental mice were examined for PrP^{Sc} by immunohistochemistry. PrP^{Sc} specific staining was absent in all age-matched negative controls, confirming assay specificity.

IC cohorts (8, 12, 16, 20, and 24 WPI) displayed early and widespread neuroinvasion (Table 1). Among brains examined, 83.3% (20/24) were IHC-positive at 8 WPI, rising to 96.0% (24/25) at 12 WPI and remaining high through 16 WPI: 92.3% (24/26)**,** 20 WPI: 84.6% (22/26)**,** and 24 WPI: 95.8% (23/24)**.** Across IC cohorts overall, 90.4% (113/125) of brains were positive. Staining patterns progressed from granular to more confluent deposits across cortical and subcortical regions, paralleling RT-QuIC seeding kinetics (IC mean 1/Ct for positives ≈0.054–0.082).

By contrast, IG-inoculated mice showed delayed and focal neuroinvasion. Brain IHC positivity was 6.7% (1/15) at 40 WPI, 8.3% (1/12) at 48 WPI, and 11.8% (2/17) at 56 WPI—9.1% (4/44) overall. The four IHC-positive brains of intragastrically inoculated mice corresponded to mice 5264, 5270, 5290, 5318. These limited brain findings are consistent with weaker RT-QuIC signals in IG cohorts (IG mean 1/Ct for positives ≈0.021).

IHC demonstrates a clear route- and time-dependent difference in neuroinvasion: IC inoculation yields early, high-frequency PrP^{Sc} accumulation in brain, whereas IG inoculation requires prolonged incubation and remains low-frequency and focal. These histopathological results corroborate the RT-QuIC data and underscore how inoculation route shapes CWD pathogenesis in ELK-PrP mice.

Fecal sample preparation and DNA isolation

After testing the brains of intragastrically inoculated mice and spleen, fecal samples from the mice were collected and examined to determine their suitability for 16S rRNA sequencing. Given that the samples were tested in a level 2 containment facility, it must be assessed whether removing prion-contaminated tissues from the containment is sufficiently safe to perform 16S rRNA sequencing. To determine this, DNA was extracted from fecal samples of mice from the IG groups (control and infected), including the four mice inoculated intragastrically, and tested by RT-QuIC to verify whether any prion remained in the

samples. By evaluating the safety of removing prion-contaminated tissues from the containment, I can expand the range of analytical techniques available for studying CWD while maintaining strict biosafety protocols.

To prepare the sample before running RT-QuIC, DNA was extracted from the fecal pellets using the Macherey-Nagel DNA Extraction kit. The elution buffer (100 µL) was used to elute 100 µL of DNA. The DNA was then prepared in a 1:19 ratio of 1.5 µL of DNA (18.5 µL of 0.1% SDS. This ratio provided the best result, avoiding any inhibition from other reagents that could interfere with signal DNA preparation and ensuring maximum signal detection while minimizing potential interference from other reagents. This carefully calibrated mixture yielded precise and reliable results for subsequent analysis.

After running approximately 50 fecal DNA samples using Nucleospin kits and 50 samples of positive WTD brain and lymph, analysis of the data using MARS software identified which assays appeared to show sensitivity, indicating that prions may be still present in the extracted DNA. The DNA samples were further cleaned to remove residual prion. The DNA samples were submitted to CFIA sequencing facility. However, due to the other priorities of CFIA sequencing facility, my DNA samples cannot be sequenced within a reasonable timeframe.

Discussion

In this study, we examined prion seeding dynamics in transgenic TgElkPrP mice inoculated either intragastrically (IG) or intracerebrally (IC) with chronic wasting disease (CWD) prions and monitored them for up to 400 days post-inoculation. Using the real-time quaking-induced conversion (RT-QuIC) assay in conjunction with immunohistochemistry, we created a comprehensive descriptive dataset encompassing 54 IG and 125 IC mice. Median RT-QuIC amplification strengths (1/Ct) revealed clear route-dependent differences: brains, spleens and small intestines of intracerebrally inoculated mice showed medians of

0.071, 0.052, and 0.045, respectively, while the corresponding tissues of intragastrically inoculate mice had lower medians of 0.021, 0.026, and 0.043 respectively. These differences also appeared in tissue positivity. IC inoculation produced rapid, consistent, and high-efficacy prion seeding and amplification in the brain and generally showed higher positivity in peripheral tissues. In contrast, IG inoculation resulted in fewer positives and delayed or weaker seeding signals. Phenotypic progression was concordant with RT-QuIC positivity in central and peripheral tissues. Animals exhibiting overt neurological signs consistently demonstrated prion seeding activity in brain tissue, while pre-symptomatic or mildly affected animals showed either delayed or absent RT-QuIC amplification. This alignment supports the biological validity of RT-QuIC as a sensitive indicator of disease progression, though no formal statistical correlation was performed. Survival analysis similarly indicated that IC-inoculated mice died earlier than those inoculated with IG. Receiver-operating characteristic analysis of small-intestine samples (area under the curve = 0.918) confirmed the excellent diagnostic accuracy of RT-QuIC, and serial dilution experiments verified its sensitivity limits. By combining detailed descriptive statistics with rigorous assay validation, these results demonstrate that the route of inoculation significantly affects CWD pathogenesis and establish RT-QuIC, together with immunohistochemistry, as a reliable tool for mechanistic studies and future diagnostics.

Route-Dependent Differences in Pathogenesis

The findings of this study clearly demonstrate that the route of inoculation was a significant predictor of disease course after inoculation. IC infected mice produced rapid, uniform, high-efficacy seeding in the brain. This was expected when considering infectious prions were specifically injected into the central nervous system (CNS) via IC, which bypasses any potential peripheral barriers, hence the rapid time frame of amplification in the CNS and the shorter survival times in mice infected via IC relative to IG. In contrast, mice inoculated via IG were somewhat able to delay and be inconsistent in brain data seeding, and peripheral tissue data was also highly variable. The requirement of a prion to transverse the

gastrointestinal barrier makes infection via the oral route a multi-step process. The gastrointestinal barrier likely involves uptake across the follicle-associated epithelium and transfer to Peyer's patches and induction of replication in gut-associated lymphoid tissue (GALT) prior to neuroinvasion via enteric nerves or hematogenous spread. Having additional biological checkpoints in the oral transmission pathway adds variability in transmission efficiency in a type of bottleneck effect which adequately explains the variability seen in the IG animals in the present study and previous studies showing that the oral route of prion exposure is less efficient and more variable than direct inoculation into the CNS (Kobayashi et al., 2019; Johnson et al., 2007).

Tissue-Specific Seeding Patterns

The tissue-level RT-QuIC results further support seeding differences in mechanisms. In the brains of the animals the IC inoculation consistently resulted in high amplification levels and reflected early and direct neuroinvasion. In comparison, variable outcomes were observed following IG inoculation, as seeding activity was detected only in some of the animals (Fig. 11.1-11.3). The involvement of the spleen between routes differed dramatically. In the spleens of intragastrically inoculated mice, amplification was detectable in several animals early on, suggesting that peripheral replication in lymphoid organs may be a key feature of oral exposure. In the spleen of intragastrically inoculated mice, amplification was routinely seen but likely reflects the secondary spread of prions, perhaps related to the CNS, rather than amplification, as the correlation of amplification preceded DPI. The variables seen in the small intestine were the greatest. In the animals inoculated via the IG route, seeding in the small intestine was documented in some animals but not in others, again reflecting heterogeneity in oral uptake effectiveness and replication. Conversely, small intestines in the IC animals showed mostly negative and sporadically positive results. This again demonstrated that either retrograde spread was limited compared to the oral route of the prion exposure or simply indicated that seeding at this site is unlikely, given the prion was

directly inoculated into the CNS. These results highlight the significance of the gastrointestinal system and its associated lymphoid tissue as a primary site for initial seeding/replication, as well as a source of diversity in oral transmissibility.

Methodology Considerations

The strength of this study was in combining assay validation with experimental results. RT-QuIC demonstrated a strong diagnostic capability, with the ROC analysis showing an AUC of 0.918 and confirming the Ct = 28 h cutoff as the best threshold. The serial dilution series verified the assay's ability to reliably detect as low as a 10^{-4} dilution of prions, indicating high sensitivity. Kaplan–Meier survival curves further supported RT-QuIC data, with IC mice surviving less time, which is consistent with our previous findings on CNS seeding.

Despite these strengths, several limitations should be acknowledged. Initially, the absence of microbiome sequencing data was a limitation of this thesis, which was originally designed to establish connections between microbiota composition and CWD pathogenesis. While the results from the RT-QuIC emphasizes the variability of IG infection, the microbial triggers that drove such differences are unknown. Second, the intestinal controls had rare false positives that may have been due some background fluorescence or technical variability demonstrating the need for more strict cutoff thresholds. Lastly, some of the sub-analyses, like IG positives and sex-based comparisons, were limited by low sample size, leading to low statistical power.

Implications for CWD transmission

These findings have direct implications for understanding natural CWD transmission in cervid populations. Oral exposure is the predominant route of infection in the wild, and the variability observed in IG mice

mirrors the unpredictable dynamics of natural transmission. The spleen and small intestine emerged as critical sites of early prion seeding and replication following oral inoculation, aligning with studies that emphasize the role of GALT and secondary lymphoid tissues in prion pathogenesis (Donaldson et al., 2015).

By contrast, IC inoculation, while experimentally useful for establishing a uniform disease course, does not reflect natural transmission dynamics. The consistent and rapid brain seeding observed in IC animals provides an experimental benchmark but underscores that oral transmission is inherently more stochastic. These results also suggest that host-specific factors, including microbiota composition, immune function, genetics, and sex, may play important roles in modulating oral susceptibility, reinforcing the need for future integrative studies.

Limitations

The current study has limitations that should be considered. First, the absence of microbiome 16S RNA sequencing data limited my ability to interpret results as I might have liked with the original thesis question being to relate microbial composition to CWD susceptibility. Without 16S RNA sequencing I was not able to assess static changes in the gut microbiota or changes in prion pathogenesis. So, while the variants of RT-QuIC gave evidence of heterogenicity of CWD among IG-inoculated mice, the microbial commensals conferring that heterogenicity are unknown. Second, the samples among the subgroups (IG positive animals, sex stratified groups) were all relatively small. Small sample sizes give less power of the statistical tests and can obscure more slight differences, especially as concerns amplification strength and serologic variability of the male and female mice. Trends noted were indicated by descriptive comparisons, but such closure to been made completely by means of statistical tests, as larger cohorts are necessary for validation and further experimenting. Third, there were occasionally phases of visible confirmed false positives in the control tissues from the intestine, probably due to background fluorescene, technical artifacts or indifference noise from RT-QuIC. I used rigid experimental thresholds

[Brain (Ct) = 33, Spleen (Ct) = 30, Small Intestine (Ct) = 28 h] to limit the damage by false positives, but it is not obtainable for find it the fault of division cannot sometimes be cleared up. Finally, while IC inoculation was a proper experimental control in order to prove consistent CNS infectivity (and used as a prepared comparative), it entails no part of the natural transmission cycle. Thus, comparisons hereafter made between IG and IC should have regard to the biological significancy of each experimental model. IG inoculation presents a mode of more nearly complete discovering the real oral transmission of infection of natural cervids, while IC inoculation is informative artificial comparison, still on the same even scale. These limitations give a general note of caution which should be borne in mind, when interpretation of the general study, pointing out the placing of both in species greater study cohorts, with experimental microbiome study of the gut and field experiments as a resort in the way of study work.

Conclusion

In this study, we show that the route of chronic wasting disease (CWD) prion inoculation in a cervidized transgenic (TgElkPrP) mouse model impacts prion seeding, the disease progression and tissue distribution. For example, with 54 mice receiving intragastric (IG) inoculation and 125 mice receiving intracerebral (IC) inoculation, the 400-day post-inoculation follow-up data indicated the IC-inoculated mice had earlier and more consistent prion seeding, and shorter survival, than IG exposure. While IG exposure had lower and delayed seeding times (RT-QuIC positivity) and longer survival. When we measured the median amplification strengths (1/Ct), across all tissues, we found consistently higher amounts of prions in the brains, spleens, and small intestines of mice that received IC inoculation compared to IG inoculated mice. The receiver operating characteristic analysis of the RT-QuIC small intestinal data (AUC = 0.918) and serial dilution assays show the sensitivity and specificity of RT-QuIC (both based on our data) as a feasible diagnostic tool in combination with immunohistochemistry. These observations imply that the route of inoculation and local tissue microenvironment can vastly influence the propagation of prions and the

progression of the disease in this model. Additionally, the results demonstrate the time-sensitive and order-of-seeding relevance of the probability of using RT-QuIC diagnostics to find early-stage seeding in multiple tissues.

While this study suggests how the route of exposure might relate to CWD pathogenesis, they do not necessarily support that the same dynamics would occur in free-ranging cervids or other hosts. Our study was also limited by post-mortem sampling, small subgroups of each tissue, and a single transgenic line. Future studies could build on the results here by investigating specific molecular routes for gut entry or neural spread, because of the influence that microbiota would have in modifying susceptibility, and possibly genetic or hormonal predisposition to route-specific effects. Longitudinal microbiome studies and greater cross-sectional sampling in natural hosts can assist these studies. Ultimately, these findings would reinforce the premise for which the route of exposure would shape disease progression and distribution of CWD prions and give an opportunity for subsequent mechanistic and ecological research that would include disease surveillance and management.

Future Direction

The experiments and analyses described in this thesis open a number of interesting avenues for prion and CWD research. This investigation establishes a longitudinal framework for characterizing prion amplification via RT-QuIC in brain and spleen following IG and IC inoculations, allowing for a thorough temporal landscape of peripheral and central spread; mechanistic and translational hypothesis testing can now be achieved. One possible avenue to further develop this thinking would be to evaluate the gut microbiome as a true modifier of susceptibility and progression of prion disease. The changes observed in the microbial composition between CWD-positive and CWD-negative deer (e.g. greater abundance of Akkermansia, Lachnospireacea UCG-010, and RF39 taxa) provide a biologically plausible starting point for microbiome manipulation (Minich et al., 2021). In addition, a recent study looking at fecal microbiome

biomarkers in CWD reports evidence bacteria can be used as biomarkers of risk or disease, as bacteria can change with pre-symptomatic disease (Didier et al., 2024). Following on their findings, follow-up studies could use germ-free or antibiotic-treated mice, reconstitution with defined microbial consortia, or fecal transplants to examine the presence of causal relationships between specific bacteria, metabolites of bacteria, and M-cell or gut-associated lymphoid tissue-mediated prion uptake.

In parallel, potential expansion via the genetic side of prion susceptibility represents another compelling axis. The association between *prnp* polymorphisms and prion disease risk and phenotype is well characterized in human populations (e.g. codon 129 M/V and codon 219 E/K) (Kobayashi et al., 2015) and experimental studies show that host factors aside from the PrP sequence can influence prion strain phenotypes (Crowell et al., 2015). Work with CWD models, in particular, demonstrates that passages through hosts with different PrP alleles results in conformational change & new prion strains arise (Duque Velasquez et al., 2020). Subsequently, developing additional cervidized mouse lines containing additional rare or protective variants of the PRNP gene (e.g, H95, F225, S96), and passing prion isolates serially in a systematic manner would provide insight into how host genetics drives strain selection, adaptation, and cross-species potential.

Another major area of opportunity is in the development of prion detection and biomonitoring. The RT-QuIC assays optimized here for brain and spleen samples can be adapted for use with non-invasive matrices such as serum, saliva, or feces, for diagnosis of living animals prior to clinical changes (Bravo-Rizzi et al., 2023). Soil humic acids decreased or diluted the PrP^{CWD} signal and also reduced infectivity of TgElk mice (Kuznetsova et al., 2018), indicating environmental matrices will impact prion activity.

A mechanistic breakdown of neuroinvasion pathways is another logical next frontier. The disparity in temporal kinetics between IG and IC inoculations we observed here indicates that prion transport may take different routes, possibly through enteric neurons, vagus complex, or lymphoid-neural crosstalk.

Future studies could utilize neuronal tracers, in vivo imaging, or cell-type specific knockouts to elucidate the cellular route that prions take from the gut to brain. Modulating immune signaling in Peyer's patches, mesenteric lymph nodes, or follicular dendritic cells might elucidate how local immune microenvironments gate or block neuroinvasion. Such mechanistic understanding could provide intervention targets to impede prion transmission.

Finally, the methodology and conceptual foundation established here can extend beyond cervid prion related wasting disease to other prion diseases and even prion-like proteinopathies. The time of use of ultrasensitive detection methods, microbial ecology, host genetics, and mechanistic neurobiology gives rise to a prototype for exploring other diseases, such as Parkinson's, Alzheimer's or amyloid diseases especially when related to peripheral seeding or gut-brain axes. By using cross-disease approaches, scientists may identify unifying principles of protein misfolding, strain diversity, and host-microbe interactions.

The experiments provided in this thesis report go beyond making a disease progression map for CWD. They provide a flexible platform for the investigation of host-pathogen dynamics, innovation in detection, and translational strategies. Following these integrated future directions have potential benefits for not just understanding and reducing CWD but also for advancing the field of neurodegenerative disease research.

After the 16S rRNA gene sequencing has been performed, the raw DNA sequence data will be subjected to a comprehensive bioinformatic and statistical analysis to characterize the bacterial communities found in each sample. Initially, the paired-end reads will be demultiplexed and quality-filtered to remove adapters, chimeras, and low-quality bases (Bokulich et al., 2013). The denoising algorithms (for instance, DADA2 or Deblur) will be used to infer amplicon sequence variants (ASVs) or operational taxonomic units (OTUs), which represents a high-fidelity representation of microbial taxa (Callahan et al., 2016). The

identified ASVs/OTUs will be taxonomically assigned by matching ASVs/OTUs to a curated reference database (such as SILVA or Greengenes) that allows identification from phylum to genus or species level, but if possible, will be genus or species level (Quast et al., 2013).

After obtaining a taxonomic classification, microbial diversity will next be examined for within and between samples. Alpha diversity metrics (for example, Shannon index, Chao1 richness) to quantify within-sample diversity, while beta diversity will be used to identify differences in community composition across experimental groups (for example, route of inoculation; time matched controls; disease state) by comparing the total microbial community using statistical analyses (for example, Bray-Curtis dissimilarity, UniFrac distances) and ordination techniques like principal coordinate analysis (PCoA). Statistical investigations using statistical tests like PERMANOVA and differential abundance testing (for example, ANCOM or DESeq2) will allow differentiation of bacterial taxa with significant correlation with prion infection state, disease state, or other covariate. The results can then be integrated with RT-QuIC and histopathology to synthesize a common interpretation of the microbial signature identified in CWD and the subsequent prion amplification event, thus, identifying microbial taxa or metabolic pathways likely to have roles in chronic wasting disease pathogenesis.

References

- Angers, R. C., Green, M., Seward, T. S., Hoover, E., Balachandran, A., Spraker, T., O'Rourke, K., Telling, G. C., & Napier, D. (2009). Chronic Wasting Disease Prions in Elk Antler Velvet. Emerging Infectious Diseases, 15 (5): 696–703. https://doi.org/10.3201/eid1505.081458

- Arifin, M. I., Thapa, S., Gilch, S., Chang, S. C., Hannaoui, S., & Schatzl, H. M. (2021). Cervid Prion Protein Polymorphisms: Role in Chronic Wasting Disease Pathogenesis. International Journal of Molecular Sciences.22(5): 2271. https://doi.org/10.3390/ijms22052271
- Baeten, L. A., Miller, M. W., Jewell, J. E., Powers, B. E., & Spraker, T. R. (2007). A Natural Case of Chronic Wasting Disease in a Free-ranging Moose (Alces alces shirasi). Journal of Wildlife Diseases. 43(2):309–314. https://doi.org/10.7589/0090-3558-43.2.309
- Bartz, J. C., Caughey, B., Christensen, S., Mckenzie, D., Morales, R., Benavente, R., Mathiason, C. K., Hoover, E. A., Schwabenlander, M. D., Herbst, A., & Walsh, D. P. (2024). Chronic Wasting Disease: State of the Science. Pathogens (Basel, Switzerland). 13(2): 138. https://doi.org/10.3390/pathogens13020138
- Benestad, S. L., & Telling, G. C. (2018). Chapter 8 - Chronic wasting disease: an evolving prion disease of cervids. Handbook of Clinical Neurology. 153: 135–151. https://doi.org/10.1016/b978-0-444-63945-5.00008-8
- Bokoliya, S. C., Zhou, Y., Dorsett, Y., & Panier, H. (2021). Procedures for Fecal Microbiota Transplantation in Murine Microbiome Studies. *Frontiers in Cellular and Infection Microbiology*, *11*(10). https://doi.org/10.3389/fcimb.2021.711055
- Bokulich, N., Subramanian, S., Faith, J. *et al.* Quality-filtering vastly improves diversity estimates from Illumina amplicon sequencing. *Nat Methods* **10**, 57–59 (2013). https://doi.org/10.1038/nmeth.2276
- Bradford, B. M., Tetlow, L., & Mabbott, N. A. (2017). Prion disease pathogenesis in the absence of the commensal microbiota. The Journal of General Virology. 98 (7): 1943–1952. https://doi.org/10.1099/jgv.0.000860
- Bravo-Risi, F., Catumbela, C. S. G., Morales, R., Nichols, T., Soto, P., Eckland, T., Soto, C., Lockwood, M., Dittmar, R., & Ramírez, S. (2021). Detection of CWD prions in naturally infected

white-tailed deer fetuses and gestational tissues by PMCA. Scientific Reports. 11(1). https://doi.org/10.1038/s41598-021-97737-y

- Bravo-Risi, F., Soto, P., Benavente, R., Nichols, T. A., & Morales, R. (2023). Dynamics of CWD prion detection in feces and blood from naturally infected white-tailed deer. Scientific reports. *13*(1), 20170. https://doi.org/10.1038/s41598-023-46929-9
- Brown, P., Rau, E. H., Johnson, B. K., Bacote, A. E., Gibbs, C. J., Jr, & Gajdusek, D. C. (2000). New studies on the heat resistance of hamster-adapted scrapie agent: threshold survival after ashing at 600 degrees C suggests an inorganic template of replication. Proceedings of the National Academy of Sciences of the United States of America. 97 (7): 3418–3421. https://doi.org/10.1073/pnas.97.7.3418
- Bryant, D. N., Larsen, R. J., Bondo, K. J., Norton, A. S., Lindbloom, A. J., Griffin, S. L., Larsen, P. A., Wolf, T. M., & Lichtenberg, S. S. (2025). Evaluation of RT-QuIC Diagnostic Performance for Chronic Wasting Disease Detection Using Elk (Cervus canadensis) Ear Punches. Journal of Wildlife Diseases. 61(1). https://doi.org/10.7589/jwd-d-24-00071
- Callahan, B., McMurdie, P., Rosen, M. *et al.* DADA2: High-resolution sample inference from Illumina amplicon data. *Nat Methods* **13**, 581–583 (2016). https://doi.org/10.1038/nmeth.3869
- Chen, S., Gu, J., Chen, Y., & Zhou, Y. (2018). fastp: an ultra-fast all-in-one FASTQ preprocessor. Bioinformatics. 34(17): i884–i890. https://doi.org/10.1093/bioinformatics/bty560
- Christenson, P. R., Jeong, H., Li, M., Ahn, H., Schmeichel, A. M., Misra, P., Li, D., Savica, R., Low, P. A., Singer, W., Larsen, P. A., Park, H. Y., & Oh, S.-H. (2024). Blood-Based Nanoparticle-Enhanced Quaking-Induced Conversion (Nano-QuIC): Inhibitor-Resistant Detection of Seeding Activity in Patients Diagnosed with Parkinson's Disease. Nano Letters. 24(47): 15016–15024. https://doi.org/10.1021/acs.nanolett.4c03768

- Cramm, M., Kim, Y.-S., Collins, S., Satoh, K., Zerr, I., Varges, D., Raeber, A., Mitrova, E., Kuhn, F., Schmitz, M., Schroeder, B., & Karch, A. (2015). Stability and Reproducibility Underscore Utility of RT-QuIC for Diagnosis of Creutzfeldt-Jakob Disease. Molecular Neurobiology. ,53(3): 1896–1904. https://doi.org/10.1007/s12035-015-9133-2
- Crowell, J., Hughson, A., Caughey, B., & Bessen, R. A. (2015). Host Determinants of Prion Strain Diversity Independent of Prion Protein Genotype. Journal of virology. *89*(20): 10427–10441. https://doi.org/10.1128/JVI.01586-15
- Curry, K. D., Soriano, S., Reeves, E., Finzer, P., Savidge, T., Tyshaieva, A., Dilthey, A., Wu, Q., Nute, M. G., Treangen, T. J., Villapol, S., Graeber, E., Mendling, W., & Wang, Q. (2022). Emu: species-level microbial community profiling of full-length 16S rRNA Oxford Nanopore sequencing data. Nature Methods. 19(7): 845–853. https://doi.org/10.1038/s41592-022-01520-4
- Darish, J. R., Ahmed, M. S., Kaganer, A. W., Kobashigawa, E., Wolf, T. M., Zhang, S., Hanley, B. J., Lichtenberg, S., Tewari, D., Schuler, K. L., Schwabenlander, M. D., Rowden, G. R., Sreevatsan, S., Pedersen, J. A., & Larsen, P. A. (2024). Inter-laboratory comparison of real-time quaking-induced conversion (RT-QuIC) for the detection of chronic wasting disease prions in white-tailed deer retropharyngeal lymph nodes. Journal of Veterinary Diagnostic Investigation: Official Publication of the American Association of Veterinary Laboratory Diagnosticians Inc. 37(1): 86–93. https://doi.org/10.1177/10406387241285165
- Das, A. S., & Zou, W.-Q. (2016). Prions: Beyond a Single Protein. Clinical Microbiology Reviews. 29(3): 633–658. https://doi.org/10.1128/cmr.00046-15
- Dassanayake, R. P., Orrú, C. D., Knowles, D. P., Hughson, A. G., Graça, T., Madsen-Bouterse, S. A., Zhuang, D., Caughey, B., & Schneider, D. A. (2015). Sensitive and specific detection of classical scrapie prions in the brains of goats by real-time quaking-induced conversion. Journal of General Virology. 97(3): 803–812. https://doi.org/10.1099/jgv.0.000367

- Defranco, J. P., Bian, J., Kim, S., Crowell, J., Barrio, T., Webster, B. K., Atkinson, Z. N., & Telling, G. C. (2024). Propagation of distinct CWD prion strains during peripheral and intracerebral challenges of gene-targeted mice. Proceedings of the National Academy of Sciences of America.121(32). https://doi.org/10.1073/pnas.2402726121
- Delgado, M. L., Manning, S. D., Moore, J. A., Scribner, K. T., Kanesfsky, J., Singh, P., Funk, J. A., & Cannell, E. M. (2017). Intestinal Microbial Community Dynamics of White-Tailed Deer (Odocoileus virginianus) in an Agroecosystem. Microbial Ecology. 74 (2): 496–506. https://doi.org/10.1007/s00248-017-0961-7
- Dempsey, E., & Corr, S. C. (2022). Lactobacillus spp. for Gastrointestinal Health: Current and Future Perspectives. Frontiers in Immunology. *13*(4). https://doi.org/10.3389/fimmu.2022.840245
- Denkers, N. D., Dahmes, S. J., Warren, R. J., Hayes-Klug, J., Seelig, D. M., Osborn, D. A., Miller, K. V., Haley, N. J., Anderson, K. R., Mathiason, C. K., & Hoover, E. A. (2012). Aerosol Transmission of Chronic Wasting Disease in White-Tailed Deer. Journal of Virology. 87(3): 1890–1892. https://doi.org/10.1128/jvi.02852-12
- Denkers, N. D., Hoover, E. A., & Telling, G. C. (2010). Minor Oral Lesions Facilitate Transmission of Chronic Wasting Disease. Journal of Virology. 85(3): 1396–1399. https://doi.org/10.1128/jvi.01655-10
- Didier, A., Bourner, M., Kleks, G., Zolty, A., Kumar, B., Nichols, T., Durynski, K., Bender, S., Gibison, M., Murphy, L., Ellis, J. C., Dong, D. W., & Kashina, A. (2024). Prospective fecal microbiomic biomarkers for chronic wasting disease. Microbiology Spectrum. 12 (3): e0375022. https://doi.org/10.1128/spectrum.03750-22

- Donaldson, D. S., Else, K. J., & Mabbott, N. A. (2015). The Gut-Associated Lymphoid Tissues in the Small Intestine, Not the Large Intestine, Play a Major Role in Oral Prion Disease Pathogenesis. Journal of virology. *89*(18): 9532–9547. https://doi.org/10.1128/JVI.01544-15
- Donaldson, D. S., Kobayashi, A., Ohno, H., Yagita, H., Williams, I. R., & Mabbott, N. A. (2012). M cell-depletion blocks oral prion disease pathogenesis. Mucosal immunology. *5*(2): 216–225. https://doi.org/10.1038/mi.2011.68
- Donaldson, D. S., Sehgal, A., Rios, D., Williams, I. R., & Mabbott, N. A. (2016). Increased Abundance of M Cells in the Gut Epithelium Dramatically Enhances Oral Prion Disease Susceptibility. PLoS pathogens. 12(12): e1006075. https://doi.org/10.1371/journal.ppat.1006075
- Duque Velásquez, C., Kim, C., Haldiman, T., Kim, C., Herbst, A., Aiken, J., Safar, J. G., & McKenzie, D. (2020). Chronic wasting disease (CWD) prion strains evolve via adaptive diversification of conformers in hosts expressing prion protein polymorphisms. The Journal of biological chemistry. 295(15): 4985–5001.
- Erny, D., Dokalis, N., Mezö, C., Castoldi, A., Mossad, O., Staszewski, O., Frosch, M., Villa, M., Fuchs, V., Mayer, A., Neuber, J., Sosat, J., Tholen, S., Schilling, O., Vlachos, A., Blank, T., Gomez de Agüero, M., Macpherson, A. J., Pearce, E. J., & Prinz, M. (2021). Microbiota-derived acetate enables the metabolic fitness of the brain innate immune system during health and disease. Cell metabolism. 33(11): 2260–2276.e7. https://doi.org/10.1016/j.cmet.2021.10.010
- Fox, K. A., Jewell, J. E., Williams, E. S., & Miller, M. W. (2006). Patterns of PrPCWD accumulation during the course of chronic wasting disease infection in orally inoculated mule deer (Odocoileus hemionus). The Journal of General Virology. 87 (Pt 11): 3451–3461. https://doi.org/10.1099/vir.0.81999-0

- Gilch, S., Chitoor, N., Stuart, M., Jewell, J. E., Schätzl, H. M., & Taguchi, Y. (2011). Chronic Wasting Disease (Vol. 305, pp. 51–77). Springer Berlin Heidelberg. https://doi.org/10.1007/128_2011_159
- Gray, J. G., Graham, C., Dudas, S., Paxman, E., Vuong, B., & Czub, S. (2016). Defining and Assessing Analytical Performance Criteria for Transmissible Spongiform Encephalopathy-Detecting Amyloid Seeding Assays. The Journal of molecular diagnostics (JMD) 18(3): 454–467. https://doi.org/10.1016/j.jmoldx.2016.01.005
- Hajian-Tilaki, K. (2013). Receiver Operating Characteristic (ROC) Curve Analysis for Medical Diagnostic Test Evaluation. Caspian Journal of Internal Medicine. 4(2).
- Haley, N. J., Mathiason, C. K., Carver, S., Zabel, M., Telling, G. C., & Hoover, E. A. (2011). Detection of Chronic Wasting Disease Prions in Salivary, Urinary, and Intestinal Tissues of Deer: Potential Mechanisms of Prion Shedding and Transmission. Journal of Virology. 85 (13): 6309. https://doi.org/10.1128/JVI.00425-11
- Haley, N. J., Telling, G. C., Hoover, E. A., Seelig, D. M., & Zabel, M. D. (2009). Detection of CWD Prions in Urine and Saliva of Deer by Transgenic Mouse Bioassay. PLoS ONE. 4(3): e4848. https://doi.org/10.1371/journal.pone.0004848
- Hamir, A. N., Miller, J. M., O'Rourke, K. I., Cutlip, R. C., Chaplin, M. J., Miller, M. W., Kunkle, R. A., Williams, E. S., Richt, J. A., & Stack, M. J. (2005). Experimental Transmission of Chronic Wasting Disease Agent from Mule Deer to Cattle by the Intracerebral Route. Journal of Veterinary Diagnostic Investigation. 17(3); 276–281. https://doi.org/10.1177/104063870501700313
- Hamir, A. N., Richt, J. A., Cutlip, R. C., Kunkle, R. A., Miller, J. M., & Williams, E. S. (2006). Transmission of Chronic Wasting Disease of Mule Deer to Suffolk Sheep following Intracerebral Inoculation. Journal of Veterinary Diagnostic Investigation. 18(6): 558–565. https://doi.org/10.1177/104063870601800606

- Heisey, D. M., Mickelsen, N. A., Johnson, C. J., Johnson, C. J., Bochsler, P. N., Barr, D. J., Keane, D. P., Schneider, J. R., & Langenberg, J. A. (2009). Chronic wasting disease (CWD) susceptibility of several North American rodents that are sympatric with cervid CWD epidemics. Journal of Virology 84 (1): 210–215. https://doi.org/10.1128/jvi.00560-09
- Henderson, D. M., Denkers, N. D., Hoover, C. E., McNulty, E. E., Cooper, S. K., Bracchi, L. A., Mathiason, C. K., & Hoover, E. A. (2020). Progression of chronic wasting disease in white-tailed deer analyzed by serial biopsy RT-QuIC and immunohistochemistry. PLoS One. 15 (2): e0228327. https://doi.org/10.1371/journal.pone.0228327
- Holz, C. L., Straka, K., Grosjean, N., Bolin, S., Sreevatsan, S., Kiupel, M., & Darish, J. R. (2022). Evaluation of Real-Time Quaking-Induced Conversion, ELISA, and Immunohistochemistry for Chronic Wasting Disease Diagnosis. Frontiers in Veterinary Science. 8: 824815 https://doi.org/10.3389/fvets.2021.824815
- Hoover, C. E., Davenport, K. A., Henderson, D. M., Denkers, N. D., Mathiason, C. K., Soto, C., Zabel, M. D., & Hoover, E. A. (2017). Pathways of Prion Spread during Early Chronic Wasting Disease in Deer. Journal of Virology. 91 (10): e00077-17. https://doi.org/10.1128/JVI.00077-17
- Imran, M., & Mahmood, S. (2011). An overview of human prion diseases. Virology Journal 8(1). https://doi.org/10.1186/1743-422x-8-559
- Johnson, C. J., Pedersen, J. A., Chappell, R. J., McKenzie, D., & Aiken, J. M. (2007). Oral transmissibility of prion disease is enhanced by binding to soil particles. PLoS pathogens. 3(7): e93. https://doi.org/10.1371/journal.ppat.0030093
- Klindworth, A., Peplies, J., Horn, M., Glöckner, F. O., Quast, C., Schweer, T., & Pruesse, E. (2012). Evaluation of general 16S ribosomal RNA gene PCR primers for classical and next-generation sequencing-based diversity studies. Nucleic Acids Research. 41(1): e1. https://doi.org/10.1093/nar/gks808

- Kobayashi, N., Takahashi, D., Takano, S., Kimura, S., & Hase, K. (2019). The Roles of Peyer's Patches and Microfold Cells in the Gut Immune System: Relevance to Autoimmune Diseases. Frontiers in immunology, 10, 2345. https://doi.org/10.3389/fimmu.2019.02345
- Konturek, P. C. (2005). *Helicobacter pylori*upregulates prion protein expression in gastric mucosa: A possible link to prion disease. World Journal of Gastroenterology 11(48): 7651. https://doi.org/10.3748/wjg.v11.i48.7651
- Koutsokostas, C., Merkouris, E., Goulas, A., Aidinopoulou, K., Sini, N., Dimaras, T., Tsiptsios, D., Mueller, C., Nystazaki, M., & Tsamakis, K. (2024). Gut Microbes Associated with Neurodegenerative Disorders: A Comprehensive Review of the Literature. Microorganisms. 12(8): 1735. https://doi.org/10.3390/microorganisms12081735
- Kujala, P., Raymond, C. R., Romeijn, M., Godsave, S. F., Van Kasteren, S. I., Wille, H., Prusiner, S. B., Mabbott, N. A., & Peters, P. J. (2011). Prion Uptake in the Gut: Identification of the First Uptake and Replication Sites. PLoS Pathogens. 7(12): e1002449. https://doi.org/10.1371/journal.ppat.1002449
- Kupfer, L., Hinrichs, W., & Groschup, M. H. (2009). Prion Protein Misfolding. Current Molecular Medicine. 9(7): 826–835. https://doi.org/10.2174/156652409789105543
- Kuznetsova, A., Aiken, J. M., Cullingham, C., Mckenzie, D., & Bartz, J. C. (2018). Soil humic acids degrade CWD prions and reduce infectivity. PLOS Pathogens. 14(11): e1007414. https://doi.org/10.1371/journal.ppat.1007414
- Kuznetsova, A., Mckenzie, D., Banser, P., Siddique, T., & Aiken, J. M. (2014). Potential role of soil properties in the spread of CWD in western Canada. Prion. 8(1): 92–99. https://doi.org/10.4161/pri.28467

- Li, B., Song, P., Liu, D., Zhang, T., Liang, C., Gao, H., Jiang, F., & Xu, B. (2022). Captivity Shifts Gut Microbiota Communities in White-Lipped Deer (Cervus albirostris). Animals. 12(4): 431. https://doi.org/10.3390/ani12040431
- Li, Y., Zhang, M., Qi, L., Xu, S., Yang, S., Lin, S., Zhou, J., Zhang, T., Fan, M., Hu, D., Liu, S., Sun, X., Cha, M., & Hu, X. (2017). Comparative Analysis of the Gut Microbiota Composition between Captive and Wild Forest Musk Deer. Frontiers in Microbiology. 8(26191). https://doi.org/10.3389/fmicb.2017.01705
- Lloyd, S., Mead, S., & Collinge, J. (2011). Genetics of Prion Disease, (Vol. 305, pp. 1–22). springer berlin heidelberg. https://doi.org/10.1007/128_2011_157
- Loeuillet, C., Boelle, P. Y., Lemaire-Vieille, C., Baldazza, M., Naquet, P., Chambon, P., Cesbron-Delauw, M. F., Valleron, A. J., Gagnon, J., & Cesbron, J. Y. (2010). Sex effect in mouse and human prion disease. The Journal of infectious diseases. 202(4): 648–654. https://doi.org/10.1086/654818
- Losa, R., Ghiboub, M., Phan, J., Tang, S.-C., Bennett, R. E., Höllerhage, M., & Soto, C. (2024). Longitudinal microbiome investigation throughout prion disease course reveals pre- and symptomatic compositional perturbations linked to short-chain fatty acid metabolism and cognitive impairment in mice. Frontiers in Microbiology. 15:1339437. https://doi.org/10.3389/fmicb.2024.1339437
- Mabbott, N. A., Bradford, B. M., Pal, R., Young, R., & Donaldson, D. S. (2020). The Effects of Immune System Modulation on Prion Disease Susceptibility and Pathogenesis. International journal of molecular sciences. 21(19): 7299. https://doi.org/10.3390/ijms21197299
- Mandrekar, J. N. (2010). Receiver Operating Characteristic Curve in Diagnostic Test Assessment. Journal of Thoracic Oncology, 5(9), 1315–1316. https://doi.org/10.1097/jto.0b013e3181ec173d

- Mathiason CK. Large animal models for chronic wasting disease. Cell Tissue Res. 2023 Apr;392(1):21-31. doi: 10.1007/s00441-022-03590-4. Epub 2022 Feb 3. PMID: 35113219; PMCID: PMC8811588.
- Miller, M. W., Wild, M. A., & Williams, E. S. (1998). Epidemiology of chronic wasting disease in captive Rocky Mountain elk. Journal of Wildlife Diseases. 34 (3): 532–538. https://doi.org/10.7589/0090-3558-34.3.532
- Minich, D., Madden, C., Evans, M. V., Hale, V. L., Barr, D. J., Ballash, G. A., Poulsen, K. P., & Dennis, P. M. (2021). Alterations in gut microbiota linked to provenance, sex, and chronic wasting disease in white-tailed deer (Odocoileus virginianus). Scientific Reports. 11 (1). https://doi.org/10.1038/s41598-021-89896-9
- Moazami-Goudarzi, K., Andréoletti, O., Béringue, V., & Vilotte, J.-L. (2021). Review on PRNP genetics and susceptibility to chronic wasting disease of Cervidae. Veterinary Research. 52(1). https://doi.org/10.1186/s13567-021-00993-z
- Moazami-Goudarzi, K., Béringue, V., Andréoletti, O., & Vilotte, J.-L. (2021). Review on PRNP genetics and susceptibility to chronic wasting disease of Cervidae. Veterinary Research. 52(1). https://doi.org/10.1186/s13567-021-00993-z
- Nalls, A. V., Crum, J. M., Hoover, E. A., Ruder, M. G., Mayfield, A., Keel, M. K., Mcnulty, E. E., & Mathiason, C. K. (2021). Detection of Chronic Wasting Disease Prions in Fetal Tissues of Free-Ranging White-Tailed Deer. Viruses. 13 (12): 2430. https://doi.org/10.3390/v13122430
- Nichols, T. A., Hoover, E., Bian, J., Vercauteren, K. C., Hoover, C., Zabel, M. D., Michel, B., Rigg, T. D., Balachandran, A., Spraker, T. R., Gidlewski, T., Bowen, R., O'Rourke, K., Telling, G. C., & Meyerett-Reid, C. (2013). Intranasal Inoculation of White-Tailed Deer (Odocoileus virginianus) with Lyophilized Chronic Wasting Disease Prion Particulate Complexed to Montmorillonite Clay. PLoS ONE. 8(5): e62455. https://doi.org/10.1371/journal.pone.0062455

- O'Riordan, K. J., Moloney, G. M., Keane, L., Clarke, G., & Cryan, J. F. (2025). The gut microbiota-immune-brain axis: Therapeutic implications. Cell Reports. Medicine. 6(3): 101982. https://doi.org/10.1016/j.xcrm.2025.101982
- Orge, L., Lima, C., Machado, C., Tavares, P., Mendonça, P., Carvalho, P., Silva, J., Pinto, L., Bastos, E., Pereira, J. C., Gonçalves-Anjo, N., Gama, A., Esteves, A., Alves, A., Matos, A. C., Seixas, F., Silva, F., Pires, I., Figueira, L., Pires, A. (2021). Neuropathology of Animal Prion Diseases. Biomolecules. 11 (3): 466. https://doi.org/10.3390/biom11030466
- Orrú CD, Hughson AG, Groveman BR, Campbell KJ, Anson KJ, Manca M, Kraus A, Caughey B. (2016). Factors That Improve RT-QuIC Detection of Prion Seeding Activity. Viruses. 8(5):140. doi: 10.3390/v8050140. PMID: 27223300; PMCID: PMC4885095.
- Osterholm, M. T., Scheftel, J. M., Moore, K. A., Appleby, B. S., Anderson, C. J., & Zabel, M. D. (2019). Chronic Wasting Disease in Cervids: Implications for Prion Transmission to Humans and Other Animal Species. MBio. 10 (4). https://doi.org/10.1128/mbio.01091-19
- Otero, A., Mckenzie, D., Velásquez, C. D., & Aiken, J. (2021). Chronic wasting disease: a cervid prion infection looming to spillover. Veterinary Research. 52(1). https://doi.org/10.1186/s13567-021-00986-y
- Peden, A. H., Will, R. G., Mcguire, L. I., Head, M. W., Mallinson, G., Ironside, J. W., Knight, R. S., Appleford, N. E. J., Orrú, C. D., Wilham, J. M., Green, A. J. E., & Caughey, B. (2012). Sensitive and specific detection of sporadic Creutzfeldt–Jakob disease brain prion protein using real-time quaking-induced conversion. Journal of General Virology. 93(2): 438–449. https://doi.org/10.1099/vir.0.033365-0
- Plummer, I. H., Samuel, M. D., Chesney, A. R., Johnson, C. J., & Pedersen, J. A. (2018). Mineral licks as environmental reservoirs of chronic wasting disease prions. PLOS ONE. 13(5): e0196745. https://doi.org/10.1371/journal.pone.0196745

- Prasad, K. N., & Bondy, S. C. (2018). Oxidative and Inflammatory Events in Prion Diseases: Can they Be Therapeutic Targets? Current Aging Science. 11 (4): 216. https://doi.org/10.2174/1874609812666190111100205
- Prusiner SB (1982). Novel proteinaceous infectious particles cause scrapie. Science. 216(4542):136-144. doi: 10.1126/science.6801762. PMID: 6801762.
- Prusiner, S. B., Scott, M. R., DeArmond, S. J., & Cohen, F. E. (1998). Prion protein biology. Cell. 93 (3): 337–348. https://doi.org/10.1016/s0092-8674(00)81163-0
- Prusiner, S. B., Scott, M., Foster, D., Pan, K. M., Groth, D., Mirenda, C., Torchia, M., Yang, S. L., Serban, D., & Carlson, G. A. (1990). Transgenetic studies implicate interactions between homologous PrP isoforms in scrapie prion replication. Cell. 63 (4): 673–686. https://doi.org/10.1016/0092-8674(90)90134-z
- Quast C, Pruesse E, Yilmaz P, Gerken J, Schweer T, Yarza P, Peplies J, Glöckner FO. The SILVA ribosomal RNA gene database project: improved data processing and web-based tools. Nucleic Acids Res. 2013 Jan; 41(Database issue): D590-6. doi: 10.1093/nar/gks1219. Epub 2012 Nov 28. PMID: 23193283; PMCID: PMC3531112.
- Race, B., Race, R., Chesebro, B., Williams, E. S., Parnell, M., Priola, S. A., Barbian, K. D., Striebel, J., Cervenakova, L., Favara, C., Gardner, D., Rubenstein, R., Lafauci, G., Meade-White, K. D., Miller, M. W., Ward, A., & Long, D. (2009). Susceptibilities of Non-human Primates to Chronic Wasting Disease. Emerging Infectious Diseases. 15 (9): 1366–1376. https://doi.org/10.3201/eid1509.090253
- Recharla, N., Geesala, R., & Shi, X.-Z. (2023). Gut Microbial Metabolite Butyrate and Its Therapeutic Role in Inflammatory Bowel Disease: A Literature Review. Nutrients. 15(10): 2275. https://doi.org/10.3390/nu15102275

- Richards B. Distribution of chronic wasting disease in north america [USGS-NWRC]. 2023 Dec 10. Available from: https://www.usgs.gov/media/images/distribution-chronic-wasting-disease-north-america-0
- Robinson, S. J., Samuel, M. D., O'Rourke, K. I., & Johnson, C. J. (2012). The role of genetics in chronic wasting disease of North American cervids. Prion. 6(2): 153–162. https://doi.org/10.4161/pri.19640
- Schmitz, M., Collins, S., Orrù, C. D., Caughey, B., Satoh, K., Schulz-Schaeffer, W. J., Atarashi, R., Llorens, F., Cramm, M., Zerr, I., Zafar, S., Groveman, B. R., & Müller-Cramm, D. (2016). The real-time quaking-induced conversion assay for detection of human prion disease and study of other protein misfolding diseases. Nature Protocols. 11(11): 2233–2242. https://doi.org/10.1038/nprot.2016.120
- Seelig, D. M., Mason, G. L., Telling, G. C., & Hoover, E. A. (2010). Pathogenesis of chronic wasting disease in cervidized transgenic mice. The American journal of pathology. 176 (6): 2785–2797. https://doi.org/10.2353/ajpath.2010.090710
- Shin, N.-R., Whon, T. W., & Bae, J.-W. (2015). Proteobacteria: microbial signature of dysbiosis in gut microbiota. Trends in Biotechnology. 33(9): 496–503. https://doi.org/10.1016/j.tibtech.2015.06.011
- Sigurdson, C. J. (2008). A prion disease of cervids: Chronic wasting disease. Veterinary Research. 39(4): 41. https://doi.org/10.1051/vetres:2008018
- Sigurdson, C. J., Bartz, J. C., & Glatzel, M. (2018). Cellular and Molecular Mechanisms of Prion Disease. Annual Review of Pathology. 14: 497. https://doi.org/10.1146/annurev-pathmechdis-012418-013109
- Sigurdson, C. J., Williams, E. S., Miller, M. W., Spraker, T. R., O'Rourke, K. I., & Hoover, E. A. (1999). Oral transmission and early lymphoid tropism of chronic wasting disease PrPres in mule deer

fawns (Odocoileus hemionus). The Journal of general virology. 80 (Pt 10): 2757–2764. https://doi.org/10.1099/0022-1317-80-10-2757

- Silva CJ (2022). Chronic Wasting Disease (CWD) in Cervids and the Consequences of a Mutable Protein Conformation. ACS Omega. 7(15):12474-12492. doi: 10.1021/acsomega.2c00155. PMID: 35465121; PMCID: PMC9022204.
- Sing, T., Sander, O., Beerenwinkel, N., & Lengauer, T. (2005). ROCR: visualizing classifier performance in R. Bioinformatics (Oxford, England). 21(20): 3940–3941. https://doi.org/10.1093/bioinformatics/bti623
- Sommer, F., & Bäckhed, F. (2013). The gut microbiota--masters of host development and physiology. Nature reviews. Microbiology. 11(4): 227–238. https://doi.org/10.1038/nrmicro2974
- Soto, C. (2012). Transmissible Proteins: Expanding the Prion Heresy. Cell. 149(5): 968–977. https://doi.org/10.1016/j.cell.2012.05.007
- Soto, C., & Satani, N. (2010). The intricate mechanisms of neurodegeneration in prion diseases. Trends in Molecular Medicine. 17(1): 14–24. https://doi.org/10.1016/j.molmed.2010.09.001
- Sun, J. L., Crowell, J., Korpenfelt, S.-L., Lowe, D. C., Kim, S., Webster, B. K., Bian, J., Benestad, S. L., Telling, G. C., & Raisley, E. K. (2023). Novel Prion Strain as Cause of Chronic Wasting Disease in a Moose, Finland. Emerging Infectious Diseases. 29 (2): 323–332. https://doi.org/10.3201/eid2902.220882
- Takakura, I., Miyazawa, K., Kanaya, T., Itani, W., Watanabe, K., Ohwada, S., Watanabe, H., Hondo, T., Rose, M. T., Mori, T., Sakaguchi, S., Nishida, N., Katamine, S., Yamaguchi, T., & Aso, H. (2011). Orally Administered Prion Protein Is Incorporated by M Cells and Spreads into Lymphoid Tissues with Macrophages in Prion Protein Knockout Mice. The American Journal of Pathology. 179(3): 1301–1309. https://doi.org/10.1016/j.ajpath.2011.05.058

- Thaiss, C. A., Zmora, N., Levy, M., & Elinav, E. (2016). The microbiome and innate immunity. Nature. 535(7610): 65–74. https://doi.org/10.1038/nature18847
- Tingler, A. M., & Engevik, M. A. (2025). Breaking down barriers: is intestinal mucus degradation by Akkermansia muciniphila beneficial or harmful? Infection and Immunity. https://doi.org/10.1128/iai.00503-24
- Trichka, J., & Zou, W.-Q. (2021). Modulation of Neuroinflammation by the Gut Microbiota in Prion and Prion-Like Diseases. Pathogens, 10(7), 887. https://doi.org/10.3390/pathogens10070887
- Trichka, J., & Zou, W.-Q. (2021). Modulation of Neuroinflammation by the Gut Microbiota in Prion and Prion-Like Diseases. Pathogens. 10(7): 887. https://doi.org/10.3390/pathogens10070887
- Unal I. (2017). Defining an Optimal Cut-Point Value in ROC Analysis: An Alternative Approach. Computational and mathematical methods in medicin., 2017: 3762651. https://doi.org/10.1155/2017/3762651
- Vanderperre, B., Tremblay, G., Mccoy, M., Cashman, N. R., Staskevicius, A. B., O'Neill, M. A., & Roucou, X. (2011). An overlapping reading frame in the, PRNP, gene encodes a novel polypeptide distinct from the prion protein. The FASEB Journal. 25(7): 2373–2386. https://doi.org/10.1096/fj.10-173815
- Wahlström, A., Sayin, S. I., Marschall, H. U., & Bäckhed, F. (2016). Intestinal Crosstalk between Bile Acids and Microbiota and Its Impact on Host Metabolism. Cell metabolism. 24(1): 41–50. https://doi.org/10.1016/j.cmet.2016.05.005
- Wang, F., Gu, Y., Zhao, Y., Xu, C., Zhao, C., Du, K., & Liu, X. (2022). Transplantation of fecal microbiota from APP/PS1 mice and Alzheimer's disease patients enhanced endoplasmic

reticulum stress in the cerebral cortex of wild-type mice. *Frontiers in Aging Neuroscience*. *14*. https://doi.org/10.3389/fnagi.2022.858130

- Williams E. S. (2005). Chronic wasting disease. Veterinary pathology. 42 (5): 530–549. https://doi.org/10.1354/vp.42-5-530
- Williams, E. S., & Young, S. (1980). Chronic wasting disease of captive mule deer: a spongiform encephalopathy. Journal of Wildlife Diseases. 16(1): 89–98. https://doi.org/10.7589/0090-3558-16.1.89
- Yang, D., Zhao, D., Shah, S. Z. A., Wu, W., Lai, M., Zhang, X., Li, J., Guan, Z., Zhao, H., Li, W., Gao, H., Zhou, X., & Yang, L. (2019). Implications of gut microbiota dysbiosis and metabolic changes in prion disease. Neurobiology of Disease. 135: 104704. https://doi.org/10.1016/j.nbd.2019.104704
- Yilmaz, G., Morrill, T., Pilot, W., Ward, C., Mitchell, G., Soutyrine, A., Dan, H., Lin, M., & Guan, J. (2024). Optimization of RT-QuIC Assay Duration for Screening Chronic Wasting Disease in White-Tailed Deer. Veterinary Sciences. 11 (2): 60. https://doi.org/10.3390/vetsci11020060
- You, Z., Xiong, H., Deng, J., Fu, J., Luo, W., Liu, J., & Xiong, J. (2022). Seasonal variations in the composition and diversity of gut microbiota in white-lipped deer (Cervus albirostris). Zoological Science 10(6): e13753. https://doi.org/10.7717/peerj.13753
- Zabel, M. D., & Reid, C. (2015). A brief history of prions. Pathogens and Disease. 73(9): ftv087. https://doi.org/10.1093/femspd/ftv087
- Zayed, M., Jeong, B.-H., & Kook, S.-H. (2023). Potential Therapeutic Use of Stem Cells for Prion Diseases. Cells. 12(19): 2413. https://doi.org/10.3390/cells12192413
- Zhang, X., Shao, Y., Tian, J., Liao, Y., Li, P., Zhang, Y., Chen, J., & Li, Z. (2019). pTrimmer: An efficient tool to trim primers of multiplex deep sequencing data. BMC Bioinformatics. 20(1). https://doi.org/10.1186/s12859-019-2854-x

- Zhao, G., Tang, W., Wang, Q., Mishra, S. K., Ma, T., Jie, H., Li, D., & Xu, Z. (2019). Gut Microbiome of Chinese Forest Musk Deer Examined across Gender and Age. BioMed Research International. 2019(1): 1–10. https://doi.org/10.1155/2019/9291216
- Zhu, C., & Aguzzi, A. (2021). Prion protein and prion disease at a glance. Journal of Cell Science. 134(17). https://doi.org/10.1242/jcs.245605

Supplementary Materials

S1. Supplementary Data 2. RT-QuIC threshold outcomes and corresponding brain IHC results for intragastrically inoculated (IG) TgElkPrP mice.

Inoculation Route & Target Incubation Date	Sample ID	Treatment	Sex	Inoculation Date	Date of Death	Weeks Survived Post Inoculation	Tissue	RT-QuIC Result	IHC Result
IG56	5259	Infected	M	2022-07-27	2023-08-03	53	Brain	NEG	NEG
							Intestine	POS	-
							Spleen	NEG	-
IG56	5260	Infected	M	2022-07-27	2023-08-21	56	Brain	NEG	NEG
							Intestine	NEG	-
							Spleen	NEG	-
IG56	5261	Infected	M	2022-07-27	2023-08-03	53	Intestine	NEG	-
							Spleen	NEG	-
IG56	5262	Infected	M	2022-07-27	2023-08-21	56	Brain	NEG	NEG
							Intestine	POS	-
							Spleen	NEG	-
IG56	5263	Infected	M	2022-07-27	2023-08-21	56	Brain	NEG	-
							Intestine	NEG	-
							Spleen	NEG	
IG56	5264	Infected	M	2022-07-27	2023-03-06	32	Brain	POS	POS
							Intestine	POS	POS
							Spleen	POS	POS
IG56	5265	Infected	F	2022-07-27	2023-06-09	45	Brain	NEG	NEG
							Intestine	NEG	-
							Spleen	NEG	-
IG56	5267	Infected	F	2022-07-27	2023-05-24	43	Brain	NEG	NEG
							Intestine	NEG	-
							Spleen	NEG	-
IG56	5268	Infected	F	2022-07-27	2023-05-02	40	Intestine	POS	-
							Spleen	NEG	-
IG56	5269	Infected	F	2022-07-27	2023-06-09	45	Brain	NEG	NEG
							Intestine	NEG	-
							Spleen	NEG	-
IG56	5270	Infected	F	2022-07-27	2023-03-21	34	Brain	POS	POS
							Intestine	POS	POS
							Spleen	POS	POS
IG56	5271	Control	M	2022-07-27	2022-09-23	8	Brain	NEG	NEG
							Intestine	NEG	-
							Spleen	NEG	-
IG56	5272	Control	M	2022-07-27	2023-08-21	56	Brain	NEG	NEG
							Intestine	POS	-
							Spleen	NEG	-
IG56	5273	Control	M	2022-07-27	2023-08-21	56	Brain	NEG	NEG
							Intestine	NEG	-
							Spleen	NEG	-
IG56	5275	Control	M	2022-07-27	2022-10-19	12	Brain	NEG	NEG
							Intestine	NEG	-
							Spleen	NEG	-
IG56	5276	Control	F	2022-07-27	2023-05-23	43	Brain	NEG	NEG
							Intestine	NEG	-
							Spleen	NEG	-
IG56	5277	Control	F	2022-07-27	2023-08-21	56	Brain	NEG	NEG
							Intestine	NEG	-
							Spleen	NEG	-
IG56	5278	Control	F	2022-07-27	2022-09-27	9	Brain	NEG	NEG
							Intestine	NEG	-
							Spleen	NEG	-
IG56	5279	Control	F	2022-07-27	2023-08-21	56	Brain	NEG	NEG
							Intestine	NEG	-
							Spleen	NEG	-
IG56	5280	Control	F	2022-07-27	2023-07-29	52	Intestine	NEG	-
							Spleen	NEG	-

IG48	5281	Infected	F	2022-08-31	2023-07-31	48	Brain	NEG	NEG
							Intestine	NEG	-
							Spleen	NEG	-
IG48	5282	Infected	F	2022-08-31	2023-07-22	46	Intestine	NEG	-
							Spleen	NEG	-
IG48	5283	Infected	M	2022-08-31	2023-07-31	48	Brain	NEG	NEG
							Intestine	NEG	-
							Spleen	NEG	-
IG48	5284	Infected	M	2022-08-31	2022-11-14	11	Intestine	NEG	-
							Spleen	NEG	-
IG48	5285	Infected	M	2022-08-31	2023-07-31	48	Brain	NEG	NEG
							Intestine	NEG	-
							Spleen	NEG	-
IG48	5286	Infected	M	2022-08-31	2023-07-31	48	Brain	NEG	NEG
							Intestine	NEG	-
							Spleen	NEG	-
IG48	5287	Infected	M	2022-08-31	2023-07-31	48	Brain	NEG	NEG
							Intestine	NEG	-
							Spleen	NEG	-
IG48	5288	Infected	F	2022-08-31	2023-07-12	45	Intestine	NEG	-
							Spleen	NEG	-
IG48	5289	Infected	F	2022-08-31	2023-07-05	44	Intestine	NEG	-
							Spleen	NEG	-
IG48	5290	Infected	F	2022-08-31	2023-04-04	31	Brain	POS	POS
							Intestine	POS	POS
							Spleen	POS	POS
IG48	5291	Control	M	2022-08-31	2023-07-13	45	Intestine	NEG	-
							Spleen	NEG	-
IG48	5292	Control	M	2022-08-31	2023-04-18	33	Intestine	NEG	-
							Spleen	NEG	-
IG48	5293	Control	M	2022-08-31	2022-11-23	12	Brain	NEG	NEG
							Intestine	NEG	-
							Spleen	NEG	-
IG48	5294	Control	M	2022-08-31	2023-07-31	48	Brain	NEG	NEG
							Intestine	NEG	-
							Spleen	NEG	-
IG48	5295	Control	F	2022-08-31	2023-07-31	48	Brain	NEG	NEG
							Intestine	NEG	-
							Spleen	NEG	-
IG48	5296	Control	F	2022-08-31	2023-07-31	48	Brain	NEG	NEG
							Intestine	NEG	-
							Spleen	NEG	-
IG48	5297	Control	F	2022-08-31	2023-07-31	48	Brain	NEG	NEG
							Intestine	NEG	-
							Spleen	NEG	-
IG48	5298	Control	F	2022-08-31	2023-07-31	48	Brain	NEG	NEG
							Intestine	NEG	-
							Spleen	NEG	-

IG40	5315	Infected	F	2022-10-12	2023-07-17	40	Brain	NEG	NEG
							Intestine	NEG	-
							Spleen	NEG	-
IG40	5316	Infected	F	2022-10-12	2023-07-17	40	Brain	NEG	NEG
							Intestine	NEG	-
							Spleen	NEG	-
IG40	5317	Infected	F	2022-10-12	2023-07-10	39	Intestine	NEG	-
							Spleen	NEG	-
IG40	5318	Infected	F	2022-10-12	2023-05-24	32	Brain	POS	POS
							Intestine	POS	POS
							Spleen	POS	POS
IG40	5319	Control	F	2022-10-12	2023-07-17	40	Brain	NEG	NEG
							Intestine	NEG	-
							Spleen	NEG	-
IG40	5320	Infected	F	2022-10-12	2023-07-17	40	Brain	NEG	NEG
							Intestine	NEG	-
							Spleen	NEG	-
IG40	5321	Infected	F	2022-10-12	2023-07-17	40	Brain	NEG	NEG
							Intestine	NEG	-
							Spleen	NEG	-
IG40	5322	Control	F	2022-10-12	2023-07-17	40	Brain	NEG	NEG
							Intestine	NEG	-
							Spleen	NEG	-
IG40	5323	Infected	M	2022-10-12	2023-07-17	40	Brain	NEG	NEG
							Intestine	NEG	-
							Spleen	NEG	-
IG40	5324	Infected	M	2022-10-12	2023-07-17	40	Brain	NEG	NEG
							Intestine	NEG	-
							Spleen	NEG	-
IG40	5325	Infected	M	2022-10-12	2023-07-17	40	Brain	NEG	NEG
							Intestine	NEG	-
							Spleen	NEG	-
IG40	5326	Control	M	2022-10-12	2023-07-17	40	Brain	NEG	NEG
							Intestine	NEG	-
							Spleen	NEG	-
IG40	5327	Infected	M	2022-10-12	2023-07-17	40	Brain	NEG	NEG
							Intestine	NEG	-
							Spleen	NEG	-
IG40	5328	Infected	M	2022-10-12	2023-07-17	40	Brain	NEG	NEG
							Intestine	NEG	-
							Spleen	NEG	-
IG40	5329	Control	M	2022-10-12	2023-07-17	40	Brain	NEG	NEG
							Intestine	NEG	-
							Spleen	NEG	-
IG40	5330	Control	M	2022-10-12	2023-07-17	40	Brain	NEG	NEG
							Intestine	NEG	-
							Spleen	NEG	-

S2. Raw RT-QuIC fluorescence data for intragastrically inoculated (IG) TgElkPrP mice: brain, spleen, and small-intestine tissues.

Inoculation Route & Target Incubation Date	Sample ID	Treatment	Sex	Inoculation Date	Date of Death	Weeks Survived Post Inoculation	Tissue	Replicate 1	Replicate 2	Replicate 3	Replicate 4
IG56	5259	Infected	M	2022-07-27	2023-08-03	53	Brain	60	60	60	60
							Intestine	19.307	26.394	60	17.618
							Spleen	60	60	60	60
IG56	5260	Infected	M	2022-07-27	2023-08-21	56	Brain	60	60	60	60
							Intestine	43.588	33.4529	31.289	28.127
							Spleen	60	60	60	60
IG56	5261	Infected	M	2022-07-27	2023-08-03	53	Intestine	60	60	60	60
							Spleen	52.584	60	58.704	60
IG56	5262	Infected	M	2022-07-27	2023-08-21	56	Brain	60	60	60	60
							Intestine	13.8622	28.427	33.686	30.36
							Spleen	60	60	60	60
IG56	5263	Infected	M	2022-07-27	2023-08-21	56	Brain	60	60	60	60
							Intestine	24.817	32.606	29.255	36.6
							Spleen	60	60	60	60
IG56	5264	Infected	M	2022-07-27	2023-03-06	32	Brain	19.27814	17.05982	14.64306	23.3032
							Intestine	7.526	9.898	10.273	9.155
							Spleen	10.208	14.819	12.376	14.173
IG56	5265	Infected	F	2022-07-27	2023-06-09	45	Brain	60	60	60	60
							Intestine	57.718	51.671	60	55.518
							Spleen	60	60	60	60
IG56	5267	Infected	F	2022-07-27	2023-05-24	43	Brain	60	60	60	60
							Intestine	19.218	40.634	38.29	60
							Spleen	60	60	60	60
IG56	5268	Infected	F	2022-07-27	2023-05-02	40	Intestine	36.317	12.318	30.216	20.488
							Spleen	23.317	32.711	40.3811	32.492
IG56	5269	Infected	F	2022-07-27	2023-06-09	45	Brain	60	60	60	60
							Intestine	60	60	60	60
							Spleen	60	60	60	60
IG56	5270	Infected	F	2022-07-27	2023-03-21	34	Brain	58.33042	27.65625	23.59935	39.32757
							Intestine	10.049	12.095	12.241	11.158
							Spleen	26.675	60	60	60
IG56	5271	Control	M	2022-07-27	2022-09-23	8	Brain	60	60	60	60
							Intestine	31.306	42.727	35.314	37.382
							Spleen	60	60	60	60
IG56	5272	Control	M	2022-07-27	2023-08-21	56	Brain	60	60	60	60
							Intestine	8.0531	23.6381	22.346	16.682
							Spleen	51.547	60	60	60
IG56	5273	Control	M	2022-07-27	2023-08-21	56	Brain	60	56.669	59.316	48.987
							Intestine	30.298	33.622	42.047	30.254
							Spleen	60	23.353	60	41.607
IG56	5275	Control	M	2022-07-27	2022-10-19	12	Brain	60	60	60	60
							Intestine	52.725	41.423	37.543	38.021
							Spleen	60	60	60	60
IG56	5276	Control	F	2022-07-27	2023-05-23	43	Brain	60	60	60	60
							Intestine	60	60	60	60
							Spleen	60	60	60	60
IG56	5277	Control	F	2022-07-27	2023-08-21	56	Brain	60	60	60	60
							Intestine	37.381	46.45	33.428	39.92
							Spleen	53.718	60	60	39.304
IG56	5278	Control	F	2022-07-27	2022-09-27	9	Brain	60	60	60	60
							Intestine	40.325	49.391	38.398	59.953
							Spleen	60	60	60	60
IG56	5279	Control	F	2022-07-27	2023-08-21	56	Brain	17.356	52.26	55.448	47.693
							Intestine	41.106	9.89	42.405	44.61
							Spleen	60	60	60	60
IG56	5280	Control	F	2022-07-27	2023-07-29	52	Intestine	60	22.28	60	60
							Spleen	60	60	60	60

IG48	5281	Infected	F	2022-08-31	2023-07-31	48	Brain	60	60	60	60
							Intestine	60	60	60	60
							Spleen	60	60	60	60
IG48	5282	Infected	F	2022-08-31	2023-07-22	46	Intestine	26.616	58.272	43.977	60
							Spleen	60	60	60	60
IG48	5283	Infected	M	2022-08-31	2023-07-31	48	Brain	60	60	60	60
							Intestine	60	50.364	60	60
							Spleen	60	60	60	60
IG48	5284	Infected	M	2022-08-31	2022-11-14	11	Intestine	46.737	17.252	42.53	52.479
							Spleen	60	60	60	60
IG48	5285	Infected	M	2022-08-31	2023-07-31	48	Brain	60	60	60	60
							Intestine	60	60	60	60
							Spleen	60	60	60	60
IG48	5286	Infected	M	2022-08-31	2023-07-31	48	Brain	60	60	60	60
							Intestine	44.7034	29.552	29.576	51.396
							Spleen	60	60	60	60
IG48	5287	Infected	M	2022-08-31	2023-07-31	48	Brain	60	60	60	60
							Intestine	60	60	14.996	29.616
							Spleen	60	46.375	60	60
IG48	5288	Infected	F	2022-08-31	2023-07-12	45	Intestine	60	60	41.774	45.26
							Spleen	60	60	60	60
IG48	5289	Infected	F	2022-08-31	2023-07-05	44	Intestine	46.507	60	60	60
							Spleen	60	60	60	60
IG48	5290	Infected	F	2022-08-31	2023-04-04	31	Brain	31.304	25.579	25.365	18.618
							Intestine	3.1587	8.225	12.608	11.672
							Spleen	13.56	12.635	10.009	10.199
IG48	5291	Control	M	2022-08-31	2023-07-13	45	Intestine	60	52.401	60	60
							Spleen	31.358	36.033	31.449	60
IG48	5292	Control	M	2022-08-31	2023-04-18	33	Intestine	60	60	32.526	59.578
							Spleen	60	60	60	60
IG48	5293	Control	M	2022-08-31	2022-11-23	12	Brain	60	60	60	60
							Intestine	60	60	60	60
							Spleen	60	60	60	60
IG48	5294	Control	M	2022-08-31	2023-07-31	48	Brain	26.741	47.43	29.386	56.551
							Intestine	38.8	40.818	60	60
							Spleen	60	60	60	60
IG48	5295	Control	F	2022-08-31	2023-07-31	48	Brain	60	60	60	60
							Intestine	60	60	60	60
							Spleen	60	60	60	60
IG48	5296	Control	F	2022-08-31	2023-07-31	48	Brain	30.399	60	36.924	60
							Intestine	40.449	44.685	53.338	53.34
							Spleen	60	60	60	60
IG48	5297	Control	F	2022-08-31	2023-07-31	48	Brain	60	60	49.777	60
							Intestine	36.38	60	60	58.134
							Spleen	60	60	60	60
IG48	5298	Control	F	2022-08-31	2023-07-31	48	Brain	60	60	60	60
							Intestine	35.251	60	60	60
							Spleen	60	60	60	60

IG40	5315	Infected	F	2022-10-12	2023-07-17	40	Brain	31.445	33.295	60	58.374
							Intestine	20.311	20.773	39.371	35.484
							Spleen	60	60	60	60
IG40	5316	Infected	F	2022-10-12	2023-07-17	40	Brain	31.886	24.296	60	60
							Intestine	21.688	27.679	32.299	40.582
							Spleen	60	60	60	60
IG40	5317	Infected	F	2022-10-12	2023-07-10	39	Intestine	39.348	15.345	32.625	37.278
							Spleen	60	60	60	60
IG40	5318	Infected	F	2022-10-12	2023-05-24	32	Brain	17.356	5.9	23.327	13.234
							Intestine	11.971	11.122	14.963	15.345
							Spleen	13.217	14.102	16.553	14.243
IG40	5319	Control	F	2022-10-12	2023-07-17	40	Brain	60	60	60	60
							Intestine	22.519	30.26	30.489	39.371
							Spleen	45.446	60	60	60
IG40	5320	Infected	F	2022-10-12	2023-07-17	40	Brain	33.635	55.623	48.697	45.678
							Intestine	22.621	29.597	41.5	36.329
							Spleen	60	60	60	60
IG40	5321	Infected	F	2022-10-12	2023-07-17	40	Brain	60	60	60	33.712
							Intestine	27.344	29.362	60	48.453
							Spleen	60	60	60	60
IG40	5322	Control	F	2022-10-12	2023-07-17	40	Brain	60	60	60	60
							Intestine	18.338	22.284	29.616	35.577
							Spleen	60	60	60	60
IG40	5323	Infected	M	2022-10-12	2023-07-17	40	Brain	58.291	52.81	53.322	30.452
							Intestine	23.3047	33.477	50.649	40.116
							Spleen	60	60	60	60
IG40	5324	Infected	M	2022-10-12	2023-07-17	40	Brain	60	60	60	60
							Intestine	16.767	20.468	37.335	37.512
							Spleen	60	60	60	60
IG40	5325	Infected	M	2022-10-12	2023-07-17	40	Brain	60	60	60	60
							Intestine	19.278	26.355	36.499	42.627
							Spleen	60	60	60	60
IG40	5326	Control	M	2022-10-12	2023-07-17	40	Brain	60	60	60	60
							Intestine	54.364	15.209	46.321	48.784
							Spleen	60	60	60	60
IG40	5327	Infected	M	2022-10-12	2023-07-17	40	Brain	60	60	60	60
							Intestine	58.453	60	55.627	59.523
							Spleen	35.646	52.318	60	60
IG40	5328	Infected	M	2022-10-12	2023-07-17	40	Brain	60	60	60	60
							Intestine	27.738	15.348	38.669	26.371
							Spleen	60	60	60	60
IG40	5329	Control	M	2022-10-12	2023-07-17	40	Brain	60	60	60	60
							Intestine	21.311	16.883	28.425	44.304
							Spleen	60	60	60	60
IG40	5330	Control	M	2022-10-12	2023-07-17	40	Brain	46.582	43.341	60	60
							Intestine	30.713	23.772	24.265	49.233
							Spleen	60	60	60	60

S3. Supplementary Data 1. Supplementary Data 2. RT-QuIC threshold outcomes and corresponding brain IHC results for intracerebrally inoculated (IC) TgElkPrP mice.

Inoculation Route & Target Incubation Date	Sample ID	Treatment	Sex	Inoculation Date	Date of Death	Weeks survived Post Inoculation	Tissue	RT-QuIC Result	IHC Result
IC 24	TSE 5448	infected	F	2024-05-01	2024-08-29	17	Brain	POS	POS
							Small Intestine	POS	-
							Spleen	POS	-
IC 24	TSE 5449	infected	F	2024-05-01	2024-08-16	15	Brain	POS	POS
							Small Intestine	POS	-
							Spleen	POS	-
IC 24	TSE 5450	infected	F	2024-05-01	2024-08-09	14	Brain	POS	POS
							Small Intestine	POS	-
							Spleen	POS	-
IC 24	TSE 5451	infected	F	2024-05-01	2024-08-29	17	Brain	POS	POS
							Small Intestine	POS	-
							Spleen	POS	-
IC 24	TSE 5452	infected	F	2024-05-01	2024-08-22	16	Brain	POS	POS
							Small Intestine	POS	-
							Spleen	POS	-
IC 24	TSE 5453	infected	F	2024-05-01	2024-08-22	16	Brain	POS	POS
							Small Intestine	POS	-
							Spleen	POS	-
IC 24	TSE 5454	infected	M	2024-05-01	2024-08-28	17	Brain	POS	POS
							Small Intestine	POS	-
							Spleen	POS	-
IC 24	TSE 5455	infected	M	2024-05-01	2024-08-28	17	Brain	POS	POS
							Small Intestine	POS	-
							Spleen	POS	-
IC 24	TSE 5457	infected	M	2024-05-01	2024-09-21	20	Brain	POS	POS
							Small Intestine	POS	-
							Spleen	POS	-
IC 24	TSE 5458	infected	M	2024-05-01	2024-09-23	21	Brain	POS	POS
							Small Intestine	POS	-
							Spleen	POS	-
IC 24	TSE 5459	infected	M	2024-05-01	2024-08-21	16	Brain	POS	POS
							Small Intestine	POS	-
							Spleen	POS	-
IC 24	TSE 5460	control	F	2024-05-01	2024-10-17	24	Brain	NEG	NEG
							Small Intestine	NEG	-
							Spleen	NEG	-
IC 24	TSE 5461	control	F	2024-05-01	2024-10-17	24	Brain	NEG	NEG
							Small Intestine	NEG	-
							Spleen	NEG	-
IC 24	TSE 5462	control	F	2024-05-01	2024-10-17	24	Brain	NEG	NEG
							Small Intestine	NEG	-
							Spleen	NEG	-
IC 24	TSE 5463	control	F	2024-05-01	2024-10-17	24	Brain	NEG	NEG
							Small Intestine	NEG	-
							Spleen	NEG	-
IC 24	TSE 5464	control	F	2024-05-01	2024-10-17	24	Brain	NEG	NEG
							Small Intestine	NEG	-
							Spleen	NEG	-
IC 24	TSE 5465	control	F	2024-05-01	2024-10-17	24	Brain	NEG	NEG
							Small Intestine	NEG	-
							Spleen	NEG	-
IC 24	TSE 5466	control	M	2024-05-01	2024-10-17	24	Brain	NEG	NEG
							Small Intestine	NEG	-
							Spleen	NEG	-
IC 24	TSE 5467	control	M	2024-05-01	2024-10-17	24	Brain	NEG	NEG
							Small Intestine	NEG	-
							Spleen	NEG	-
IC 24	TSE 5468	control	M	2024-05-01	2024-10-17	24	Brain	NEG	NEG
							Small Intestine	NEG	-
							Spleen	NEG	-
IC 24	TSE 5469	control	M	2024-05-01	2024-10-17	24	Brain	NEG	NEG
							Small Intestine	NEG	-
							Spleen	NEG	-
IC 24	TSE 5471	control	M	2024-05-01	2024-10-17	24	Brain	NEG	NEG
							Small Intestine	NEG	-
							Spleen	NEG	-

IC 20	TSE 5496	infected	F	2024-05-15	2024-08-29	15	Brain	POS	POS
							Small Intestine	NEG	-
							Spleen	POS	-
IC 20	TSE 5498	infected	F	2024-05-15	2024-08-23	14	Brain	POS	POS
							Small Intestine	POS	-
							Spleen	POS	-
IC 20	TSE 5499	infected	F	2024-05-15	2024-08-30	15	Brain	POS	POS
							Small Intestine	POS	-
							Spleen	POS	-
IC 20	TSE 5500	infected	F	2024-05-15	2024-08-30	15	Brain	POS	POS
							Small Intestine	POS	-
							Spleen	POS	-
IC 20	TSE 5501	infected	F	2024-05-15	2024-08-23	14	Brain	POS	POS
							Small Intestine		-
							Spleen	POS	-
IC 20	TSE 5502	infected	M	2024-05-15	2024-10-02	20	Brain	POS	POS
							Small Intestine		-
							Spleen	POS	-
IC 20	TSE 5503	infected	M	2024-05-15	2024-08-23	14	Brain	POS	POS
							Small Intestine	NEG	-
							Spleen	POS	-
IC 20	TSE 5505	infected	M	2024-05-15	2024-09-27	19	Brain	POS	POS
							Small Intestine		-
							Spleen	POS	-
IC 20	TSE 5506	infected	M	2024-05-15	2024-09-13	17	Brain	POS	POS
							Small Intestine	NEG	-
							Spleen	POS	-
IC 20	TSE 5507	infected	M	2024-05-15	2024-09-16	18	Brain	POS	POS
							Small Intestine	NEG	-
							Spleen	POS	-
IC 20	TSE 5508	infected	M	2024-05-15	2024-08-27	15	Brain	POS	POS
							Small Intestine	POS	-
							Spleen	POS	-
IC 20	TSE 5509	infected	M	2024-05-15	2024-08-23	14	Brain	POS	POS
							Small Intestine	POS	-
							Spleen	POS	-
IC 20	TSE 5510	control	F	2024-05-15	2024-10-02	20	Brain	NEG	POS
							Small Intestine	NEG	-
							Spleen	NEG	-
IC 20	TSE 5511	control	F	2024-05-15	2024-10-02	20	Brain	NEG	POS
							Small Intestine	NEG	-
							Spleen	NEG	-
IC 20	TSE 5512	control	F	2024-05-15	2024-10-02	20	Brain	NEG	POS
							Small Intestine	NEG	-
							Spleen	NEG	-
IC 20	TSE 5514	control	F	2024-05-15	2024-09-13	17	Brain	NEG	POS
							Small Intestine	NEG	-
							Spleen	NEG	-
IC 20	TSE 5516	control	M	2024-05-15	2024-10-02	20	Brain	NEG	POS
							Small Intestine	NEG	-
							Spleen	NEG	-
IC 20	TSE 5517	control	M	2024-05-15	2024-10-02	20	Brain	NEG	POS
							Small Intestine	NEG	-
							Spleen	NEG	-
IC 20	TSE 5518	control	M	2024-05-15	2024-10-02	20	Brain	NEG	POS
							Small Intestine	NEG	-
							Spleen	NEG	-
IC 20	TSE 5519	control	M	2024-05-15	2024-10-02	20	Brain	NEG	POS
							Small Intestine	NEG	-
							Spleen	NEG	-
IC 20	TSE 5520	control	M	2024-05-15	2024-10-02	20	Brain	NEG	POS
							Small Intestine	NEG	-
							Spleen	NEG	-
IC 20	TSE 5521	control	M	2024-05-15	2024-10-02	20	Brain	NEG	POS
							Small Intestine	NEG	-
							Spleen	NEG	-

IC 16	TSE 5522	infected	M	2024-06-19	2024-10-09	16	Brain	POS	POS
							Small Intestine		-
							Spleen	POS	-
IC 16	TSE 5523	infected	M	2024-06-19	2024-10-09	16	Brain	POS	POS
							Small Intestine		-
							Spleen	POS	-
IC 16	TSE 5524	infected	M	2024-06-19	2024-10-09	16	Brain	POS	POS
							Small Intestine		-
							Spleen	POS	-
IC 16	TSE 5525	infected	M	2024-06-19	2024-09-11	12	Brain	POS	POS
							Small Intestine		-
							Spleen	POS	-
IC 16	TSE 5526	infected	M	2024-06-19	2024-10-03	15	Brain	POS	POS
							Small Intestine		-
							Spleen	POS	-
IC 16	TSE 5527	infected	M	2024-06-19	2024-08-29	10	Brain	POS	POS
							Small Intestine		-
							Spleen	POS	-
IC 16	TSE 5528	infected	F	2024-06-19	2024-10-09	16	Brain	POS	POS
							Small Intestine		-
							Spleen	POS	-
IC 16	TSE 5529	infected	F	2024-06-19	2024-09-23	14	Brain	POS	POS
							Small Intestine		-
							Spleen	POS	-
IC 16	TSE 5530	infected	F	2024-06-19	2024-09-13	12	Brain	POS	POS
							Small Intestine		-
							Spleen	POS	-
IC 16	TSE 5532	infected	F	2024-06-19	2024-09-23	14	Brain	POS	POS
							Small Intestine		-
							Spleen	POS	-
IC 16	TSE 5533	infected	F	2024-06-19	2024-10-09	16	Brain	POS	POS
							Small Intestine		-
							Spleen	POS	-
IC 16	TSE 5534	infected	F	2024-06-19	2024-09-11	12	Brain	POS	POS
							Small Intestine		-
							Spleen	POS	-
IC 16	TSE 5536	control	M	2024-06-19	2024-08-27	10	Brain		POS
							Small Intestine		-
							Spleen	NEG	-
IC 16	TSE5535	control	F	2024-06-19	2024-10-10	16	Brain	NEG	NEG
							Small Intestine	NEG	-
							Spleen	NEG	-
IC 16	TSE 5537	control	M	2024-06-19	2024-10-09	16	Brain	NEG	NEG
							Small Intestine		-
							Spleen	NEG	-
IC 16	TSE 5538	control	M	2024-06-19	2024-10-09	16	Brain	NEG	NEG
							Small Intestine		-
							Spleen	NEG	-
IC 16	TSE 5540	control	M	2024-06-19	2024-10-09	16	Brain	NEG	NEG
							Small Intestine		-
							Spleen	NEG	-
IC 16	TSE 5541	control	M	2024-06-19	2024-10-10	16	Brain	NEG	NEG
							Small Intestine		-
							Spleen	NEG	-
IC 16	TSE 5542	control	F	2024-06-19	2024-10-10	16	Brain	NEG	NEG
							Small Intestine		-
							Spleen	NEG	-
IC 16	TSE 5543	control	F	2024-06-19	2024-10-10	16	Brain	NEG	NEG
							Small Intestine		-
							Spleen	NEG	-
IC 16	TSE 5544	control	F	2024-06-19	2024-10-10	16	Brain	NEG	NEG
							Small Intestine		-
							Spleen	NEG	-
IC 16	TSE 5545	control	F	2024-06-19	2024-10-10	16	Brain	NEG	NEG
							Small Intestine		-
							Spleen	NEG	-
IC 16	TSE 5546	control	F	2024-06-19	2024-10-10	16	Brain	NEG	NEG
							Small Intestine		-
							Spleen	NEG	-
IC 16	TSE 5547	control	F	2024-06-19	2024-10-10	16	Brain	NEG	NEG
							Small Intestine		-
							Spleen	NEG	-

IC 12	TSE 5599	infected	M	2024-08-28	2024-11-19	12	Brain	POS	POS
							Small Intestine		-
							Spleen	POS	-
IC 12	TSE 5601	infected	M	2024-08-28	2024-10-07	6	Brain	POS	POS
							Small Intestine		-
							Spleen	POS	-
IC 12	TSE 5602	infected	M	2024-08-28	2024-10-11	6	Brain	POS	POS
							Small Intestine	POS	-
							Spleen	NEG	-
IC 12	TSE 5603	infected	M	2024-08-28	2024-11-19	12	Brain	NEG	POS
							Small Intestine	POS	-
							Spleen	POS	-
IC 12	TSE 5604	infected	M	2024-08-28	2024-11-19	12	Brain	POS	POS
							Small Intestine	POS	-
							Spleen	POS	-
IC 12	TSE 5605	infected	F	2024-08-28	2024-11-19	12	Brain	POS	POS
							Small Intestine	NEG	-
							Spleen	POS	-
IC 12	TSE 5606	infected	F	2024-08-28	2024-11-19	12	Brain	POS	POS
							Small Intestine	POS	-
							Spleen	POS	-
IC 12	TSE 5607	infected	F	2024-08-28	2024-11-19	12	Brain	POS	POS
							Small Intestine	POS	-
							Spleen	POS	-
IC 12	TSE 5608	infected	F	2024-08-28	2024-11-19	12	Brain	POS	POS
							Small Intestine	POS	-
							Spleen	POS	-
IC 12	TSE 5609	infected	F	2024-08-28	2024-11-19	12	Brain	POS	POS
							Small Intestine	POS	-
							Spleen	POS	-
IC 12	TSE 5610	infected	F	2024-08-28	2024-11-19	12	Brain	POS	POS
							Small Intestine		-
							Spleen	POS	-
IC 12	TSE 5611	infected	F	2024-08-28	2024-11-19	12	Brain	POS	POS
							Small Intestine		-
							Spleen	POS	-
IC 12	TSE 5612	control	M	2024-08-28	2024-11-20	12	Brain	NEG	NEG
							Small Intestine	NEG	-
							Spleen	NEG	-
IC 12	TSE 5613	control	M	2024-08-28	2024-11-20	12	Brain	NEG	NEG
							Small Intestine	POS	-
							Spleen	NEG	-
IC 12	TSE 5614	control	M	2024-08-28	2024-11-20	12	Brain	NEG	NEG
							Small Intestine	NEG	-
							Spleen	NEG	-
IC 12	TSE 5615	control	M	2024-08-28	2024-11-20	12	Brain	NEG	NEG
							Small Intestine	NEG	-
							Spleen	NEG	-
IC 12	TSE 5616	control	M	2024-08-28	2024-11-20	12	Brain	NEG	NEG
							Small Intestine	NEG	-
							Spleen	NEG	-
IC 12	TSE 5617	control	M	2024-08-28	2024-11-20	12	Brain	NEG	NEG
							Small Intestine	NEG	-
							Spleen	NEG	-
IC 12	TSE 5618	control	F	2024-08-28	2024-11-20	12	Brain	NEG	NEG
							Small Intestine	NEG	-
							Spleen	NEG	-
IC 12	TSE 5619	control	F	2024-08-28	2024-11-20	12	Brain	NEG	NEG
							Small Intestine	NEG	-
							Spleen	NEG	-
IC 12	TSE 5620	control	F	2024-08-28	2024-11-20	12	Brain	NEG	NEG
							Small Intestine	NEG	-
							Spleen	NEG	-
IC 12	TSE 5621	control	F	2024-08-28	2024-11-20	12	Brain	NEG	NEG
							Small Intestine	NEG	-
							Spleen	NEG	-
IC 12	TSE 5622	control	F	2024-08-28	2024-11-20	12	Brain	NEG	NEG
							Small Intestine	NEG	-
							Spleen	NEG	-
IC 12	TSE 5623	control	F	2024-08-28	2024-11-20	12	Brain	NEG	NEG
							Small Intestine	NEG	-
							Spleen	NEG	-

IC 8	TSE 5472	infected	F	2024-05-08	2024-07-03	8	Brain	POS	POS
							Small Intestine	POS	-
							Spleen	POS	-
IC 8	TSE 5474	infected	F	2024-05-08	2024-07-03	8	Brain	POS	POS
							Small Intestine	NEG	-
							Spleen	POS	-
IC 8	TSE 5475	infected	F	2024-05-08	2024-07-03	8	Brain	POS	POS
							Small Intestine		-
							Spleen	POS	-
IC 8	TSE 5476	infected	F	2024-05-08	2024-07-03	8	Brain	POS	POS
							Small Intestine	POS	-
							Spleen	POS	-
IC 8	TSE 5478	infected	M	2024-05-08	2024-07-03	8	Brain	POS	POS
							Small Intestine	POS	-
							Spleen	POS	-
IC 8	TSE 5479	infected	M	2024-05-08	2024-07-03	8	Brain	POS	POS
							Small Intestine	POS	-
							Spleen	POS	-
IC 8	TSE 5480	infected	M	2024-05-08	2024-07-03	8	Brain	POS	POS
							Small Intestine	NEG	-
							Spleen	POS	-
IC 8	TSE 5481	infected	M	2024-05-08	2024-07-03	8	Brain	POS	POS
							Small Intestine	POS	-
							Spleen	POS	-
IC 8	TSE 5482	infected	M	2024-05-08	2024-07-03	8	Brain	POS	POS
							Small Intestine	NEG	-
							Spleen	POS	-
IC 8	TSE 5483	infected	M	2024-05-08	2024-07-03	8	Brain	POS	POS
							Small Intestine	POS	-
							Spleen	POS	-
IC 8	TSE 5484	control	F	2024-05-08	2024-07-03	8	Brain	NEG	POS
							Small Intestine	POS	-
							Spleen	NEG	-
IC 8	TSE 5485	control	F	2024-05-08	2024-07-03	8	Brain	NEG	POS
							Small Intestine		-
							Spleen	NEG	-
IC 8	TSE 5486	control	F	2024-05-08	2024-07-03	8	Brain	NEG	NEG
							Small Intestine		-
							Spleen	NEG	-
IC 8	TSE 5488	control	F	2024-05-08	2024-07-03	8	Brain	NEG	NEG
							Small Intestine		-
							Spleen	NEG	-
IC 8	TSE 5489	control	F	2024-05-08	2024-07-03	8	Brain	NEG	NEG
							Small Intestine	NEG	-
							Spleen	NEG	-
IC 8	TSE 5490	control	M	2024-05-08	2024-07-03	8	Brain	POS	NEG
							Small Intestine	NEG	-
							Spleen	NEG	-
IC 8	TSE 5491	control	M	2024-05-08	2024-07-03	8	Brain	NEG	NEG
							Small Intestine		-
							Spleen	NEG	-
IC 8	TSE 5492	control	M	2024-05-08	2024-07-03	8	Brain	NEG	NEG
							Small Intestine	POS	-
							Spleen	NEG	-
IC 8	TSE 5494	control	M	2024-05-08	2024-07-03	8	Brain	NEG	NEG
							Small Intestine	NEG	-
							Spleen	NEG	-
IC 8	TSE 5495	control	M	2024-05-08	2024-07-03	8	Brain	NEG	NEG
							Small Intestine	NEG	-
							Spleen	NEG	-

S4. Supplementary Data 4. Raw RT-QuIC fluorescence data for intracerebrally inoculated (IC) TgElkPrP mice: brain, spleen, and small-intestine tissues.

Inoculation Route & Target Incubation Date	Sample ID	Treatment	Sex	Inoculation Date	Date of Death	Weeks Survived Post Inoculation	Tissue	Replicate 1	Replicate 2	Replicate 3	Replicate 4
IC 24	TSE 5448	infected	F	2024-05-01	2024-08-29	17	Brain	9.2021	7.075	7.5322	10.169
							Small Intestine	11.201	12.247	10.064	11.193
							Spleen	60	35.417	15.9925	39.62788
IC 24	TSE 5449	infected	F	2024-05-01	2024-08-16	15	Brain	11.755	11.1957	12.4856	10.0107
							Small Intestine	13.261	11.187	13.92	11.19
							Spleen	10.17089	10.623	10.1825	16.9726
IC 24	TSE 5450	infected	F	2024-05-01	2024-08-09	14	Brain	5.49521	9.5022	13.1255	7.2643
							Small Intestine	6.832	10.101	9.462	10.511
							Spleen	7.5325	6.5551	7.5325	6.5551
IC 24	TSE 5451	infected	F	2024-05-01	2024-08-29	17	Brain	8.3715	8.1947	6.8331	10.95955
							Small Intestine	9.554	10.308	10.206	5.522
							Spleen	7.3179	8.1994	7.2646	6.2707
IC 24	TSE 5452	infected	F	2024-05-01	2024-08-22	16	Brain	9.2073	10.344	8.8518	9.153
							Small Intestine	12.22	12.6	13.143	9.67
							Spleen	22.3712	25.2643	19.4925	9.359
IC 24	TSE 5453	infected	F	2024-05-01	2024-08-22	16	Brain	9.2835	7.57992	9.3139	7.5914
							Small Intestine	12.297	12.212	10.385	10.493
							Spleen	4.2726	6.223	6.2741	5.1339
IC 24	TSE 5454	infected	M	2024-05-01	2024-08-28	17	Brain	6.6731	7.203	7.17184	8.6274
							Small Intestine	19.647	21.587	16.279	24.587
							Spleen	7.6467	5.6818	7.177	6.2707
IC 24	TSE 5455	infected	M	2024-05-01	2024-08-28	17	Brain	6.578	9.0259	11.2331	11.4485
							Small Intestine	12.29	11.209	9.06	10.928
							Spleen	7.9779	7.6386	10.6145	7.5439
IC 24	TSE 5457	infected	M	2024-05-01	2024-09-21	16	Brain	11.2229	10.2554	14.8602	23.2026
							Small Intestine	60	16.262	13.525	12.91
							Spleen	34.41644	29.254	25.5239	28.73545
IC 24	TSE 5458	infected	M	2024-05-01	2024-09-23	21	Brain	12.213	13.267	11.2202	12.8232
							Small Intestine	14.864	13.448	13.223	14.967
							Spleen	12.2104	60	60	22.493
IC 24	TSE 5459	infected	M	2024-05-01	2024-08-21	16	Brain	10.8284	31.489	10.1967	9.5287
							Small Intestine	10.357	11.755	11.623	11.418
							Spleen	11.2245	10.6535	9.5559	10.03867
IC 24	TSE 5460	control	F	2024-05-01	2024-10-17	24	Brain	60	60	60	60
							Small Intestine	60	60	59.734	60
							Spleen	60	60	60	60
IC 24	TSE 5461	control	F	2024-05-01	2024-10-17	24	Brain	60	60	60	60
							Small Intestine	60	60	60	60
							Spleen	34.50367	60	60	60
IC 24	TSE 5462	control	F	2024-05-01	2024-10-17	24	Brain	60	60	60	60
							Small Intestine	23.291	34.599	40.26	39.615
							Spleen	42.4198	27.3594	33.4806	41.4512
IC 24	TSE 5463	control	F	2024-05-01	2024-10-17	24	Brain	60	60	60	60
							Small Intestine	60	60	38.358	60
							Spleen	60	60	60	60
IC 24	TSE 5464	control	F	2024-05-01	2024-10-17	24	Brain	60	60	60	60
							Small Intestine	51.251	28.637	58.748	53.323
							Spleen	60	60	60	60
IC 24	TSE 5465	control	F	2024-05-01	2024-10-17	24	Brain	60	60	60	60
							Small Intestine	43.573	58.789	52.361	24.293
							Spleen	60	60	60	60
IC 24	TSE 5466	control	M	2024-05-01	2024-10-17	24	Brain	60	60	60	60
							Small Intestine	46.5	57.615	47.377	39.042
							Spleen	60	60	60	60
IC 24	TSE 5467	control	M	2024-05-01	2024-10-17	24	Brain	60	60	60	60
							Small Intestine	54.678	60	60	60
							Spleen	60	47.5444	46.73	60
IC 24	TSE 5468	control	M	2024-05-01	2024-10-17	24	Brain	31.2858	60	60	60
							Small Intestine	60	60	60	60
							Spleen	60	60	60	34.4322
IC 24	TSE 5469	control	M	2024-05-01	2024-10-17	24	Brain	60	60	60	15.8735
							Small Intestine	37.38	37.671	34.476	34.504
							Spleen	60	60	60	60
IC 24	TSE 5471	control	M	2024-05-01	2024-10-17	24	Brain	60	60	60	60
							Small Intestine	40.724	52.742	42.788	60
							Spleen	60	60	60	47.4323

IC 20	TSE 5496	infected	F	2024-05-15	2024-08-29	15	Brain	9.1723	11.9595	10.5053	12.6659
							Small Intestine	60	60	60	60
							Spleen	43.59	23.5499	32.1714	38.7201
IC 20	TSE 5498	infected	F	2024-05-15	2024-08-23	14	Brain	5.6695	9.1978	7.7693	5.6202
							Small Intestine	13.686	10.854	11.263	12.2091
							Spleen	8.6295	8.3261	8.0608	9.6697
IC 20	TSE 5499	infected	F	2024-05-15	2024-08-30	15	Brain	8.9898	5.4581	11.4671	7.3934
							Small Intestine	13.224	14.234	12.963	14.423
							Spleen	19.27814	17.05982	14.64306	23.3032
IC 20	TSE 5500	infected	F	2024-05-15	2024-08-30	15	Brain	9.5239	9.938	10.8276	8.9162
							Small Intestine	6.3	6.41	6.293	6.698
							Spleen	12.8339	10.31798	10.2178	10.9647
IC 20	TSE 5501	infected	F	2024-05-15	2024-08-23	14	Brain	11.6252	7.466	11.3728	5.6295
							Small Intestine	13.224	18.292	12.921	35.729
							Spleen	9.5225	9.1707	8.2032	8.8869
IC 20	TSE 5502	infected	M	2024-05-15	2024-10-02	20	Brain	9.7279	12.5714	10.2777	13.2398
							Small Intestine	32.518	60	9.269	10.433
							Spleen	11.3646	7.1476	8.2333	11.2826
IC 20	TSE 5503	infected	M	2024-05-15	2024-08-23	14	Brain	8.5121	3.414	10.3438	9.813
							Small Intestine	60	60	42.474	60
							Spleen	8.5289	10.6904	10.2929	8.0528
IC 20	TSE 5505	infected	M	2024-05-15	2024-09-27	19	Brain	8.5021	8.2333	12.2157	10.1798
							Small Intestine	12.963	9.5225	4.9777	7.884
							Spleen	20.274	14.477	12.788	12.761
IC 20	TSE 5506	infected	M	2024-05-15	2024-09-13	17	Brain	10.0714	13.246	2.4191	9.3248
							Small Intestine	60	60	60	60
							Spleen	5.953	7.594	4.2726	6.223
IC 20	TSE 5507	infected	M	2024-05-15	2024-09-16	18	Brain	7.3529	7.7302	10.3127	9.3266
							Small Intestine	60	60	60	60
							Spleen	6.2741	5.1339	8.7752	14.477
IC 20	TSE 5508	infected	M	2024-05-15	2024-08-27	15	Brain	7.3271	8.2218	4.9777	10.2097
							Small Intestine	11.732	12.07	14.273	11.235
							Spleen	10.9316	9.5598	16.1177	10.367
IC 20	TSE 5509	infected	M	2024-05-15	2024-08-23	14	Brain	11.4749	6.2935	11.2128	10.2097
							Small Intestine	9.836	8.083	8.404	7.884
							Spleen	8.7752	7.214	6.5443	5.3591
IC 20	TSE 5510	control	F	2024-05-15	2024-10-02	20	Brain	60	60	60	60
							Small Intestine	60	60	60	60
							Spleen	60	60	60	60
IC 20	TSE 5511	control	F	2024-05-15	2024-10-02	20	Brain	60	60	60	60
							Small Intestine	60	60	60	60
							Spleen	60	60	60	60
IC 20	TSE 5512	control	F	2024-05-15	2024-10-02	20	Brain	60	60	60	60
							Small Intestine	60	60	60	60
							Spleen	60	60	60	60
IC 20	TSE 5514	control	F	2024-05-15	2024-09-13	17	Brain	60	60	60	60
							Small Intestine	60	60	60	60
							Spleen	60	60	60	60
IC 20	TSE 5516	control	M	2024-05-15	2024-10-02	20	Brain	60	60	60	60
							Small Intestine	60	60	60	44.497
							Spleen	60	60	60	60
IC 20	TSE 5517	control	M	2024-05-15	2024-10-02	20	Brain	60	60	60	60
							Small Intestine	60	60	38.385	36.265
							Spleen	60	60	60	60
IC 20	TSE 5518	control	M	2024-05-15	2024-10-02	20	Brain	60	60	43	60
							Small Intestine	60	60	60	60
							Spleen	60	60	60	60
IC 20	TSE 5519	control	M	2024-05-15	2024-10-02	20	Brain	60	60	60	60
							Small Intestine	60	60	33.2577	60
							Spleen	60	60	60	60
IC 20	TSE 5520	control	M	2024-05-15	2024-10-02	20	Brain	60	60	60	60
							Small Intestine	60	60	60	60
							Spleen	60	60	60	60
IC 20	TSE 5521	control	M	2024-05-15	2024-10-02	20	Brain	60	60	60	60
							Small Intestine	60	60	60	60
							Spleen	60	60	60	60

IC 16	TSE 5522	infected	M	2024-06-19	2024-10-09	16	Brain	9.9729	10.3235	15.6272	9.495
							Small Intestine	8.214	7.538	10.376	5.862
							Spleen	24.36882	60	60	60
IC 16	TSE 5523	infected	M	2024-06-19	2024-10-09	16	Brain	6.8554	11.2021	11.3352	6.0882
							Small Intestine	60	60	60	60
							Spleen	14.80456	20.3089	17.48021	15.3724
IC 16	TSE 5524	infected	M	2024-06-19	2024-10-09	16	Brain	3.5075	7.5049	9.2117	6.532
							Small Intestine	60	60	60	11.837
							Spleen	60	24.2602	8.501886	60
IC 16	TSE 5525	infected	M	2024-06-19	2024-09-11	12	Brain	6.7653	11.5024	10.3583	9.5066
							Small Intestine	60	60	60	60
							Spleen	10.34365	11.30884	10.39629	9.3277
IC 16	TSE 5526	infected	M	2024-06-19	2024-10-03	15	Brain	5.8319	7.1552	9.77	4.5709
							Small Intestine	8.829	13.464	13.219	11.416
							Spleen	33.15538	30.3847	29.5343	28.3765
IC 16	TSE 5527	infected	M	2024-06-19	2024-08-29	10	Brain	9.5299	11.1954	13.2546	10.554
							Small Intestine	8.0786	3.096	3.682	4.998
							Spleen	4.5921	4.769	7.6538	8.323
IC 16	TSE 5528	infected	F	2024-06-19	2024-10-09	16	Brain	4.5005	9.5422	9.4304	5.2181
							Small Intestine	60	60	8.0786	18.281
							Spleen	4.93439	5.48795	4.361873	4.487635
IC 16	TSE 5529	infected	F	2024-06-19	2024-09-23	14	Brain	11.0785	11.2	9.6269	9.3876
							Small Intestine	6.777	8.205	8.907	8.343
							Spleen	3.735797	3.635946	5.19296	3.681541
IC 16	TSE 5530	infected	F	2024-06-19	2024-09-13	12	Brain	10.5023	10.2207	10.3093	9.3889
							Small Intestine	6.7653	11.5024	10.3583	9.5066
							Spleen	5.12029	5.253517	7.280124	7.286968
IC 16	TSE 5532	infected	F	2024-06-19	2024-09-23	14	Brain	10.222	11.05311	12.2464	10.2085
							Small Intestine	7.3271	8.2218	4.9777	10.2097
							Spleen	8.83647	8.324705	10.4735	8.234818
IC 16	TSE 5533	infected	F	2024-06-19	2024-10-09	16	Brain	8.692651	9.166246	Negative	7.67661
							Small Intestine	60	60	5.504	60
							Spleen	60	60	32.56599	35.57518
IC 16	TSE 5534	infected	F	2024-06-19	2024-09-11	12	Brain	10.2314	9.1812	11.40009	12.3241
							Small Intestine	60	60	60	60
							Spleen	10.66981	10.235	10.2209	10.6131
IC 16	TSE5535	control	F	2024-06-19	2024-10-10	16	Brain	60	60	60	58.6868
							Small Intestine	60	44.5708	39.629	47.581
							Spleen	60	60	60	60
IC 16	TSE 5537	control	M	2024-06-19	2024-10-09	16	Brain	60	60	7.5398	60
							Small Intestine	60	60	60	60
							Spleen	60	60	60	60
IC 16	TSE 5538	control	M	2024-06-19	2024-10-09	16	Brain	35.4434	60	60	60
							Small Intestine	60	60	60	34.378
							Spleen	60	60	60	60
IC 16	TSE 5540	control	M	2024-06-19	2024-10-09	16	Brain	33.5029	60	60	60
							Small Intestine	60	60	60	60
							Spleen	60	60	60	60
IC 16	TSE 5541	control	M	2024-06-19	2024-10-10	16	Brain	60	58.25367	60	60
							Small Intestine	60	60	60	60
							Spleen	60	60	60	60
IC 16	TSE 5542	control	F	2024-06-19	2024-10-10	16	Brain	60	60	60	60
							Small Intestine	60	60	60	60
							Spleen	60	60	60	60
IC 16	TSE 5543	control	F	2024-06-19	2024-10-10	16	Brain	60	60	60	60
							Small Intestine	60	60	60	60
							Spleen	60	60	60	60
IC 16	TSE 5544	control	F	2024-06-19	2024-10-10	16	Brain	60	60	60	60
							Small Intestine	60	60	60	60
							Spleen	60	60	60	60
IC 16	TSE 5545	control	F	2024-06-19	2024-10-10	16	Brain	60	60	60	60
							Small Intestine	60	60	60	60
							Spleen	60	60	60	60
IC 16	TSE 5546	control	F	2024-06-19	2024-10-10	16	Brain	60	60	60	60
							Small Intestine	60	60	60	60
							Spleen	60	60	60	60
IC 16	TSE 5547	control	F	2024-06-19	2024-10-10	16	Brain	60	60	60	57.912
							Small Intestine	60	60	60	60
							Spleen	60	60	60	60
IC 16	TSE5535	control	F	2024-06-19	2024-10-10	16	Brain	60	60	60	58.6868
							Small Intestine	60	44.5708	39.629	47.581
							Spleen	60	60	60	60

IC 12	TSE 5599	infected	M	2024-08-28	2024-11-19	12	Brain	8.1707	11.2134	9.0878	8.7029
							Small Intestine	4.511	5.094	4.511	5.76
							Spleen	9.8816	16.03385	15.02365	13.52246
IC 12	TSE 5601	infected	M	2024-08-28	2024-10-07	6	Brain	7.3529	7.7302	10.3127	9.3266
							Spleen	9.157	8.1573	4.6698	6.7773
IC 12	TSE 5602	infected	M	2024-08-28	2024-10-11	6	Brain	8.9898	5.4581	11.4671	7.3934
							Small Intestine	14.32	40.31	21.643	26.245
							Spleen	36.5678	60	53.4929	39.6267
IC 12	TSE 5603	infected	M	2024-08-28	2024-11-19	12	Brain	60	8.261	12.008	17.905
							Small Intestine	11.397	12.047	17.274	26.526
							Spleen	11.3023	7.2607	60	8.7277
IC 12	TSE 5604	infected	M	2024-08-28	2024-11-19	12	Brain	13.216	8.636	10.462	9.586
							Small Intestine	12.251	14.089	10.346	8.187
							Spleen	60	9.8989	15.0748	11.3989
IC 12	TSE 5605	infected	F	2024-08-28	2024-11-19	12	Brain	5.132	4.693	4.768	4.845
							Small Intestine	60	60	60	46.536
							Spleen	16.5122	13.7498	14.2992	15.8436
IC 12	TSE 5606	infected	F	2024-08-28	2024-11-19	12	Brain	8.403	9.147	9.34	8.97
							Small Intestine	5.294	15.693	5.085	11.234
							Spleen	10.6368	60	16.1833	9.315
IC 12	TSE 5607	infected	F	2024-08-28	2024-11-19	12	Brain	5.458	5.193	5.128	4.767
							Small Intestine	8.1832	14.876	9.0127	12.181
							Spleen	60	12.9109	12.552	14.5025
IC 12	TSE 5608	infected	F	2024-08-28	2024-11-19	12	Brain	4.074	4.865	4.688	4.319
							Small Intestine	6.271	6.351	4.463	7.432
							Spleen	19.2918	15.6776	12.9029	11.6233
IC 12	TSE 5609	infected	F	2024-08-28	2024-11-19	12	Brain	8.763	8.24	9.938	13.056
							Small Intestine	8.1832	6.271	7.218	5.421
							Spleen	7.1377	8.3068	7.5499	6.4997
IC 12	TSE 5610	infected	F	2024-08-28	2024-11-19	12	Brain	9.2163	8.279	7.135	7.551
							Small Intestine	60	60	60	12.232
							Spleen	13.0211	9.6932	16.6374	9.7585
IC 12	TSE 5611	infected	F	2024-08-28	2024-11-19	12	Brain	7.372	9.817	7.3825	10.221
							Small Intestine	60	60	11.817	8.697
							Spleen	11.1889	8.0134	8.5321	8.4998
IC 12	TSE 5612	control	M	2024-08-28	2024-11-20	12	Brain	60	60	60	60
							Small Intestine	60	60	60	60
							Spleen	60	60	60	60
IC 12	TSE 5613	control	M	2024-08-28	2024-11-20	12	Brain	60	60	60	60
							Small Intestine	15.658	18.766	27.387	23.292
							Spleen	60	60	60	60
IC 12	TSE 5614	control	M	2024-08-28	2024-11-20	12	Brain	60	60	60	60
							Small Intestine	60	60	60	60
							Spleen	60	60	60	60
IC 12	TSE 5615	control	M	2024-08-28	2024-11-20	12	Brain	60	60	60	60
							Small Intestine	32.5	60	60	60
							Spleen	60	60	60	60
IC 12	TSE 5616	control	M	2024-08-28	2024-11-20	12	Brain	60	60	60	60
							Small Intestine	60	60	60	60
							Spleen	60	60	60	60
IC 12	TSE 5617	control	M	2024-08-28	2024-11-20	12	Brain	60	60	60	60
							Small Intestine	60	60	60	60
							Spleen	36.5678	60	60	60
IC 12	TSE 5618	control	F	2024-08-28	2024-11-20	12	Brain	60	60	60	60
							Small Intestine	60	60	60	60
							Spleen	60	60	60	60
IC 12	TSE 5619	control	F	2024-08-28	2024-11-20	12	Brain	60	60	60	60
							Small Intestine	60	60	60	60
							Spleen	60	60	60	60
IC 12	TSE 5620	control	F	2024-08-28	2024-11-20	12	Brain	60	60	60	60
							Small Intestine	60	60	60	39.545
							Spleen	60	60	60	60
IC 12	TSE 5621	control	F	2024-08-28	2024-11-20	12	Brain	60	60	60	60
							Small Intestine	60	60	60	39.428
							Spleen	60	60	60	60
IC 12	TSE 5622	control	F	2024-08-28	2024-11-20	12	Brain	60	60	60	60
							Small Intestine	60	60	60	32.216
							Spleen	60	60	24.36882	60
IC 12	TSE 5623	control	F	2024-08-28	2024-11-20	12	Brain	60	60	60	60
							Small Intestine	60	60	60	60
							Spleen	60	60	60	60

IC 8	TSE 5472	infected	F	2024-05-08	2024-07-03	8	Brain	10.454	10.669	9.528	13.286
							Small Intestine	36.268	38.351	19.293	27.083
							Spleen	26.2868	20.8868	14.3758	9.7973
IC 8	TSE 5474	infected	F	2024-05-08	2024-07-03	8	Brain	13.8	11.685	16.551	14.436
							Small Intestine	60	60	60	39.38
							Spleen	37.93	23.394	13.377	6.47
IC 8	TSE 5475	infected	F	2024-05-08	2024-07-03	8	Brain	14.244	14.613	12.633	13.511
							Small Intestine	14.621	44.094	49.378	60
							Spleen	20.274	14.477	12.788	12.761
IC 8	TSE 5476	infected	F	2024-05-08	2024-07-03	8	Brain	11.656	10.543	12.209	11.248
							Small Intestine	25.2547	11.486	13.657	17.257
							Spleen	5.953	7.594	10.183	9.263
IC 8	TSE 5478	infected	M	2024-05-08	2024-07-03	8	Brain	10.64	12.568	8.126	12.434
							Small Intestine	6.777	8.205	8.907	8.343
							Spleen	60	11.137	21.323	13.973
IC 8	TSE 5479	infected	M	2024-05-08	2024-07-03	8	Brain	12.318	10.6	12.434	14.713
							Small Intestine	28.648	10.681	11.595	18.294
							Spleen	35.391	28.134	26.387	22.292
IC 8	TSE 5480	infected	M	2024-05-08	2024-07-03	8	Brain	13.223	13.578	15.29	14.322
							Small Intestine	60	60	60	60
							Spleen	60	6.819	9.775	7.255
IC 8	TSE 5481	infected	M	2024-05-08	2024-07-03	8	Brain	5.429	11.371	13.238	12.434
							Small Intestine	60	24.252	14.234	23.342
							Spleen	38.713	22.35	18.507	12.76
IC 8	TSE 5482	infected	M	2024-05-08	2024-07-03	8	Brain	8.829	13.464	13.219	11.416
							Small Intestine	25.258	33.333	32.08	32.403
							Spleen	31.44	18.274	8.534	10.765
IC 8	TSE 5483	infected	M	2024-05-08	2024-07-03	8	Brain	14.026	21.308	18.47	16.761
							Small Intestine	18.297	14.563	21.339	14.884
							Spleen	60	12.474	16.435	10.634
IC 8	TSE 5484	control	F	2024-05-08	2024-07-03	8	Brain	60	60	60	60
							Small Intestine	22.365	14.526	24.851	25.328
							Spleen	60	60	60	60
IC 8	TSE 5485	control	F	2024-05-08	2024-07-03	8	Brain	60	60	60	60
							Small Intestine	60	60	60	60
							Spleen	60	60	60	60
IC 8	TSE 5486	control	F	2024-05-08	2024-07-03	8	Brain	60	60	60	60
							Small Intestine	7.631	29.145	23.361	23.401
							Spleen	60	60	34.188	32.324
IC 8	TSE 5487	control	F	2024-05-08	2024-05-08	0	Brain	60	60	60	60
							Small Intestine	38.1095	29.32	28.383	38.485
							Spleen	60	60	60	60
IC 8	TSE 5488	control	F	2024-05-08	2024-07-03	8	Brain	60	60	60	60
							Small Intestine	47.626	44.559	51.583	26.574
							Spleen	60	60	60	60
IC 8	TSE 5489	control	F	2024-05-08	2024-07-03	8	Brain	60	60	60	60
							Small Intestine	60	52.392	60	60
							Spleen	60	60	60	60
IC 8	TSE 5490	control	M	2024-05-08	2024-07-03	8	Brain	60	60	60	60
							Small Intestine	53.565	60	40.929	32.37
							Spleen	60	60	60	60
IC 8	TSE 5491	control	M	2024-05-08	2024-07-03	8	Brain	60	60	60	60
							Small Intestine	10.94	23.29	35.997	52.819
							Spleen	60	60	60	60
IC 8	TSE 5492	control	M	2024-05-08	2024-07-03	8	Brain	60	60	60	60
							Small Intestine	24.346	23.548	11.078	15.741
							Spleen	60	60	60	60
IC 8	TSE 5494	control	M	2024-05-08	2024-07-03	8	Brain	60	60	60	60
							Small Intestine	60	60	60	60
							Spleen	60	60	60	60
IC 8	TSE 5495	control	M	2024-05-08	2024-07-03	8	Brain	60	60	60	60
							Small Intestine	31.295	34.996	60	35.732
							Spleen	60	60	60	60